PRODUCTION AND CHARACTERIZATION OF HYDROXYAPATITE-GRAPHENE OXIDE-CHITOSAN SCAFFOLD FOR BONE TISSUE ENGINEERING APPLICATION

by

Pelin Yılmaz

B.S., Chemical Engineering, Yıldız Technical University, 2015

Submitted to the Institute for Graduate Studies in
Science and Engineering in partial fulfilment of
the requirements for the degree of
Master of Science

Graduate Program in Chemical Engineering
Boğaziçi University
2019

PRODUCTION AND CHARACTERIZATION OF
HYDROXYAPATITE-GRAPHENE OXIDE-CHITOSAN SCAFFOLD
FOR BONE TISSUE ENGINEERING APPLICATION

APPROVED BY:

Prof. Kutlu Ülgen (Thesis Supervisor)	…….
Prof. Belma Özbek (Thesis Co-Supervisor)	…….
Assoc. Prof. Sezen Soyer Uzun	…….
Assoc. Prof. Elçin Demirhan Yılmaz	…….
Assist. Prof. Nazar İleri Ercan	…….

DATE OF APPROVAL: 19/12/2018

ACKNOWLEDGEMENTS

First and foremost, I would like to express my sincerest gratitude to my supervisor, Prof. Kutlu Ülgen. I am aware that this study would not be completed without her guidance, support and insight.

I would like to express my sincerest gratitude to my co-supervisor, Prof. Belma Özbek who gave me an opportunity about my master thesis subject and she continuously supported me with her endless help. I surely know that this work would not be even possible without her help. Even if I offer my endless thanks to her, it will be always deficient when it compared with her helps.

I would also like to thank to Prof. Sezgin Bakırdere who is the professor at chemistry department in Yıldız Technical University and without for his help and support, it would be difficult to complete of this study.

I would like to express my heart-felt thanks to Specialist Elif Öztürk Er for her endless guidance. She has valuable contribute to this study and I learned many of things from her. Whenever I confused, she gave me hand and it was encouraged me to carry out the study. I would like to thank to Assoc. Prof. Elçin Demirhan Yılmaz and Res.Assist. Sinem Şimşek Kekevi for their ideas and support. I have so many friends who always share their moral support with me and I would like to thanks all; Ecem Güler, Anıl Tevfik Koçer, Benan İnan, Sinem Yakarsönmez are just some of them.

I would like to also thank to Yıldız Technical University Scientific Research Projects Coordination Department since this research has been financially supported by Project Number FBA-2018-3210. Additionally, I would like to express my special thanks to Yıldız Technical University Science and Technology Application and Research Center since they provide me enhanced information about the different analysis techniques applied in the present study.

I would like to express my special thanks to my lovely family members; my mother Tülay Yılmaz, my father İlhan Yılmaz, my sister Tülin Yilmaz Nayır and my brother-in-law Tanju Nayır for their endless love and also moral support. I always feel lucky that I have such a family**.** Finally, I would like to thank to my dear boyfriend, Samet Çetiner for his patience and love.

ABSTRACT

PRODUCTION AND CHARACTERIZATION OF HYDROXYAPATITE-GRAPHENE OXIDE-CHITOSAN SCAFFOLD FOR BONE TISSUE ENGINEERING APPLICATION

Bone tissue engineering is a strategy to regenerate diseased or damaged bone tissues by providing the biological microenvironment with the use of appropriate scaffolds that can mimic the native extracellular matrix for bone tissue cells. In the literature, there are many studies performed on this subject, but, no studies have been conducted on the investigation of the production of three-component scaffold, which composed of hydroxyapatite (HAp) derived from eggshells, graphene oxide (GO) and chitosan (CS), by using the supercritical gel drying method, and on the examination of the possible toxicity effects of GO additions. In the present study, HAp derived from the eggshells, which is used for the production of three-component scaffolds composed of HAp-GO-CS, was synthesized by using the precipitation method. Improved Hummer method was used for the synthesis of GO, which was used as an osteoconductive agent. The mixtures of scaffolds were prepared by mixing the solutions of HAp, GO and CS, and these mixtures were frozen after molded. Then, the water-acetone substitution procedure was applied to the frozen samples, the supercritical gel drying was performed to produce scaffolds. Three-component scaffolds, produced at different GO ratios to examine the toxic effect of GO, were characterized by FTIR, XRD, SEM, TEM, EDS, BET and TG/DTA analyses. For the evaluation of the mechanical properties of the produced scaffolds, Universal Instron Mechanical Test System was used. The scaffolds were subjected to MTT testing for cytotoxicity analysis. MTT analysis showed that the use of GO ratio more than 1% (w/w) had a toxic effect on MC3T3-E1 cells. According to the characterization studies performed, it was determined that HAp-GO(1%)-CS three-component scaffold including 1% (w/w) of GO ratio had three-dimensional porous structure, highest cell viability and reasonable mechanical properties. According to the findings, it was concluded that HAp-GO(1%)-CS based composite is a promising scaffold, and could be used for the applications in bone tissue engineering.

ÖZET

KEMİK DOKU MÜHENDİSLİĞİ UYGULAMASI İÇİN HİDROKSİAPATİT-GRAFEN OKSİT-KİTOSAN DOKU İSKELESİ ÜRETİMİ VE KARAKTERİZASYONU

Kemik dokusu mühendisliği, kemik doku hücreleri için doğal hücre dışı matriksi taklit edebilen uygun doku iskeleleri kullanımı ile biyolojik mikroçevreyi sağlayarak hastalıklı veya hasarlı kemik dokularını iyileştirme stratejisidir. Literatürde; bu konuya yönelik çok sayıda çalışma mevcuttur. Ancak literatürde, yumurtadan elde edilen hidrokoksiapit (HAp), grafen oksit (GO), kitosan (CS) içeren üç bileşenli doku iskelesinin süper kritik jel kurutma işlemiyle üretimi ve üretilen doku iskelesi üzerinde GO'nun toksik etkisinin incelenmesine yönelik bir çalışmaya rastlanılamamıştır. Bu çalışmada, HAp-GO-CS'dan oluşan üç bileşenli doku iskelelerin üretilmesinde kullanılan HAp, kalsiyum kaynağı olan yumurta kabuklarından çöktürme yöntemi ile sentezlenmiştir. Osteokondüktif ajanı olarak kullanılan GO'in sentezi için Geliştirilmiş Hummer yöntemi kullanılmıştır. HAp, GO ve CS çözeltilerinin karıştırılmasıyla hazırlanan doku iskelesi karışımları kalıplanarak dondurulmuştur. Dondurulmuş örneklere su-aseton ikame işlemi uygulandıktan sonra, süperkritik jel kurutma işlemi uygulanarak doku iskeleleri üretilmiştir. GO'in toksik etkisini inceleyebilmek için farklı GO oranlarında üretilen üç bileşenli doku iskeleleri; FTIR, XRD, SEM, TEM, EDS, BET ve TG/DTA analizleri ile karakterize edilmiştir. Üretien doku iskelelerinin mekanik özelliklerini değerlendirmek için Universal Instron Mekanik Test Sistemi kullanılmıştır. Sitotoksisite analizi için doku iskeleleri MTT testine tabi tutulmuştur. MTT analizi ile GO'nun % 1'lik (g/g) orandan fazla kullanılmasının MC3T3-E1 hücreleri üzerinde toksik etkisinin olduğu tespit edilmiştir. Yapılan karakterizasyon çalışmaları ile % 1'lik (g/g) GO oranına sahip HAp-GO(%1)-CS üç bileşenli doku iskelesinin; üç boyutlu gözenekli yapıya, yüksek hücre canlılığına, uygun mekanik özelliklere sahip olduğu belirlenmiştir. Elde edilen bulgulara göre, HAp-GO(%1)-CS bir kompozit olarak üretilen üç bileşenli doku iskelesinin kemik doku mühendisliğindeki uygulamalar için kullanılabilir olduğu sonucuna varılmıştır.

TABLE OF CONTENTS

LIST OF FIGURES

LIST OF TABLES

LIST OF ABBREVIATIONS

3D	Three Dimensional
BET	Brunauer-Emmett-Teller
CP	Calcium Phosphate
CS	Chitosan
DCPD	Dicalcium Phosphate Dehydrate
DCPD	Dicalcium Phosphate Dihydrate
ECM	Extracellular Matrix
EDS	Energy Dispersive X-Ray Spectroscopy
FET	Field Effect Transistor Sensors
FTIR	Fourier Transform Infrared Spectrometer
GAGs	Glycosaminoglycans
GO	Graphene Oxide
HAp	Hydroxyapatite
HIV	Human Immmunodeficiency Virus
LDI-MS	Laser Desorption/Ionization Mass Spectrometry
MCP	Monocalcium Phosphate
MCPH	Monohydrate Calcium Phosphate
MRI	Magnetic Resonance Imaging
MTT	3-(4,5-dimethyl-2-yl)-2,5-diphenyltetrazolium bromide
NAG	N-acetyl D-glucosamine
OCP	Octacalcium Phosphate
rGO	Reduced Graphene Oxide

SC-CO_2	Supercritical Carbon Dioxide
SEM	Scanning Electron Microscope
SERS	Surface Enhanced Raman Scattering
TCP	Tricalcium Phosphate
TEM	Transmission Electron Microscopy
TG/DTA	Thermogravimetric/Differential Thermal Analyzer
UV	Ultraviolet
XRD	X-Ray Powder Diffraction

1. INTRODUCTION

Bone is a large connective tissue, which is responsible for locomotion, support and protection of soft tissues. It has calcium and phosphate reservoir which provides the structural integrity of the body (Florencio-Silva *et al.*, 2015).

Bone tissue is composed of organic components (mainly collagens), water and inorganic nanocrystalline hydroxyapatite (HAp) (Roseti *et al.*, 2017). Collagen has natural binding sites that modulate the adhesion of osteoblasts and fibroblasts. Otherwise, HAp is osteoconductive and it is a source of calcium and phosphate ions for bone tissue cells (Wahl, *et al.*, 2007). While these components are responsible for the mechanical strength and accommodation of bone cells, bone cells are mainly responsible for bone formation and initiating bone remodeling in necessary conditions. Bone cells types and their functions are summarized in Table 1.1.

Table 1.1. Bone cell types and functions

Cell type	**Function**
Osteoblasts	These cells are responsible to synthesize of bone tissue extracellular matrix. They evolve into osteocytes (Bhattacharjee *et al.*, 2017).
Osteocytes	Calcification of the osteoid matrix, blood-calcium homeostasis (Salgado *et al.*, 2004).
Osteoclasts	They are chief constituent for mature bones and they are responsible for release of hydroxloric acid to digest HAp crystals and collagen fibers via proteases at the fracture site.

Remodeling of bone tissue is a cycle organized by osteoblasts, osteocytes and osteoclasts and has three phases; initiation of bone resorption by osteoclasts, the transition from resorption to new bone formation and finally bone formation by osteoblasts. In this way, defected bone is naturally replaced by a new bone (Florencio-Silva *et al.*, 2015).

The worldwide incidence of bone disorders are becoming higher in populations due to the increase of aging rate coupled with increased obesity and poor physical activity. Although, the bone tissue has high capacity of regeneration, complicated large defects cannot regenerate via normal physiological process and require additional treatment to proper regeneration such as intervention in the form of bone grafts.

Conventionally, there are two ways for bone grafting such as autografts and allografts. Autografts are extracted from another site in patients while the allografts are extracted from cadavers and they need to be sterilized (Lan Levengood and Zhang, 2015). Transplantation is another way which is conventionally applied to treat the bone defects. However, it is known that after the transplant, patients are treated with immunosuppressasnts to prevent rejection of the transplanted tissue or organs during the rest of their lives. In this point, the ideal way to overcome this consequence is to use patients own cells or a tissue engineering biomaterials which are capable of the cell growth, differentiation, migration and finally regeneration of the new tissue. Bone tissue engineering strategy, which is associated with the regeneration of diseased or damaged bone tissues by controlling the biological microenvironment using the proper biomaterials, arise as a promising alternative to conventional methods. This strategy can be a way to reduce the long waiting time for organ transplants, minimize the risk of transplant rejection and the necessity for high-risk surgery (Naahidi *et al.*, 2017).

In the present study, the scaffold composed of hydroxyapatite (HAp), graphene oxide (GO) and chitosan (CS) was produced by supercritical gel drying and the toxicity effect of GO was investigated by preparing the scaffolds including various GO ratios. For determination of the physical, chemical and biological properties of the produced scaffolds, the characterization studies were performed. In the following sections; the bone tissue engineering (Chapter 2), HAp (Section 2.3), GO (Section 2.4), CS (Section 2.5) were

explained in detail to enhance the basic approaches of bone tissue engineering and the components used in the present study. The experimental procedure to synthesize the components and produce the scaffolds were explained in Chapter 3. The results of the characterization studies, which were applied for synthesized components and produced scaffolds, were discussed in Chapter 4. According to the results obtained, the major findings of the present study and the recommendations for further studies were given in Chapter 5.

2. BONE TISSUE ENGINEERING

Bone tissue engineering strategy is a complex cascade of steps including cell proliferation, differentiation and synthesis of extracellular matrix (Sivashankari and Prabaharan, 2016). In this strategy, fabrication of scaffolds plays a critical role for the success of the strategy, as a scaffolds pretend to be a natural extracellular matrix (ECM) for bone tissue cells. It contributes to bone regeneration process via seeding of bone tissue cell population into the scaffold in a laboratory culture. These cells attach to proper scaffold which is responsible for accommodation of the cells and growth factor placement in the scaffold-cell complex promotes of the growth of premature tissue. Afterwards; when the premature tissue become a mature tissue for physiologic environment of the defected area, it is surgically transplanted to the area and provide the regeneration of the bone tissue cells (Velasco *et al.,* 2015).

Normal cells in human tissues attach the solid matrix called as ECM, which is usually composed of tissue-specific compounds (Chan and Leong, 2008). The ECM in native tissues consist of cell adhesion proteins (e.g., fibronectin and laminin), structural proteins (e.g., collagen and elastin), and glycans [e.g., glycosaminoglycans (GAGs) and proteoglycans] (Keane and Badylak, 2014). ECM is responsible for providing structural support (e.g., rigidity and elasticity) and physical environment for cells and stimulating them to attach, grow, migrate and respond to the biological signals which are specific for each tissue (Chan and Leong, 2008).

The scaffold typically made of metal, polymeric, and ceramic biomaterials (Venkatesan *et al.,* 2015a) and it acts as a natural ECM in defected site. Mainly, it provides a biological environment to the cells and promote them to bone regeneration (Wahl *et al.*, 2007). An ideal scaffold should be biocompatible, biodegradable and it should promotes cell adhesion and proliferation and maintains the metabolic activity of the cells (Sivashankari and Prabaharan, 2016). The design considerations of scaffolds and their brief explanations were represented in Table 2.1 and Table 2.2.

In this respect, manufactured scaffolds must exhibit the analogous functions with ECM which is specific for each tissue. However, the multiple functions, complex composition and the dynamic nature of ECM in native tissues make it difficult to mimic exactly. For this reason, selected biomaterials should possess the similar structure with the natural bone tissue. In addition to the biomaterial selection, the fabrication methods of scaffolds have an importance as much as the biomaterial choice since they affect the mechanical and structural properties of scaffolds and in this way their biological functionality. In Section 2.1 and Section 2.2 scaffold fabrication methods and bone tissue engineering biomaterials are explained, respectively.

Table 2.1. Design parameters of tissue engineered scaffolds (Velasco *et al.*, 2015)

General Design Considerations	**Explanation**
Biofunctionality	This term refers to interaction between the tissue engineering materials and host cells.
Biocompatibility	It is term used for appropriate host response to the biomaterial. When the biomaterial is transplanted to the defected area, it should not be toxic or cause to any immunological rejection.
Biodegradability	It is degradation ability of the biomaterials with time in physiological environment and degradation rate of the material should be ideal for growth rate of the cells during the healing or regeneration process. Additionally, as the biomaterial, the degradation materials should also be non-toxic.
Mechanical compatibility	This property is related with the compatibility in terms of elastic modulus, tensile strength, fracture toughness, fatigue, and elongation percentage of biomaterials. These properties should be as close as possible as to the replaced tissue.
Pore size and porosity	Natural extracellular matrix are porous to allow the mass transfer of oxygen, nutrients, and waste metabolic products within the structure. For this reason scaffolds should mimic the similar microenvironment for cell proliferation and differentiation.

Table 2.2. Design parameters of bone tissue engineered scaffolds (Velasco *et al.,* 2015)

Bone Tissue Engineering Specific Design Considerations	**Explanation**
Osteoconductivity	It is defined as an ability of the biomaterials for bone cells adhesion, proliferation and formation of ECM on its surface and pores.
Osteoinductivity	It is ability to induce new bone formation.
Osteointegrity	It is ability to form strong bonds with surrounding osseous tissue allowing material continuity and proper transfer load.

2.1. Scaffold Fabrication Methods

The most important part of the scaffold fabrication depends on the complete elimination of the solvent which is used to formation of polymeric solutions. Otherwise, the remains of organic solvents damage the cells and nearby tissues with their toxicity. For this reason, different fabrication methods are used to dry the scaffolds with desired structural properties. These methods can be applied specifically to each scaffolds with taking into consideration of their different properties. It should be noted that these methods are developed to anticipate different desired properties such as; high porosity, fiber like structure and high mechanical properties. Thus, choice of scaffold fabrication is also based on the final desired properties of the scaffold according to its application area.

2.1.1. Freeze Drying

This method is based on the sublimation of solvent which is allowed the preparation of a stable products and it is used to obtain porous scaffolds. The polymer solution is obtained by dissolving the polymer in a solvent with a desired concentration. Afterwards, this solution is frozen and solvent is removed via sublimation because of the applied vacuum and heat conditions. In this way, frozen solvent directly pass from the solid phase to the gas

phase and the scaffolds with high porosity and inter connectivity are fabricated (Subia *et al.,* 2010).

2.1.2. Solvent Casting

This process is inexpensive and highly applicable since it does not require any specific equipment. It is basically depend on the evaporation of the solvent from the casted polymer solution in a mold (Subia *et al.,* 2010).

2.1.3. Particulate Leaching

This method is depend on the dissolving of a porous agent into the polymeric solution and after the washing step removing of the porogen result in a porous structure into the polymeric solution. In this method, generally, salt is used as porous agent to make small pieces of preferred size. The amount of porogen added, the size and shape of the porogen is affected the pore size of the final scaffold (Sughanthy *et al.,* 2015).

2.1.4. Phase Separation

This technique depends on separation of polymeric solution in two phases which one is polymer rich phase and the second one is polymer lean phase. Firstly, the polymer is dissolved in an organic solvents at high temperature and required bioactive materials are added. Then, the formed mixture is treated with decreased temperature which induced the phase separation into polymer rich phase and solvent rich phase. Afterwards, the solvent is removed by extraction, evaporation and sublimation and the porous structure of the scaffold is formed (Subia *et al.,* 2010).

2.1.5. Electrospinning

In this method, the electrostatic force is used to produce the polymeric fibers ranging from nanoscale to microscale (Subia *et al.,* 2010) and it requires the combination of the following equipments; a syringe pump, a high voltage source and a collector (Lu *et al.,*

2013). Basically, the polymer solution is prepared and injected out through the needle and this step results in forming of a drop solution. Then, high voltage applied and this leads to the electric charge on the droplet and this droplet migrate towards the collector. Consequently, droplet elongates to form fiber (Athira *et al.*, 2014).

2.1.6. Three Dimensional (3D) Printing

In this method, 3D-porous scaffolds are designed by a computer aided programs for example; AutoCAD, AutoDesk. After the modelling, the composition of the scaffold materials are loaded into a printer which is capable of spraying the solution layer by layer to form the 3D structure in diverse geometries (Dutta *et al.*, 2017).

2.1.7. Supercritical Gel Drying

A supercritical fluid is obtained once it is exposed to higher temperature and pressure than its critical temperature and pressure points. In this point, fluid exhibits liquid-like densities, gas-like viscosities and diffusivities (Quirk *et al.*, 2004).

Carbon dioxide (CO_2) is often used as a supercritical fluid because of its availability, low toxicity, stability and low cost. Additionally, the critical point conditions of 31°C and 73.8 bar are readily attainable (Quirk *et al.*, 2004). Supercritical carbon dioxide (SC-CO_2) assisted processes include various techniques to form 3D porous scaffolds such as; supercritical foaming, supercritical phase separation, supercritical gel drying and electrospinning in SC-CO_2 (Reverchon and Cardea, 2012).

The general aim of these methods is to improve the weak points of conventional scaffold fabrication methods suffering various limitations. For instance; many of conventional scaffold fabrication methods are not sufficient to produce porous scaffolds with pore connectivity and mechanical resistance. Additionally, many of these methods are only limited to produce thin disks or films and it causes to lack of 3D structure of scaffolds (Reverchon and Cardea, 2012). Another major challenge of the scaffold fabrication is elimination of the liquid solvent from the gel without collapsing porous structure of the

produced scaffolds. SC-CO_2 assisted processes used the characteristic features of SC-CO_2 to control scaffolds morphology and removing of the solvent from the scaffold structure.

Supercritical gel drying method is frequently used to generate 3D scaffolds maintaining the macro and nano structure of the gel due to the fact that it does not cause formation of vapor-liquid transition and surface tensions in the hydrogel pores (García-González *et al.,* 2012). As this method requires a supercritical fluid, SC-CO_2 is the mostly used fluid due to its high affinity with almost all the organic solvents, its low toxicity and availability. In this method, the hydrogel is loaded into a vessel which is connected with the SC-CO_2 flow and when the supercritical conditions of the fluid is reached, the hydrogel is put in contact with continuous flow of SC-CO_2. After a certain process time, the system is depressurized and aerogels (hydrogels are transformed into aerogels when they are contacted with SC-CO_2 flow) are collected from the vessel (García-González *et al.*, 2012).

Although, this process has many advantages when it is compared with other methods, it cannot be directly applied to polymeric hydrogels. The underlying reason of this challenge can be explained with very limited compatibility of SC-CO_2 with water at supercritical conditions of carbon dioxide. Water has limited solubility at the supercritical conditions of CO_2, and this property prevents the affinity of CO_2 with water. For this reason, before the drying procedure, the water inside of the hydrogels should be substituted with an organic solvent such as; acetone or ethanol. In this way, the water is eliminated from the hydrogel and the high affinity of CO_2 with organic solvent provide the completely removal of solvent from the hydrogel and effective drying (Reverchon and Cardea, 2012).

2.2. Bone Tissue Engineering Biomaterials

Biomaterials used for scaffold synthesizing can be broadly classified two main categories depend on the obtaining sources, such as natural and synthetic biomaterials.

Natural biomaterials are obtained from their natural sources and they usually have favorable immune recognition by the recipient, however, their limited physical and mechanical stability make their usage to be difficult in tissue engineering applications. For

this reason, these biomaterials should be recovered by developing composites with synthetic materials (Chan & Leong, 2008). In this way, when composites are formed in tissue engineering applications, deficiency of the signaling functions and mechanical strength are prevented and the scaffolds which are similar as much as the natural ECM are obtained (Keane and Badylak, 2014). Naturally derived polymeric biomaterials were represented in Table 2.3.

Table 2.3. Natural biomaterials classification (Keane and Badylak, 2014)

Naturally Derived Polymeric Biomaterials	
Polysaccharides	**Proteins**
Chitosan	Collagen, Gelatin
Alginate	Elastin
Hyaluronic acid	Fibrin, Silk

Synthetic biomaterials cannot occur naturally and can be classified as metals, ceramics and polymers. The classification of synthetic biomaterials were represented in Table 2.4. Thus, they need to be synthesized via engineering approaches. These type of biomaterials are often preferred in different tissue engineering applications due to their controlled physical and mechanical properties. For this reason, they can be properly used for both soft and hard tissues. However, biocompatibility becomes the major problem for synthetic biomaterials, because cells may have difficulties in attachment and growth on this type of biomaterials (Keane and Badylak, 2014).

Success of tissue engineering applications depend on finding an appropriate scaffold materials that can accommodate biological design variables inherent to each application. For instance, in bone tissue applications, composite materials are preferred due to composite structure of natural bone tissue which is composed of 70 % of inorganic compounds and 30 % of organic compounds (Bhattacharjee *et al.*, 2017). In this way, the scaffolds can become more similar to natural ECM and mechanically more strength.

Table 2.4. Synthetic biomaterials classification (Keane and Badylak, 2014)

Group	Examples
Metals	Titanium, tantalum
Ceramics	Hydroxyapatite, tricalciumphosphate, calcium carbonate
Polymers	Polyesters, Poly(glycolide) (PGA), Poly(lactide) (PLA), Poly(caprolactone) (PCL), Poly(trimethlenecarbonate), Poly(Ether-Ester), Poly(dioxanone) (PDS) Poly(EthyleneGlycol)

In bone tissue engineering, ceramics such as hydroxyapatite, and tricalcium phosphate (TCP) are widely used in bone tissue engineering scaffolds because of their structural similarity with the mineral components in native bone tissue. However, their low mechanical strength and brittleness need them to be combined with naturally or synthetically occurred polymers to produce appropriate scaffolds which have desirable properties.

2.3. Hydroxyapatite

Apatite is the general name used for calcium phosphate (CP) based minerals and has general formula $Ca1_4Ca2_6(MO_4)_6X_2$, where Ca1 and Ca2 are considered as two different calcium ions with respect to their crystallographic positions, MO_4 is designated as phosphate group and X represents the presence of OH^- group in the apatite structure (Akram *et al.*, 2014).

CP based ceramic biomaterials are group of compounds having Ca/P molar ratio in the range of 0.5-2 and they are attractive materials due to their biocompatibility, osteoconductivity and osteointegration. The brief list of important CP-based ceramic materials is given in Table 2.5.

Table 2.5. Brief list of important CP-based ceramic materials (Koutsopoulos, 2002)

Compound	Ca/P Ratio	Formula
Monohydrate Calcium Phosphate (MCPH)	0.50	$Ca(H_2PO_4)_2.H_2O$
Monocalcium Phosphate (MCP)	0.50	$Ca(H_2PO_4)_2$
Dicalcium Phosphate Dihydrate (DCPD)	1.0	$Ca(HPO_4).2H_2O$
Tricalcium Phosphate (TCP)	1.50	α and β $Ca_3(PO_4)_2$
Octacalcium Phosphate (OCP)	1.33	$Ca_4H(PO_4)_3.2.5H_2O$
Hydroxyapatite (HAp)	1.67	$Ca_{10}(PO_4)_6(OH)_2$

Hydroxyapatite (HAp) is one of a CP based biomaterial with a Ca/P molar ratio of 1.67 and it is a principal inorganic constituent of bones and teeth (Koutsopoulos, 2002). Its structural and chemically similarity with mineral portion of bone tissue leads to use it in the biomedical field (Wang *et al.*, 2010). Additionally, among the CP based biomaterials, the hydroxyapatite is the most stable crystalline phase at the temperature, pH and composition of physiological fluids (Sadat-Shojai *et al.*, 2013).

Although, hydroxyapatite is similar to the inorganic component of natural bone, there are differences with respect to the total chemical composition of bone and synthetic hydroxyapatite. For example, biologically synthesized hydroxyapatite is not stoichiometric and it has an atomic ratio Ca/P<1.67 and does not contain only ions and radicals of hydroxyapatite but also traces of carbonate, magnesium, sodium and clor ions (Rivera-Muñoz, 2011). The ratio of Ca/P is also changing with age and when bone ages, the Ca/P ratio increases which means carbonate species increases (Chetty *et al.*, 2012). Additionally, the stoichiometric ratio of Ca/P determines the stability of hydroxyapatite in human body and it becomes more stable and inert for the closer values of Ca/P to 1.67.

2.3.1. Structure and Properties of Hydroxyapatite

Hydroxyapatite has highly crystalline structure and it displays a needle-like morphology (Chetty *et al.*, 2012). Two different calcium ions, Ca1 and Ca2, are located in hydroxyapatite crystal structure: columnar and hexagonal. The four of them are situated in Ca1 position and other six calcium atoms, Ca2, which are coordinated by six oxygen atoms and phosphate groups are also located in these planes (Lee *et al.*, 2015). This crystal structure of hydroxyapatite was represented in Figure 2.1. The hexagonal structure of hydroxyapatite includes two triangles of calcium atoms on two different planes at each corner. Hydroxyl groups are specific for hydroxyapatite structure and they give hydroxyapatite significant properties such as high surface area and good adsorption ability (Lee *et al.*, 2015).

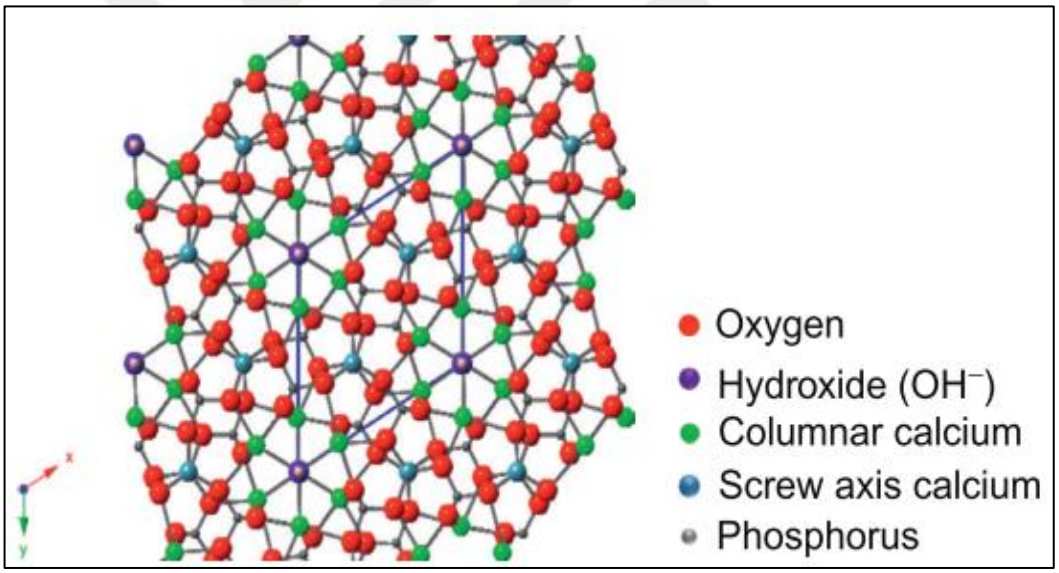

Figure 2.1. Crystalline structure of hydroxyapatite (Lee *et al.*, 2015)

2.3.2. Synthesis of Hydroxyapatite

The synthesis methods and reaction parameters have an impact on the HAp morphology, particle size and crystallinity. For instance, at higher pH values (pH>9) the reaction product is usually HAp and other calcium based products cannot be found in the reaction medium. Additionally, at acidic pH level, the products have larger particle size (Sadat-Shojai *et al.*, 2013).

Hydroxyapatite powders can be synthesized via different methods and these methods are classified into three different categories; dry methods, wet methods and high temperature processes (Sadat-Shojai *et al.*, 2013). These methods and their subgroups are listed in Table 2.6. The basic idea behind the production process is to choose the best way to obtain hydroxyapatite particles with desirable properties. High specific surface area, fine grain size and size distribution including small in particle agglomeration can be given as examples for the desirable properties.

Table 2.6. Hydroxyapatite synthesis methods (Sadat-Shojai *et al.*, 2013)

Method	**Subgroups**
Dry methods	Solid-state method Mechanochemical method
Wet methods	Chemical precipitation Hydrolysis method Sol-gel method Hydrothermal method
High temperature processes	Combustion method Pyrolysis method Synthesis methods based on biogenic sources

In dry methods, solvent is not used and synthesized HAp powders are generally large in size and irregular in shape. These methods are suitable for mass production of HAp since the process parameters do not have strong effect on the HAp powders (Sadat-Shojai *et al.*, 2013).

Calcium and potassium containing chemicals are used as precursors for the HAp in solid-state reaction and in a typical method precursors are first grinded and then calcined in high temperatures to obtain HAp powders in high crystallinity. The limited diffusion of ions during the reaction leads to develop of the mechanochemical method as an alternative

approach. This method includes mixing dry powders of calcium and potassium precursors and they are dry-milled at various rotation speeds (Chetty *et al.*, 2012). Hydroxyapatite properties are affected by milling medium, the type and diameter of the milling balls, type of reagents, the duration of the milling steps and rotational speed (Sadat-Shojai *et al.*, 2013).

The hydroxyapatite can be synthesized in nanosized structure with a regular morphology via wet methods. These methods allow to control of the morphology and the mean size of the final product. In these methods, low temperature is required to prepare hydroxyapatite powders. Despite the outcoming properties of these methods, the resulting powder usually has lower crystallinity than the powders produced by dry methods (Sadat-Shojai *et al.*, 2013).

The wet chemical precipitation route is the most common route because of the superiority of the reaction conditions such as; low working temperature, high percentages of pure products and inexpensive equipment requirement (Monmaturapoj, 2008). Precipitation method involves a reaction between orthophosphoric acid and dilute calcium hydroxide at pH 9 (Chetty *et al.*, 2012). The reaction can be written as following;

$$10\mathrm{Ca(OH)_2} + 6\mathrm{H_3PO_4} \rightarrow \mathrm{Ca_{10}(PO_4)_6(OH)_2} + 18\mathrm{H_2O} \qquad (2.1)$$

In the precipitation method; reactant addition rate and reaction temperature have an effect on the hydroxyapatite nanoparticles structure such as; shape, size and specific surface area. The purity of the synthesized hydroxyapatite is directly associated with the reactant addition rate. It is also linked to the pH obtained at the end of the synthesis and the suspension stabilization. The basic steps of this method are precipitation reaction, washing, filtering, drying and calcination. The pH value of the reaction can be adjusted using ammonium hydroxide (Sadat-Shojai *et al.*, 2013).

HAp can be also synthesized by hydrolysis of other CP based ceramic materials such as: dicalcium phosphate dehydrate (DCPD) and tricalcium phosphate (TCP). The hydrolysis of CP based bioceramics can be achieved by dissolution and precipitation processes (Sadat-Shojai *et al.*, 2013).

In sol-gel method, the solid particles are dissolved in aqueous or an organic phase and aged at room temperature and afterward the steps of gelation, drying and calcination are applied, respectively. In this method, reaction between calcium and phosphorus precursors is carried out slowly with longer aging time. The insufficient aging, uncontrolled gelation and heat treatment can lead to formation of various impurities. A general reaction of sol-gel method can be written like following (Sadat-Shojai *et al.*, 2013);

$$6Ca(NO_3)_2 + 6(C_2H_5O)_3P(O) \rightarrow Ca_{10}(PO_4)_6(OH)_2 + \text{byproducts} \quad (2.2)$$

The brief representation of sol-gel method can be seen in Figure 2.2 (Sadat-Shojai *et al.*, 2013).

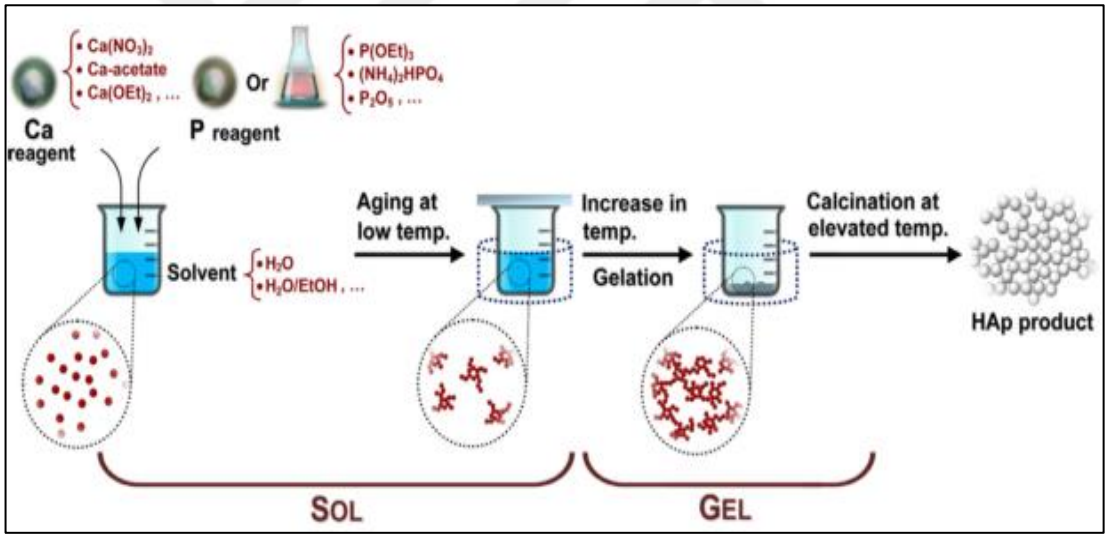

Figure 2.2. Preparation of HAp via sol-gel method (Sadat-Shojai *et al.*, 2013)

In hydrothermal method; very high temperatures are used to synthesize HAp via reaction between the calcium and phosphate solutions. Calcium chloride, calcium carbonate, calcium hydroxide and calcium nitrate materials can be used as calcium precursors and calcium hydrogen phosphate and dipotassium and diammonium hydrogen phosphates can be used as phosphate precursors. The following reaction is carried out in the temperature range of 60-250°C for 24 hour to produce crystalline HAp crystals (Chetty *et al.*, 2012).

$$4Ca(OH)_2 + 6CaHPO_4.2H_2O \rightarrow Ca_{10}(PO_4)_6(OH)_2 + 18H_2O \quad (2.3)$$

In this way, hydrothermal method can be considered as a chemical precipitation in which the aging step is conducted at a high temperature (Sadat-Shojai *et al.*, 2013).

High temperature processes are associated with burning or partially burning the precursors in elevated temperature, and this process can be explained in two different approach: combustion and pyrolysis.

The combustion method mainly involves the mixing of the aqueous stock solutions of $Ca(NO_3)_2$ and $(NH_4)_2HPO_4$ and adding concentrated HNO_3 to obtain homogen white solution. Afterwards, the reaction medium is heated at a fairly low temperature but suddenly the temperature is increased which leads to combustion and final step is cooling of the products.

In pyrolysis method, precursor solution is sprayed into a flame or hot zone of electric furnace using an ultrasonic generator. The final products are collected in agglomerated form (Sadat-Shojai *et al.*, 2013).

Hydroxyapatite can be derived from biogenic sources with different chemical procedures. To synthesize hydroxyapatite from biogenic sources, different steps are required in respect to source types. However, the main idea underlying the synthesis of HAp is to obtain calcium precursors to perform a reaction with the phosphate precursors. HAp can be synthesized by utilizing the eggshells waste or exoskeleton of marine organisms and extracted by bovine bones of fish scales (Sadat-Shojai *et al.*, 2013). Additionally, the common step for all of these synthesis methods is thermal treatment (calcination) of sources to obtain calcium precursor. The next steps can be carried out by any HAp synthesis strategies.

2.3.3. Biomedical Applications of Hydroxyapatite

Hydroxyapatite is commonly preferred for tissue engineering applications and drug delivery systems due to its excellent biocompatibility and bioactivity. Generally, hydroxyapatite is firstly calcined, which is the way for treatment of hydroxyapatite to remove impurities and volatiles from the material at high temperature in air medium, for medical applications. This treatment provides pure phase of hydroxyapatite with high crystallinity degree. The parameters in calcination process such as; temperature and soaking time have directly impact on the physical and mechanical properties of hydroxyapatite (Chetty *et al.*, 2012).

HAp materials can be used as a carrier for drug/protein delivery due to their excellent biocompatibility, easily tuneable physical-chemical properties (e.g., size, morphology, porous structure and surface composition), low toxicity, low production cost, excellent storage stability and pH-dependent dissolution (Lin and Chang, 2015).

The pH-dependent dissolution is the attractive feature for drug delivery systems. The degradation rate of HAp increases when the pH value of the medium is changed from alkaline to acidic conditions. This accelerates the release of the drug molecules from the HAp surfaces. While the normal cells have pH value of 7.4, pH value of ECM environment of solid tumors is observed around 5. This pH difference enables a preferential active drug release from HAp surface in a pH-dependent way in the tumor region (Lin and Chang, 2015).

Important properties that enable the hydroxyapatite to be useful material in tissue engineering applications area are; its bioactivity which means that it stimulates a specific biological reaction at material-tissue interface, biocompatibility, osteoconduction and osteointegration. It is also known that hydroxyapatite supports osteoblastic cell adhesion, growth and differentiation.

Despite the significant properties, weak mechanical properties of hydroxyapatite specifically brittles, low tensile strength and poor impact resistance restrict the unique usage of hydroxyapatite in bone tissue engineering applications (Cengiz *et al.,* 2008). To improve

the mechanical properties of hydroxyapatite, the reinforcement with various fillers such as ceramics, polymers, metals and inorganics are applied. In this way, hydroxyapatite mechanical strength could be increased (Chetty *et al.*, 2012) and used in bone tissue engineering applications due to its similarity with natural bone tissue ECM.

2.4. Graphene Oxide

Graphene oxide (GO) is defined as single-atomic-layered material composed of carbon, hydrogen, and oxygen molecules, and produced by the oxidation of graphite crystals (Ray, 2014). The graphene skeleton and oxygen containing functional groups located in the GO structure enable it to exhibit the fascinating chemical, optical and electrical properties.

Graphite is oxidized with strong oxidizing agents and oxygen containing functional groups are joined to the graphite structure and the hydrophilic structure of graphite oxide is formed. This property provides the exfoliation of graphite oxide in water using the sonication and single layer graphene oxide is produced (Ray, 2015). The oxygen functionalities can be considered as defects, which lead to the conversion of electrically conductive graphene into an insulator because of the disruption of its sp^2 bonding networks (Dimiev and Eigler, 2016).

The thermal or electrochemical reduction of GO is used to partially recovering process of the electrical conductivity and this process results in the formation of the graphene-like sheets that is called as reduced graphene oxide (rGO) (Chowdhury and Balasubramanian, 2014). In this way, the oxygen containing groups are removed and a transitional material, rGO, between graphene and GO offering the solubility and the partial recovery of the electrical properties is occurred (Pei and Cheng, 2011).

On the other hand, these functional groups can provide potential advantages of using GO in different applications. For instance; GO has good dispersibility in many solvents, particularly in water, and the resulting GO-stable dispersion can be deposited on various substrates in order to prepare thin conductive films (Chen *et al.*, 2004). These functional groups also give a chance to produce other graphene based materials for different applications (Guerrero-Contreras and Caballero-Briones, 2015).

2.4.1. Chemical Structure of Graphene Oxide

Although the precise structure of GO is still unknown due to its complexity and nonstoichiometric atomic composition, there are different suggestions about the chemical structure of the GO.

On a simple level, GO consists of individual sheets of graphene decorated with oxygen functional groups on both the basal planes and edges. The functional groups introduced into the graphite powders have been identified as mostly in the form of hydroxyl and epoxy groups on the basal plane with smaller amounts of carboxy, carbonyl, phenol, lactone at the sheet of edges (Chen, Feng and Li, 2004).

The earliest studies about the GO chemical structure is given by Hoffman (1947) and Ruess (1934) as stated in the study performed by (Guerrero-Contreras and Caballero-Briones, 2015). Hoffman suggested that 1, 2-epoxies is spread across the basal planes of graphite. The proposed chemical structure of graphene oxide according to this model can be seen in Figure 2.4.

Ruess's model reported that the basal plane structure is mainly composed of the sp^3 hybridized system rather than the sp^2 hybridized model of Hofmann (Dreyer *et al.,* 2015). The proposed chemical structure of graphene oxide according to these models can be seen in Figure 2.4.

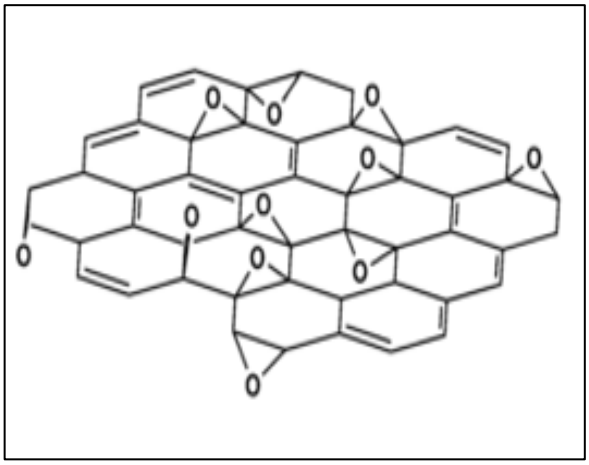

Figure 2.3. The chemical structure of GO suggested by Hoffman (Dreyer *et al.*, 2015)

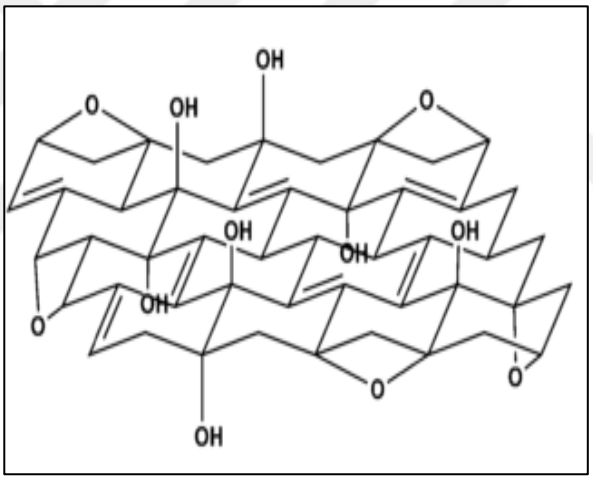

Figure 2.4. The chemical structure model of GO suggested by Ruess (Dreyer *et al.*, 2015)

The final and the widely accepted model is called as Lerf-Klinowski model and it focuses on a nonstoichiometric, amorphous alternative. This model reports the decoration of the carbon basal plane with epoxides and hydroxyls, with sheet edges terminated by carboxylic acid functional groups (Figure 2.5). In addition, the distribution of functional groups in every oxidized aromatic ring need not be identical, and both the oxidized rings and aromatic entities are distributed randomly (Lerf *et al.*, 1998).

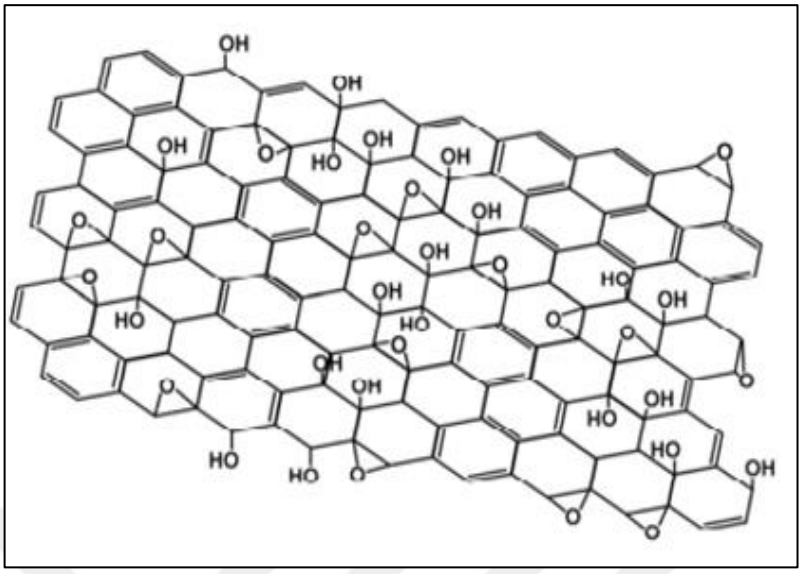

Figure 2.5. The chemical structure of GO according to the Lerf–Klinowski model (Chowdhury and Balasubramanian, 2014)

2.4.2. Synthesis of Graphene Oxide

GO is synthesized via the oxidation of graphite in acid solution with oxidizing agents. It is quantified by the C:O ratio and dependent upon the oxidation ratio and also the length of the oxidation reaction (Compton and Nguyen, 2010). This ratio affects the structural properties of graphene oxide such as; exfoliation level, number of layers, sheet size, number of defects (Guerrero-Contreras and Caballero-Briones, 2015).

GO can be produced by three main methods depending on the oxidation agent and acidic medium; Brodie's method, Staudenmaier's method and Hummers method or by a variation of the latter one, namely, Modified Hummers Method or Improved Hummers Method (Dimiev and Eigler, 2017). Basically, in the Brodie and Staudenmair methods, combination of potassium chlorate with nitric acid is used to oxidize graphite, while in the Hummers method treatment of graphite is achieved with potassium permanganate and sulfuric acid (Chowdhury and Balasubramanian, 2014). The summary of oxidants and toxicity conditions of each methods can be seen in Table 2.7.

Table 2.7. Synthesis methods of graphene oxide (Lavin-Lopez *et al.*, 2016)

Method Name	**Oxidants**	**Toxicity**
Brodie Method	$KClO_3$, HNO_3	Yes
Staudenmaier Method	$KClO_3$, HNO_3, H_2SO_4	Yes
Hummers Method	$KMnO_4$, H_2SO_4, $NaNO_3$	No
Improved Hummers Method	$KMnO_4$, H_2SO_4, H_3PO_4	No

Toxicity of Brodie and Staudenmaier methods is directly associated with the ClO_2 gas formation in the reaction medium and it must be handled with caution. The Hummers method has relatively shorter reaction time than the Brodie and Staudenmaier method and it is superior to them in terms of toxicity due to the absence of the ClO_2 gas. On the other hand, one drawback of this method is the potential contamination by excess permanganate ions which must be removed by treatment with H_2O_2 (Compton and Nguyen, 2010).

In Brodie method, ratio of 1:3 of graphite and potassium chlorate ($KClO_3$) is mixed and reacted with fuming nitric acid (HNO_3) in 3 or 4 days with 60^oC (Zaaba *et al.*, 2017). However, this method is not effective because it is not complete in one step and in one vessel. (Dimiev and Eigler, 2017).

Staudenmaier improved Brodie's procedure by using concentrated sulfuric acid and fuming sulfuric acid mixture. The chlorate is gradually added to this acid mixture. This method is slightly different from the Brodie's method and provides a practical way to be performed the reaction in one vessel (Zaaba *et al.*, 2017).

Because of the hazardous effects of both methods, there should be new and more effective methods to obtain graphene oxide and Hummers & Offeman developed an alternative method to synthesize of graphene oxide. This new method is called as Hummers method, and currently, it or its derivatives are used to synthesize graphene oxide.

In Hummers method, graphite is oxidized with a concentrated water free sulfuric acid, potassium permanganate and sodium nitrate mixture (Khan *et al.,* 2016). Potassium permanganate is used instead of potassium chlorate to avoid spontaneous explosion during oxidation process and sodium nitrate is replaced to fuming nitric acid to eliminate fog acid produced (Dimiev and Eigler, 2017). After the oxidation reactions, the graphite oxide is exfoliated in water by sonication and GO sheets are formed in water (Phiri *et al.,* 2017).

Marcano *et al.* (2010) reported a new method to synthesize the graphene oxide. In this method (Improved Hummers Method), sodium nitrate was excluded and amount of potassium permanganate ($KMnO_4$) was increased. The oxidation reaction of graphite was performed with $KMnO_4$ in a mixture of H_2SO_4/H_3PO_4 (9:1) and it produced GO with higher extent of oxidation (Marcano *et al.,* 2010). Absence of toxic gases (NO_2, ClO_2, and N_2O_4) in the reaction medium is one of the advantages of this procedure. In addition, this method does not involve a large exothermic reactions and it can be used for large scale production of graphene oxide.

2.4.3. Properties of Graphene Oxide

GO exhibits various excellent properties which make it preferable material in different applications, because of the existence of oxygenated functional groups. Graphene oxide can be evaluated in terms of physical, mechanical, electronic and reactivity properties.

GO can be easily dispersed in the water because of its hydrophilic structure. In addition, GO is dispersed in all solvents excluding dichloromethane, n-hexane and to a smaller extent in o-xylene and methanol (Khan *et al.*, 2016). The mechanical properties of GO is significantly lower than the pure graphene, the comparation of main properties of graphene, graphene oxide and reduced graphene oxide was given in Table 2.8. Electronic properties of GO is directly depend upon the degree of sp^3 carbon fraction thus, the intrinsic insulating nature of GO is strongly correlated to the amount of sp^3 C-O bonding (Chen *et al*., 2015).

Table 2.8. Overview of main properties of graphene based nanomaterials (Perreault *et al.*, 2015)

Properties	**Graphene**	**Graphene Oxide**	**Reduced Graphene Oxide**
Synthesis	Chemical vapor deposition Thermal decomposing of SiC Graphite exfoliation	Oxidation and exfoliation of graphite	Reduction of graphene oxide
C:O ratio	No oxygen	2-4	8-246
Young's modulus (TPa)	1	0.2	0.25
Electron mobility ($cm^2\ V^{-1}\ s^{-1}$)	10000-50000	insulator	0.05-200
Production cost	High	Low	Low

The chemical and physical properties of GO can be manipulated by chemical functionalization method (Boukhvalov and Katsnelson, 2009). The functional groups located on GO are used as sites for the functionalization. Non-covalent and covalent functionalization principles can be used to functionalize GO. The covalent functionalization is depend on the chemical bonds formed between the GO and additive substances while the non-covalent functionalization involves mainly π-π interactions, van der Waals forces, hydrogen bonding, ionic interactions to improve the performance of GO in various applications.

Various functionalization agents are used such as; biomolecules, drugs and polymers, depending on the target applications in the fields of environment science, catalysis, biosensors, biomedicine, green chemistry (Georgakilas *et al.*, 2016).

2.4.4. Applications of Graphene Oxide

The application areas of GO should be handled into different categories due to the wide application area of GO and these areas can be classified as energy and environment, biomedical and electronic devices. In this section, the biomedical applications of GO were explained in details.

Energy and environment applications: GO is used in energy conversion, storage and environmental protection applications and these applications were represented in Table 2.9. The applications of GO in energy conversion and storage is based on the electronic properties of the GO, while the applications of GO in environmental protection is based on the adsorption ability of the GO.

Table 2.9. Overview of energy and environment applications of GO (Li *et al.,* 2015)

Applications of GO in energy conversion and storage	**Applications of GO in environmental protection**
Photocatalytic water splitting Hydrogen storage Lithium batteries and Supercapacitors	Management of harmful gases Water purification

Biomedical Applications: GO is considered as a promising material for biological applications due to its excellent aqueous processability, amphiphilicity, surface functionalization capability, surface enhanced Raman scattering (SERS), and fluorescence quenching ability *(Nandae et al.,* 2015). The biomedical applications of GO can be given as; biosensors, bioimaging, drug and gene delivery, phototherapy and tissue engineering.

Biosensors are used to accurate detection of the biomolecules to diagnosis and GO is used to construct various biosensors because of its high sensitivity, low cost, quick response and easy operation.

The fluorescent feature of the GO provide the using of it in construction of fluorescent-based biosensors. These type of biosensors are mainly used for the detection of DNA and proteins corresponding to HIV (Human Immmunodeficiency Virus) (Ray, 2015). The underlying mechanism of this detection can be explained by the strong binding ability of GO with biomolecules through π-π stacking and/or hydrogen bonding (Lee *et al.*, 2016).

GO is can be used for biomolecule detection, signal amplification, enzyme assay in different detection technique such as Field Effect Transistor Sensors (FET) and Laser Desorption/Ionization Mass Spectrometry (LDI-MS) (Lee *et al.*, 2016).

GO is used for magnetic resonance imaging (MRI) in biomedical applications due to its high light transmittance, photoluminescence and high charge mobility (Nanda *et al.*, 2015).

GO is capable of loading of drugs or genes via chemical conjugation or physisorption approaches thanks to its excellent biocompatibility and physiological solubility and stability (Nanda *et al.*, 2015). However, due to its solubility in water, it can aggregate in the presence of salts and components of serum. Thus, it is often chemically modified to improve its bioavailability, which includes either non-covalent (electrostatic or π–π interactions) or covalent modification (Dimiev and Eigler, 2017).

Phototherapy includes photothermal therapy and photodynamic therapy and it is able to control disease by specific light irradiation (Yang *et al.*, 2013). These technologies are promising approaches with the capability to destroy cancer cells and they have an advantage, when they compared with the conventional cancer therapies, in terms of their selectivity and ability to kill cancer cells specifically on tumor sites without undesirable side-effects (Goenka *et al.*, 2014).

Disease-causing cells including cancer cells in tumors and bacteria in wounds are loaded with a reagent which absorbs near-infrared (NIR) light in photothermal therapy. NIR is responsible to heat up the system and includes hyperthermia and thereby causes cell death.

GO is suitable for this method since it absorbs light in the NIR range (Dimiev and Eigler, 2017).

The critical properties of biomaterials can be enhanced by additive materials having good bioactivity and high tensile strength. It was found that GO based composites exhibits significant improvements in cell adhesion, differentiation and proliferation (Goenka *et al.*, 2014).

2.5. Chitosan

Chitosan is a naturally occurring cationic biopolymer, which is structurally similar to the major component of the ECM called as glycosaminoglycans (Bedian *et al.*, 2017). It is composed of N-acetyl D-glucosamine (NAG) and D-glucosamine components, and it can be derived from chemical or enzymatic partial deacetylation of chitin, which is produced from the exoskeleton of crustaceans (Venkatesan *et al.*, 2015b).

Chitosan is chemically organized by linear structure consisting of β(1-4) glycosidic bonds linked to D-glucoasmine residues with a variable number of randomly located N-acetyl-D-glucosamine groups (Saravanan *et al.*, 2016). The chemical structure of chitin and chitosan were represented in Figure 2.6.

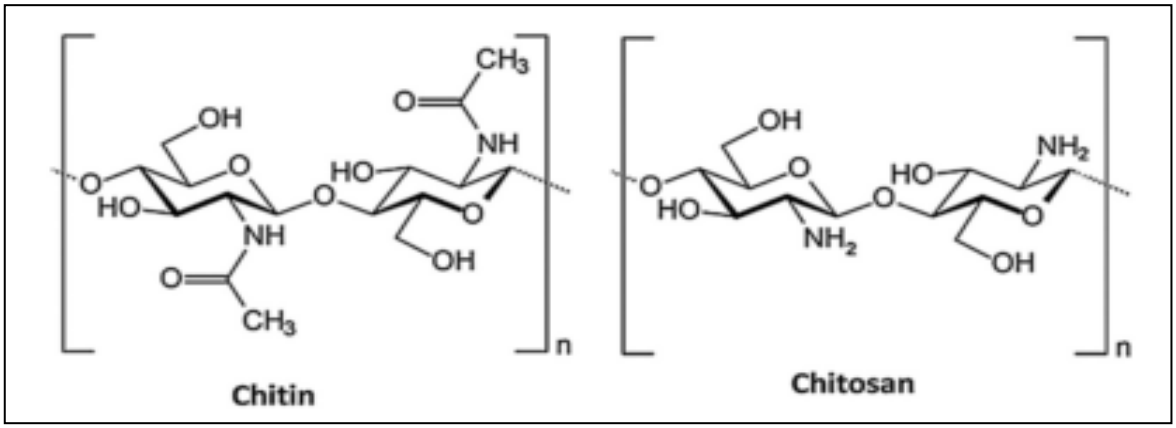

Figure 2.6. Chemical structures of chitin and chitosan (Logithkumar *et al.*, 2016)

2.5.1. Synthesis of Chitosan

Chitosan is derived from the chitin which is the secondly abundant biopolymer in the world. Although chitin is also biocompatible, bioactive and biodegradable, its poor solubility limits its usage. For this reason, chitin is converted into the chitosan via enzymatic or chemical processes.

Shells of crustaceans such as crabs, prawns, lobsters and shrimps are the source of the chitin and these sources are used as industrial sources for the large-scale production of chitin (Islam *et al.*, 2016). Currently, chitin is extracted from marine shell waste streams in large-scale usually using chemical methods. Then, the smaller size of shells are obtained and the mineral components (calcium carbonate) are removed by the hydrochloric acid treatment. This step is called demineralization. The next step is associated with the extraction of protein from the residual protein, and it is performed by treatment with dilute aqueous sodium hydroxide. Final step to obtain chitin product is discoloration performed by treatment with an alkaline solution (Muxika *et al.,* 2017).

Finally, the deacetylation of the chitin is carried out in sodium hydroxide solution at higher temperature for 1-3 h in absence of oxygen. In this way, the acetyl groups of chitin are removed, and the final amount of free amine groups ($-NH_2$) are determined. The deacetylation degree is directly based on sodium hydroxide concentration, the reaction temperature and time. This deacetylation degree can be different based on the production method and resources used, and the solubility of the chitosan is directly affected by this degree. For instance, at least 85% deacetylation degree is required for good solubility of chitosan (Islam *et al.,* 2016).

2.5.2. Physicochemical Properties of Chitosan

The physicochemical properties of chitosan determining the chitosan behavior in different applications can be given as pH dependence and solubility, degree of deacetylation and molecular weight.

The solubility of chitosan depends on the distribution of free amino and N-acetyl groups. In diluted acid solutions, free amino groups are protonated and confer a polycationic behavior and the molecule becomes soluble. Chitosan which have low deacetylation degree; is soluble at the pH=9.0 and upper, in contrast, chitosan which have high deacetylation degree; is soluble at the pH=6.5 and under. Depending on this property, drug delivery system is improved by using chitosan (Rodríguez-Vázquez *et al.,* 2015).

The degree of deacetylation is defined as the molar ratio of the D-glucosamine units to the sum of both NAG and D-glucosamine units (Logithkumar *et al.,* 2016).

Deacetylation is defined as a removing of the acetyl group in different processes and the chitosan should have at least 60 or 70% of deacetylation degree. The degree of deacetylation determines some physical and chemical properties such as solubility limit in acid solutions, molecular weight and mechanical properties. The higher degree of deacetylation result in higher percentage of positively charged primary amines and an overall higher charge density (Levengood and Zhang, 2014).

The deacetylation degree of chitosan has an effect on cell adhesion and proliferation. For instance, the lower deacetylation degree of chitosan leads to lower cell adhesion (Rodríguez-Vázquez *et al.*, 2015). Additionally, the degree of deacetylation inversely affects the chitosan degradation rate, for instance; the higher degree of deacetylation corresponds with lower degradation rate (Levengood and Zhang, 2014).

Molecular weight of chitosan can change depending on where and how the synthesis of chitosan is done and ranges from 300 to 1000 kDa. Both of the molecular weight and deacetylation degree have direct effect on the biodegradation rate of chitosan in vitro and as well as in vivo system. For instance; the greater molecular weight leads to delay of the degradation process (Rodríguez-Vázquez *et al.*, 2015).

2.5.3. Biological Properties of Chitosan

The biological properties of chitosan can be sorted as its strong antibacterial effect, biocompatibility, non-toxicity and water adsorption capacity. Majority of these properties are affected by the physicochemical properties of the chitosan. The hydrophilic structure and cationic behavior of chitosan provide the osteogenetic adhesion and proliferation. In this way, chitosan takes place in many biomedical applications.

2.5.4. Biomedical Applications of Chitosan

Chitosan offers several advantages in biomedical applications due to its biocompatibility, biodegradability properties and the main applications of chitosan can be classified into three categories such as drug delivery, wound healing, tissue engineering.

Chitosan is used as a drug delivery material due to its unique properties such as hydrophilic character and permeation enhancing. The drug delivery system is developed for the carrying of the drug to the target location. Then, drug gains the ability to reach the target location and take action in there.

The major problem comes up in the wound healing applications is the antibacterial resistance of the microorganisms, and this caused to develop the new antibacterial to prevent the tissue from the injection. In this field, chitosan is utilized as a wound healing material for the treatment of deep burns or wounds due to its antibacterial properties (Jayakumar *et al.*, 2010).

Chitosan is a promising material to produce of the tissue engineering scaffolds due to its excellent biological properties. Production of chitosan in various forms like sponges, fibers, films was resulted in increase on the usage of the chitosan in tissue engineering applications.

The structural functional groups give chitosan desirable properties such as biocompatibility, biodegradability and nontoxicity for bone tissue engineering applications. In addition to these properties, hydrophilic surface of chitosan which is capable of the enhancing osteoblast adhesion, proliferation and differentiation and mineralization have an importance (Saravanan *et al.,* 2016).

The cationic nature of chitosan is another important property for bone tissue engineering applications since it provides the formation of polyelectrolyte complexes with anionic biological macromolecules such as glycosaminoglycans. In bone regeneration, chitosan association with glycosaminoglycans plays a critical role in utilizing growth factors to aid in bone formation (Levengood and Zhang, 2014).

Although, chitosan has most of the desirable properties required in tissue engineering applications, however, chitosan has a disadvantage in terms of its mechanical properties since it is very stiff and brittle. To improve its low mechanical resistance, crosslinking agents are used, or different biomaterials are reinforced to chitosan structure (Rodríguez-Vázquez *et al.,* 2015).

2.6. Reported Studies on Three-Component Scaffolds

Multicomponent porous scaffolds have gained an attention due to the fact that their ability to mimic the natural bone tissue properties. In this field, naturally derived components and chemically synthesized components are composed to obtain required properties for scaffolds such as; porous structure, high mechanical strength, providing an environment to host cells and promote them to proliferation and differentiation. In various studies, it was proved that three-component scaffolds have better compatibility with natural bone tissue since it has composite structure made from inorganic and organic materials.

In recently, various components have been combined with Hydroxyapatite-Chitosan composite scaffolds to achieve the desired properties of the bone tissue engineering scaffolds. These components are: zein (Shahbazarab *et al.*, 2018), silica (Dong *et al.*, 2018), dextran (El-Meliegy *et al.*, 2018), reduced graphene oxide (Yu *et al.*, 2017), gelatin-alginate

(Sharma *et al.*, 2016), β-tricalciumphosphate (β-TCP) (Shavandi *et al.*, 2015), alginate (Kim *et al.*, 2015), graphene oxide (Mohandes and Salavati-Niasari, 2014), collagen (Pallela *et al.*, 2012), chondroitin sulphate (Venkatesan *et al.*, 2012), amylopectin (Venkatesan *et al.*, 2012) and carbon nanotube (Venkatesan *et al.*, 2011).

In the present study, three-component scaffolds composed of HAp-GO-CS were produced by supercritical gel drying and the toxicity effect of GO was investigated by preparing the scaffolds including various GO ratios. The scaffolds were prepared by blending of the solutions of HAp, GO and CS, and this scaffold mixture was molded and freezed. After the water-acetone substitution step, the supercritical gel drying procedure was applied. To the best of our knowledge, this is the first report on the production of three-component scaffold, which composed of hydroxyapatite (HAp) derived from eggshells, graphene oxide (GO), chitosan (CS), by using the supercritical gel drying method, and also the examination of the possible toxicity effects of GO additions. The results showed that produced scaffold, which includes 60% of HAp, 1% of GO, 39% of CS, had essential properties such as; 3D porous structure, highest cell viability and reasonable mechanical properties for the requirements for bone tissue engineering materials.

Shahbazarab *et al.* (2018) prepared the scaffold composed of zein (ZN), chitosan (CS) and nanohydroxyapatite (nHAp) in different inorganic/organic weight ratios. In this study, the hydroxyapatite was synthesized via high temperature processing using the $Ca(NO_3)_2 \cdot 4H_2O$ and $(NH_4)_2HPO_4$ as calcium and phosphate precursor, respectively. The ZN solution was prepared with dissolving the ZN into the alcohol, and then chitosan solution was transferred to this solution. Afterwards, the hydroxyapatite was added to the ZN-CS solution and stirred for 24 h. The glutaraldehyde solution (0.25% (v/v)) was added to the resultant mixture and stirred additional 2 h. The final solution was transferred to 24 well-plates and frozen at −20ºC for 12 h; this was followed by freeze-drying at −80ºC for 48 h, and it was then stored for further use. The scaffolds were prepared in different weight ratios of ZN, CS and Hap, and the effect of each component on the scaffold properties were investigated. According to the results, it was suggested that ZN/CS/nHAp porous scaffolds would be used as a suitable template for bone regeneration.

Dong *et al.* (2018) studied to produce the bioactive hydroxyapatite-chitosan-silica hybrid scaffolds via combining of the sol-gel and 3D plotting technique. In this study, the plotting pastes using for the 3D plotting were prepared by the sol-gel process. In this step, appropriate amount of Ca $(NO_3)_2$ (dissolved in acetic acid solution) and H_3PO_4 were added into the prepared chitosan solution, then the formation of HAp was achieved simultaneously. The tetraethyl orthosilicate (TEOS) was used as a silica gel precursor, and then silica solution was added to the chitosan-hydroxyapatite solution. After being mixed, the hybrid solution was loaded into plotting cartridges and allowed to gel for 48 h. The design of the scaffold was performed by CAD software and manufactured in a layer by layer manner. The prepared scaffold was dried at 40°C for future use. This study showed that the synthesized scaffold possessed interconnected pores, biocompatibility and adequate mechanical strength.

El-Meliegy *et al.* (2018) used HAp as an incorporated material into the polymer matrix Dextran/Chitosan to obtain a composite scaffold by freeze drying technique. In this study, the HAp was synthesized using the calcium nitrate tetrahydrate ($Ca(NO_3)_2 \cdot 4H_2O$) and di-ammonium hydrogen orthophosphate ($(NH_4)2HPO_4$). The HAp powder was added with different proportions into a dextran-chitosan aqueous solution, and this solution was stirred overnight at room temperature. Afterwards, the mixture was molded, frozen and lyophilized in a freeze-dryer at -90 °C for 48 h to achieve porous scaffolds. The produced scaffolds had 0.2-0.9 MPa compressive strength values depending on the proportion of the HAp. This study revealed that the produced scaffolds had desirable properties to anticipate the essential requirements for bone tissue engineer materials.

Yu *et al.* (2017) reported high strength composite hydrogel composed of HAp, GO and chitosan. In this study; GO, HAp and chitosan self-assembled into a 3-dimensional hydrogel with the assistance of crosslinking agent genipin (GNP) for CS and reducing agent sodium ascorbate (NaVC) for GO simultaneously. In this study, the GO was synthesized via Hummers method and HAp was purchased. The composite hydrogel showed the desirable features for bone tissue engineering applications. This study revealed that the simultaneous crosslinking and reduction reactions can be hopefully applied for bone tissue engineering materials and time-saving procedure.

Sharma *et al.* (2016) studied to produce of the nano-biocomposite scaffold composed of natural polymers such as; chitosan, gelatine, alginate and bioceramic compound, hydroxyapatite. In this study, the composite polymer solution was prepared in bead form with using the sodium hydrogen carbonate ($NaHCO_3$) as a foaming agent for the porous structure and glutaraldehyde as a crosslinking agent. Firstly, the mixture of alginate and gelatine was prepared in specific ratio and $NaHCO_3$, and glutaraldehyde was added to this mixture and waited for the formation of polymer foam. This polymer foam was extruded drop-wise to the solution containing HAp particles dispersed in chitosan solution. This step was resulted in formation of composite scaffold beads. The applied characterization studies showed that the developed scaffold could be potentially applied for bone regeneration.

Shavandi *et al.* (2015) reported the chitosan composite reinforced by HAp and β-TCP derived from waste mussel shells. In this study, it was investigated the effect of the crosslinking agent tripolyphosphate (TPP) and plasticizing agent (glycerol) on the structural and biological properties of the prepared composites. The prepared scaffold mixture including HAp-β-TCP-chitosan was molded and freezed at -80°C. After the freeze drying procedure, the composites were treated with different amount of TPP and washed with distilled water to remove the TPP. The crosslinked samples were again freeze dried and ultimately characterized. This study revealed that the ideal concentration of the glycerol and TPP should be equal to 1% and 2.5%, respectively, to achieve the desirable properties of composite scaffolds in terms of porosity, cytotoxicity and mechanical.

Kim *et al.* (2015) produced the three-component scaffold including HAp, alginate (AG) and chitosan (CS) utilizing AG as a dispersing agent for nano-HAp and CS. The low molecular weight of chitosan solution was prepared at 4 wt % concentration in acetic acit solution. Alginate solution was prepared at specific concentrations for HAp dispersion. HAp was dispersed in the alginate solution using the magnetic stirrer for 1 h, and the pH of the mixture was adjusted to 9.5-10.0 by adding the NH_4OH solution. The composite scaffold material was prepared by mixing the HAp-AG mixture with CS solution using the planetary mixer. The whole mixture was molded and frozen -20 °C overnight, and then lyophilized for 24 h with a freeze drier. The composites were crosslinked $CaCl_2$ solution, then washed with deionized water. Finally, the wet composites were freezed dried following the procedure

described above. This study revealed that alginate solution at pH 10 can be utilized as a bio-inspired dispersant for nano-HAp. The HAp addition to the scaffolds at various proportions led to improvement of compressive strength values from 0.2 to 0.68 MPa. The composite scaffolds exhibited an improvement on the osteoblastic differentiation.

Mohandes & Salavati-Niasari (2014) studied on nanocomposite composed of HAp, graphene oxide (GO) and chitosan via freeze drying method. In this study, the HAp was synthesized via precipitation method using the new agent based on Schiff base compounds and GO was synthesized via Improved Hummers method. The bioactivity of the synthesized nanocomposite and HAp was evaluated. The results showed that the nanocomposite had higher bioactivity rather than the pure HAP nanoparticles.

Pallela *et al.* (2012) prepared a three-component scaffold composed of chitosan, HAp and marine sponge collagen (MSCol) using freeze-drying method. The resultant solution prepared by adding the components was transferred to the small petri dish and freezed −80°C for 5 h and finally lyophilized in freeze dryer to form scaffolds. The characterization studies revealed that the prepared scaffolds had following properties; good thermal stability, interconnected porosity, and in vitro cell proliferation. Based on these features, it was suggested that the scaffolds had potential prospects in the field of bone tissue engineering.

Venkatesan *et al.* (2012) developed the three-component scaffolds of chitosan/natural hydroxyapatite with chondroitin sulfate (chitosan-CS/HAp) and amylopectin (chitosan-AP/HAp) via freeze-drying method. The prepared scaffold mixture was transferred to the small petri dish and freezed -80°C for 5 h and finally lyophilized in freeze dryer to form scaffolds. This study revealed that the cross linking between chitosan, HAp, CS and AP. Additionally, both of the produced scaffolds had desirable properties such as; interconnected porosity, controlled degradation structure and enhanced cell proliferation.

Venkatesan *et al.* (2011) prepared chitosan grafted with functionalized multiwalled carbon nanotube (f-MWCNT) in addition to HAp (f-MWCNT-g-chitosan/HAp) scaffolds via freeze drying method. After the scaffold mixture was prepared with mixing the all components at specific ratio, the mixture was molded and freezed. These samples were lyophilized with freeze dryer to form scaffolds. In this study, cross linkage of [NH_3^+] group of chitosan with [COO^-] group of f-MWCNT was clearly observed by FTIR spectroscopy and the performed characterization studies showed that f-MWCNT-g-chitosan/HAp had a great potential applications in the field of bone tissue engineering due to its cell proliferation, interconnected porosity, thermal stability and controlled in vitro degradation properties.

Most of the studies demonstrated in the literature were found to be related to the three-component scaffold fabrication carried out with the freeze drying procedure. The studies on the production of three-component scaffolds were summarized in Table 2.10.

Table 2.10. Various studies on the production of three-component scaffolds

Reference	Components	Crosslinking Agent	HAp Synthesis Method	Drying Method
Present study	HAp	Glutaraldehyde	Derived from eggshells	Supercritical gel drying
	GO			
	Chitosan			
Shahbazarab *et al.*, 2018	Zein	Glutaraldehyde	Hydrothermal	Freeze drying
	Chitosan			
	HAp			
Dong *et al.*, 2018	HAp	-	Simultaneously synthesis	3D plotting
	Chitosan			
	Silica			
El-Meliegy *et al.*, 2018	Dextran	-	Precipitation	Freeze drying
	Chitosan			
	HAp			
Yu *et al.*, 2017	Chitosan	Genipin	-	-
	GO			
	HAp			
Sharma *et al.*, 2016	Chitosan	Glutaraldehyde	Purchaced	Foaming
	Gelatine			
	Alginate			
	HAp			

Table 2.10. Various studies on the production of three-component scaffolds (cont.)

Reference	Components	Crosslinking Agent	HAp Synthesis Method	Drying Method
Kim *et al.*, 2015	HAp	0.2 M $CaCl_2$	Hydrothermal	Freeze drying
	AG			
	Chitosan			
Shavandi *et al.*, 2015	HAp	TPP Glycerol (plasticizer)	Derived from waste mussel shells	Freeze drying
	β-TCP			
	Chitosan			
Mohandes & Salavati-Niasari, 2014	Chitosan	-	Precipitation method using Schiff base	Freeze drying
	GO			
	HAp			
Pallela *et al.*, 2012	Chitosan	-	Derived from Thunnus Obesus bone	Freeze drying
	HAp			
	Collagen			
Venkatesan *et al.*, 2012	Chitosan	-	Derived from Thunnus Obesus bone	Freeze drying
	AP			
	HAp			
Venkatesan *et al.*, 2012	Chitosan	-	Derived from Thunnus Obesus bone	Freeze drying
	CS			
	HAp			
Venkatesan *et al.*, 2011	MWCNT	-	Derived from Thunnus Obesus bone	Freeze drying
	Chitosan			
	HAp			

3. MATERIALS AND METHODS

3.1. Materials

3.1.1. Chemicals

Graphite rods have high purity value to 99.9995% and purchased from Alfa Aesar. Low molecular weight of chitosan was supplied from Acros firm with 9012-76-4 CAS number. The crosslinking agent glutaraldehyde (50% aqueous solution) was supplied from AppliChem firm. Potassium permanganate ($KMnO_4$), hydrogen peroxide solution (35%) (H_2O_2), hydrochloric acid (37%) (HCl), ortho-Phosphoric acid (85%) (o-H_3PO_4), sulfuric acid (95-98%) (H_2SO_4), acetone, and ammonia solution (25%) (NH_4OH) were supplied from Merck.

3.1.2. Apparatus

Analytical Balance: RADWAG AS 220.R2 analytical balance was used and it has 220 g capacity with 0.1 mg readability. In Figure 3.1, RADWAG AS 220.R2 analytical balance was represented.

Figure 3.1. RADWAG AS 220.R2 analytical balance

Magnetic Stirrer: DAIHAN MaXtir™ 500S Hi-performance digital magnetic stirrer was used for mixing of the samples at defined temperature value (0-500°C) and speed rate (0-1500 rpm). The magnetic stirrer used was represented in Figure 3.2.

Figure 3.2. DAIHAN MaXtir™ 500S Hi-performance digital magnetic stirrer

pH meter: During the experiments, Hanna HI-2211 pH meter (Figure 3.3) was used to adjust the pH value of the hydroxyapatite solution. Its standard pH range was within -2 to 16 with 0.01 resolution.

Figure 3.3. Hanna HI-2211 pH meter

Ultrasonic Bath: During the experiments, Elma TI-H-5 ultrasonic bath (Figure 3.4) was used for sonication of the mixtures. It has 3.5 L capacity and the temperature of the ultrasonic bath can be adjusted in the range of 20-80°C. The frequency can be arranged at 25 kHz and 45 kHz.

Figure 3.4. Elma TI-H-5 ultrasonic bath

Oven: Memert Drying-oven was used to dry the samples in required temperature. Its temperature range was within 30-200°C. It was represented in Figure 3.5.

Figure 3.5. Drying oven

Centrifuge: HERMLE Z206A Compact Research Centrifuge was used for centrifugation of the samples. The speed range is within the range of 200 rpm - 6000 rpm. It holds six rotors with 50 mL capacity per one. The centrifuge was represented in Figure 3.6.

Figure 3.6. Hermle Centrifuge

High Temperature Laboratory Furnace: Protherm PLF 110/30 high temperature laboratory furnace was used for calcination of the hydroxyapatite (Figure 3.7).

Figure 3.7. Protherm PLF 110/30 high temperature laboratory furnace

Supercritical Extraction Equipment: The supercritical gel drying procedure was performed using the Applied Separations Helix-7409 equipment. It was represented in Figure 3.8. The temperature and pressure can be adjusted to the highest value as 240°C and 10000 bar, respectively. Different size of vessel can be used for the specific applications. In the present study, 1000 mL of vessel was used.

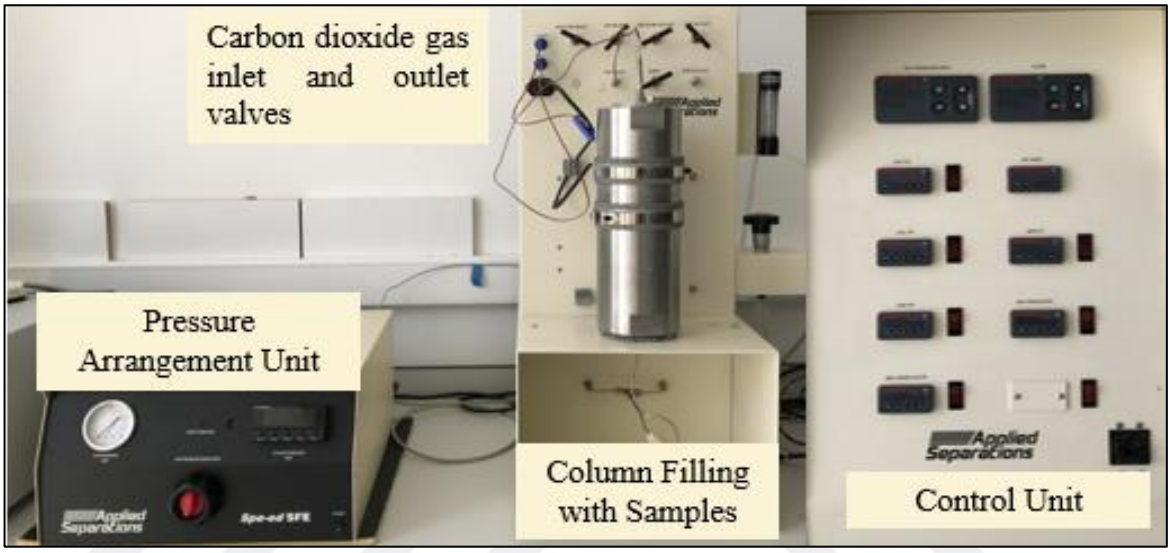

Figure 3.8. Applied Separations Helix-7409

3.2. Experimental Procedure

The experimental procedure of the present study includes the synthesis of the HAp and GO, mixing of these components with chitosan solution to prepare scaffold mixture, molding and freezing of the prepared scaffold mixture, water-acetone substitution to apply the supercritical gel drying method and finally, supercritical gel drying which is the last step to produce the scaffolds. Then, the produced scaffolds were characterized in terms of their physical, chemical and biological properties. These steps of experimental procedure was basically represented in Figure 3.9.

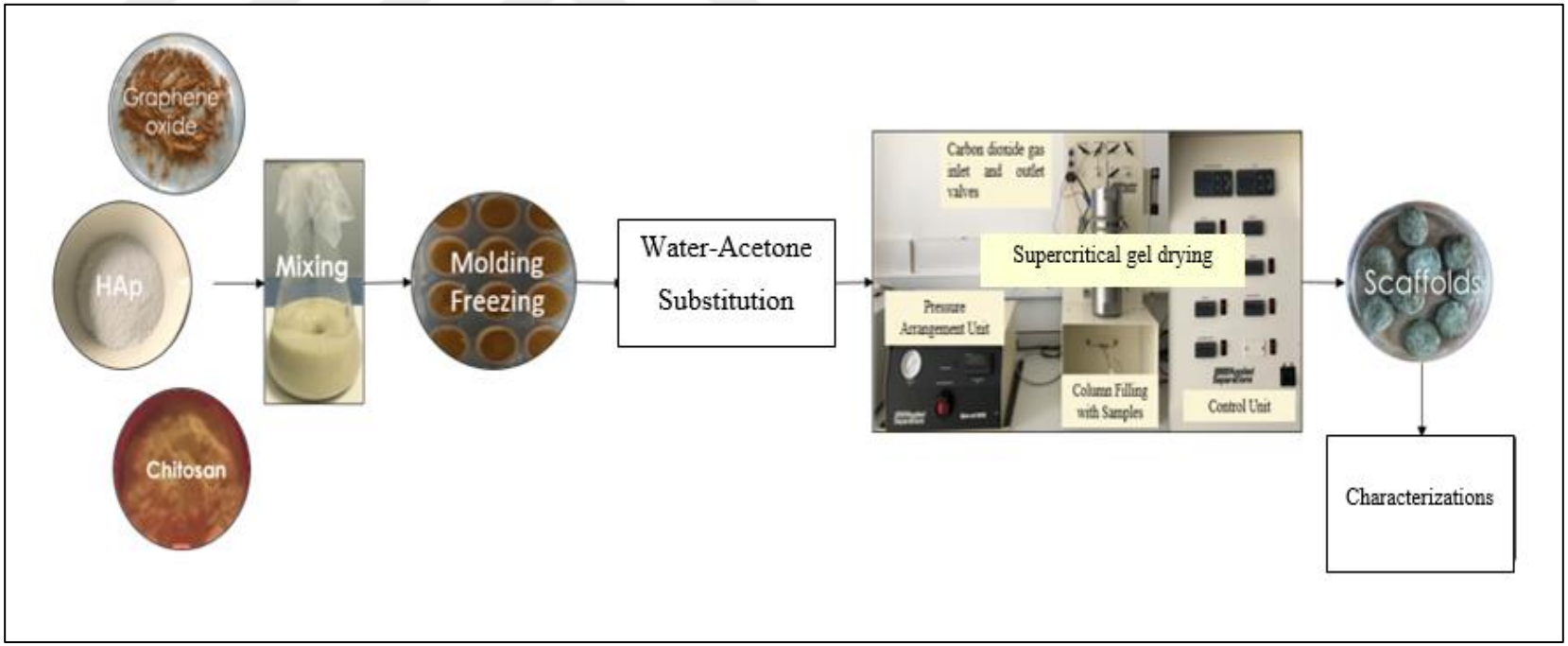

Figure 3.9. Graphical representation of the present study

3.2.1. Hydroxyapatite Synthesis

Hydroxyapatite was synthesized using the calcium precursor derived from eggshells and ortho-phosphoric acid (85%) via wet chemical precipitation method (Kamalanathan *et al.*, 2014).

Preparation of calcium precursor using eggshells: Eggshells were washed with excess amount of distilled water, boiled in distilled water and, their inside membranes were removed. The eggshells were dried at 100°C for 12 h to eliminate the odor and any volatile contaminants, and grinded using a grinder. Finally, eggshell powder (calcium carbonate) was calcined in a laboratory furnace at 900°C with 10°C heat rate for 2 hours to obtain substance of calcium oxide (calcined eggshell powder). The eggshell conversion to calcium oxide was represented in Figure 3.10.

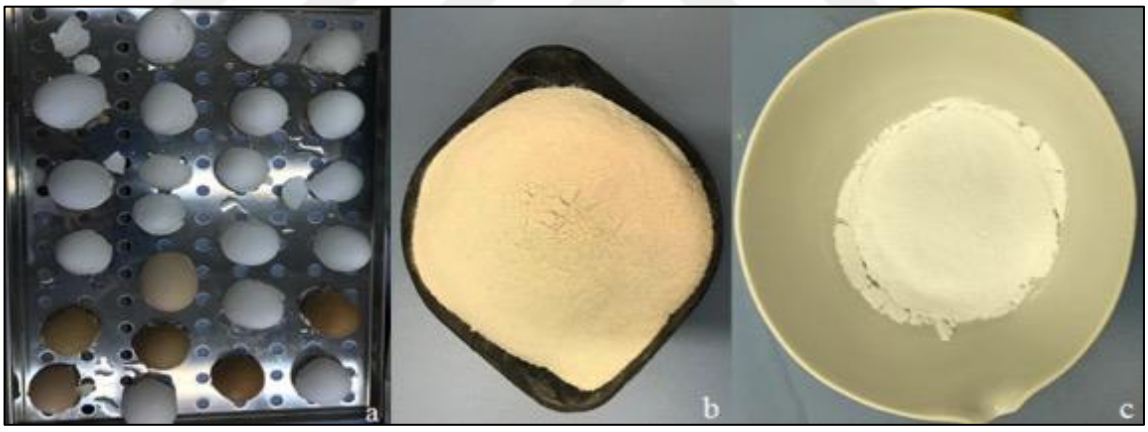

Figure 3.10. Eggshell conversion to calcium oxide a) washed and dried eggshells, b) eggshell powder (calcium carbonate) and c) calcium oxide (calcined eggshell powder)

The chemical conversion reactions from calcium carbonate to calcium hydroxide was expressed in Equations 3.1 and 3.2 (Khandelwal and Prakash, 2016).

$$CaCO_3(s) \rightarrow^{\text{calcination}}_{900°C} CaO(s) + CO_2(g) \quad (3.1)$$

$$CaO(s) + H_2O\ (l) \rightarrow Ca(OH)(aq) + \text{Heat} \quad (3.2)$$

Preparation of hydroxyapatite by precipitation method: Calcium oxide was dissolved in sufficient amount of water to obtain 1 M calcium hydroxide. The mixture was heated at 40°C and stirred at 600 rpm using a magnetic stirrer. When the required temperature was achieved, 0.6 M of phosphoric acid solution was added to the calcium oxide solution with help of a dropper. The pH of the resultant mixture was adjusted to 9.0 with using the 25% (v/v) ammonium hydroxide and stirred for 2 h. The mixture is then left for 24 h to complete the formation of precipitation.

The precipitate was washed for three times of 200 ml distilled water, and then solid part was separated by centrifugation at 6000 rpm for 30 minutes. The washed solid part was transferred into a petri dish and dried in an oven at 100°C for 12 h. Then, the dried solid part (hydroxyapatite powders) was ground using a mortar and pestle to produce a fine powder.

Finally, the hydroxyapatite was calcined in the laboratory furnace at 900°C with 10°C/min heating rate for 2 hours to obtain higher crystallinity degree. In Figure 3.11, the synthesis steps of hydroxyapatite procedure were represented.

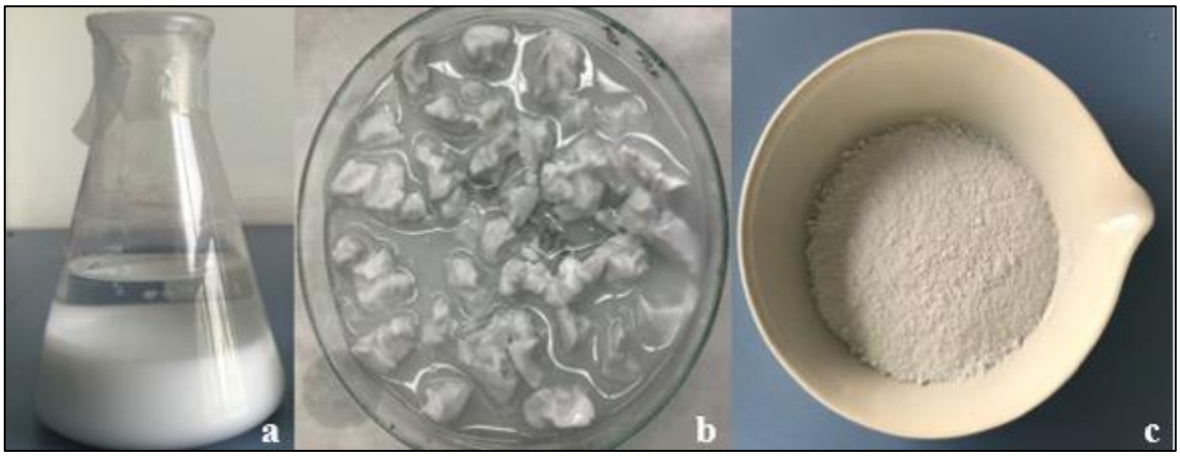

Figure 3.11. Synthesis of hydroxyapatite with precipitation method a) precipitated hydroxyapatite, b) separated hydroxyapatite and c) calcined hydroxyapatite

3.2.2. Graphene Oxide Synthesis

Graphene oxide was synthesized by Improved Hummers Method (Marcano *et al.*, 2010). The oxidation reaction of graphite was performed with $KMnO_4$ in a mixture of H_2SO_4/H_3PO_4 (9:1 v/v) for production of GO with higher extent of oxidation (Marcano *et al.*, 2010). 3 gr of graphite powder and 9 gr of $KMnO_4$ were added into the oxidation medium including 360 ml of H_2SO_4 and 40 ml of H_3PO_4. The reaction medium was then heated to 50°C and stirred for 12 h at 150 rpm.

Afterwards, reaction medium was cooled down to room temperature and poured into ice (400 ml) with H_2O_2 30% (3 ml). This mixture was centrifuged at 6000 rpm for 30 minutes to remove the liquid part. The solid part was washed in succession with 200 ml of water (twice), 5 N 200 ml HCl (twice) and 200 ml of ethanol (twice) and solid part was separated from the liquid part using the centrifugation. Finally, the washed solid part was transferred into a petri dish and dried at 50°C for 18 h. Figure 3.12 represents the graphene oxide synthesis steps. As it can be clearly seen from this figure, the color of graphene oxide obtained after washing and drying was open-brown.

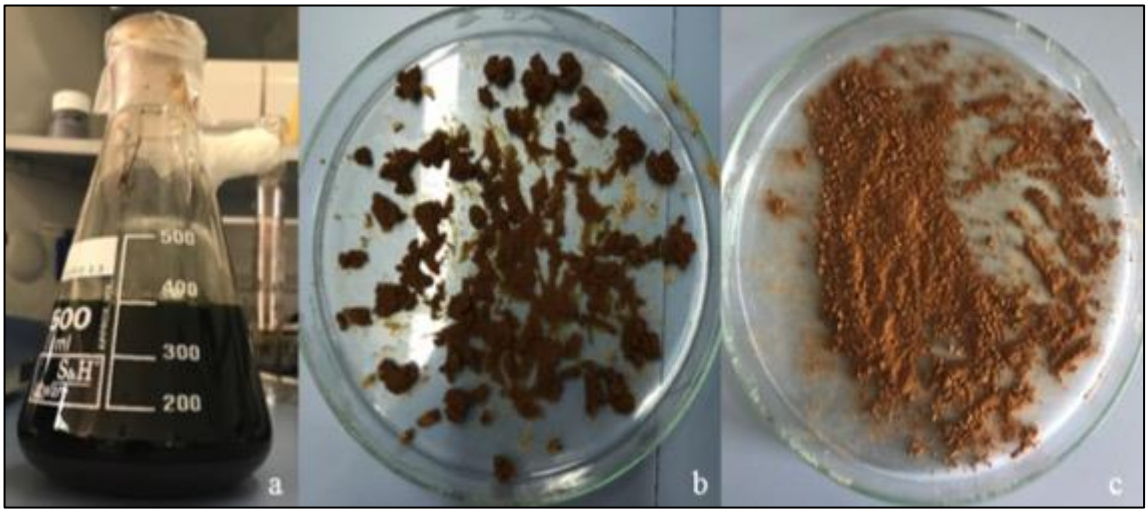

Figure 3.12. Graphene oxide synthesis method a) reaction medium, b) solid part of the reaction medium and c) dried solid part (graphene oxide)

3.2.3. Preparation of Scaffolds

Graphene oxide-Chitosan (GO-CS) and Hydroxyapatite-Chitosan (HAp-CS) scaffolds were synthesized to compare their physical and biological properties with three-component scaffolds composed of graphene oxide, hydroxyapatite and chitosan components (HAp-GO-CS). The ratio of the components for produced scaffolds were given in Table 3.1.

Table 3.1. The ratio of the components for produced scaffolds

Name	Scaffold Components	Ratio of Components (w/w)
A	Graphene Oxide	1%
	Chitosan	99%
B	Hydroxyapatite	60%
	Chitosan	40%
C	Hydroxyapatite	60%
	Graphene Oxide	0.5%
	Chitosan	39.5%
D	Hydroxyapatite	60%
	Graphene Oxide	1%
	Chitosan	39%
E	Hydroxyapatite	60%
	Graphene Oxide	2%
	Chitosan	38%
F	Hydroxyapatite	60%
	Graphene Oxide	4%
	Chitosan	36%

1% (v/v) glutaraldehyde solution was prepared with dissolving defined amount of glutaraldehyde in distilled water to be used as a crosslinking agent. In this way, the stability of produced scaffolds were increased. Otherwise, the water-acetone substitution, which is

the necessary step for supercritical gel drying, could not be achieved as the scaffold structure was tend to collapse.

The scaffold production basically includes of the following steps; dissolving of chitosan in required concentration, preparation the solutions of other components, addition of these components to the chitosan solution, addition of crosslinking agent to the mixture, molding and, finally, drying. The steps were explained in details as given below:

Preparation of chitosan solution: Chitosan was weighted and dissolved in 2% (v/v) acetic acid solution to reach 4% (w/v) concentration, and this mixture was continuously stirred for 2 hours at 45°C.

Preparation of Graphene oxide-Chitosan scaffolds: Graphene oxide was weighted in according to its ratio in the scaffolds and dissolved in distilled water by sonication for 2 hours. The homogeneous graphene oxide solution was transferred to the chitosan solution (4% (w/v)) with help of a dropper. This mixture was stirred for 1 h at 40°C, and the solution of 1% (v/v) glutaraldehyde was added into this solution as a crosslinking agent in a specific ratio (10% v/v), and then, the final mixture was stirred for additional 2 h at 40°C.

The resultant solution was transferred to the 21 well plates, and they were frozen at -18°C for 24 h for formation of hydrogel. Then, these hydrogels were put an acetone bath at -18°C for 24 h to achieve the water-acetone substitution. Then, this samples were subjected to dry based on the supercritical gel method. Unless otherwise stated, the same procedures were followed for molding, water-acetone substitution and drying steps of the prepared scaffolds.

Preparation of Hydroxyapatite-Chitosan scaffolds: Hydroxyapatite was weighted in according to its ratio in the scaffolds and dissolved in distilled water by sonication for 2 hours. The hydroxyapatite solution was transferred to the chitosan solution (4% (w/v)) with a help of dropper. This mixture was stirred for 1 h at 40°C, and the solution of 1% (v/v) glutaraldehyde was added to this solution to be used as a crosslinking agent in a specific

ratio (10% v/v) and mixed for additional 2 h at 40°C. The homogenous solution was moulded, frozen and then, dried.

Preparation of Hydroxyapatite-Graphene Oxide-Chitosan scaffolds: Firstly, the hydroxyapatite, graphene oxide and chitosan solutions were individually prepared. The graphene oxide solution was transferred to the chitosan solution (4% (w/v)) with the help of a dropper, and this mixture was stirred for 1 h at 40°C. Secondly, the hydroxyapatite solution was transferred to the graphene oxide-chitosan solution with a help of dropper, and the final mixture was stirred at 500 rpm for 2 hours. Following this, the crosslinking agent, glutaraldehyde of 10% v/v was added to this mixture and stirred for additional 2 h at 40°C. After all, the homogenous solution obtained was moulded, frozen and then dried.

The scaffolds were prepared at various GO ratios for the investigation of the toxicity effect of GO ratios on MC3T3-E1 cell lines. The same procedures were followed for molding and drying steps of the samples prepared at various GO ratios.

3.2.4. Drying of Prepared Scaffolds

Supercritical gel drying was performed in the following procedure: after water-acetone substitution, samples were put in a high pressure vessel, and vessel was filled from the bottom with SC-CO_2. When the desired temperature (70°C) and pressure (200 bar) were achieved, the drying procedure was performed at constant flow rate of SC-CO_2 (1 kg/h) for 4 h. The basic steps for the scaffold synthesis were shown in Figure 3.13. After depressurization of the system, the produced scaffolds were characterized in terms of their physical, chemical and biological properties.

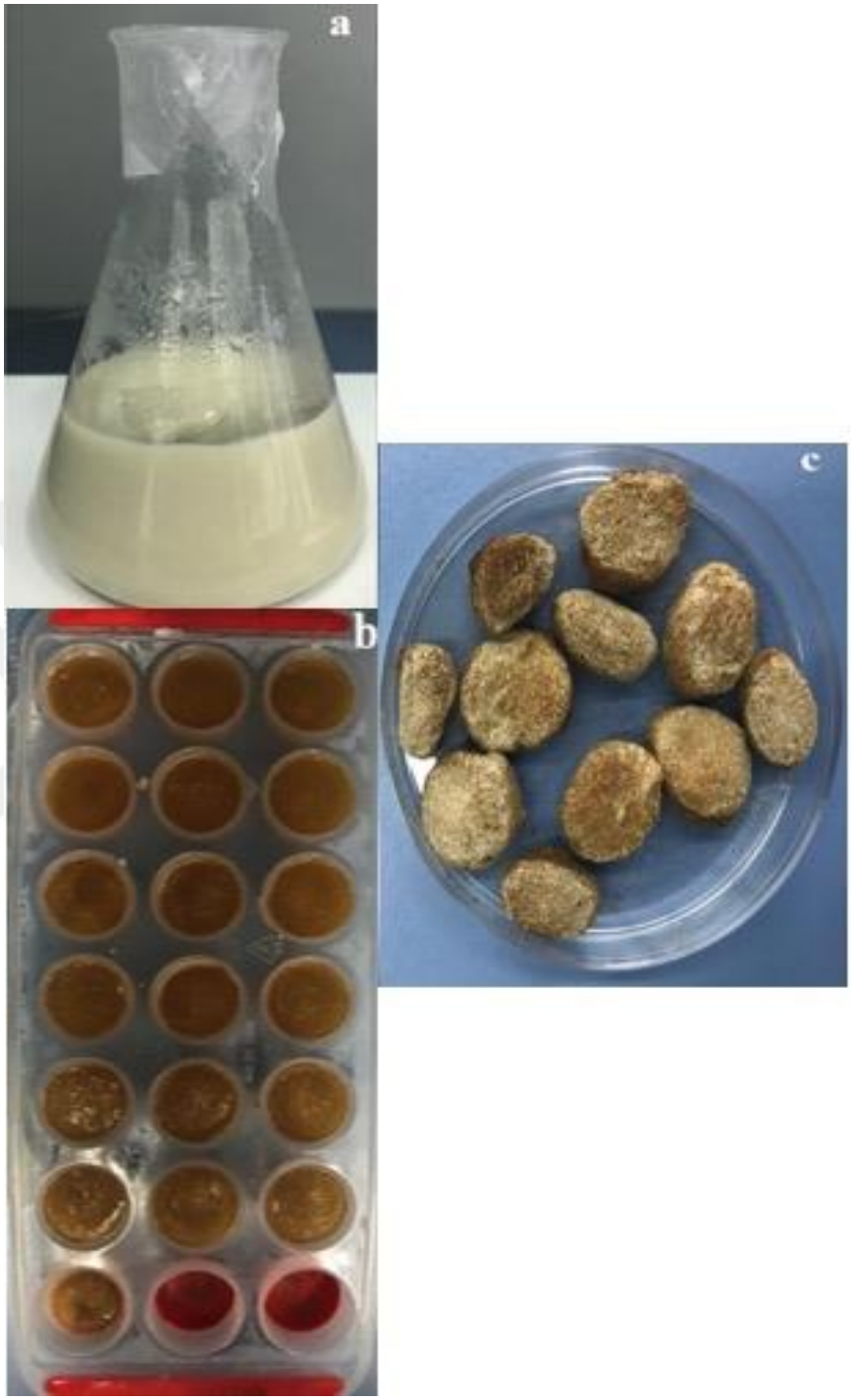

Figure 3.13. Experimental procedure; a) mixing of the components, b) molding and freezing and c) produced scaffolds after drying procedure

3.3. Characterization Studies

3.3.1. UV-Visible Spectrophotometer

UV-Visible spectrum of aqueous GO solution was determined using the UV-1800 SHIMADZU spectrophotometer (Figure 3.14). It is a double beam spectrophotometer and has a 190-1100 nm spectral range with ±0.3nm wavelength accuracy.

Figure 3.14. UV-1800 SHIMADZU spectrophotometer

3.3.2. Fourier Transform Infrared (FTIR) Spectrometer

Bruker Tensor 27 Attenuated Total Reflection (ATR) FTIR Spectrometer (Figure 3.15) was used to determine the chemical structure of the components and produced scaffolds. The analyses were carried out at room temperature and specific wavelength range (450-4000 cm^{-1} range) to determine the functional groups of the samples. The wavenumber accuracy of the equipment is ±0.01 cm^{-1} and photometric accuracy is ±0.1% T.

Figure 3.15. Bruker Tensor 27 Attenuated Total Reflection (ATR) FTIR Spectrometer

3.3.3. Raman Spectroscopy

Raman spectroscopy is a non-destructive technique which is a widely used tool to analyze the structure of carbon-based materials. In the present study, Raman spectra of GO were recorded at 785 nm laser excitation using Perkin Elmer Raman Station 400F instrument (Figure 3.16).

Figure 3.16. Perkin Elmer Raman Station 400F

3.3.4. X-Ray Powder Diffraction (XRD) Analysis

PANalytical X'Pert Pro Analyzer (Figure 3.17) was used to identify the phase of the synthesized components and scaffolds. Cu-Kα radiation source was used for XRD analyzer, and the scanning angle 2θ can be arranged from 2° to 90° with a step scanning rate of 3° min^{-1} at 45 kV and 40 mA.

Figure 3.17. PANalytical X'Pert Pro Analyzer

The crystallinity size of the samples were calculated using Scherer formula:

$$\boldsymbol{D_p = \frac{k \times \lambda}{b \times cos\theta}} \quad (3.3)$$

In this formula; D_p is the average particle size of the powder, k is the constant (0.9), λ is the X-ray emission wavelength (Cu=1,54 A), b is the half-width of the diffraction line (002) for the reference polycrystalline sample and θ represents the Bragg's angle of the diffraction line (Goloshchapov *et al.*, 2013).

3.3.5. Thermogravimetric/Differential Thermal Analyzer (TG/DTA)

EXSTAR SII TG/DTA6300 Analyzer (Figure 3.18) was used to determine the thermal behavior of the components and produced scaffolds in inert atmosphere. The working temperature of the instrument can be arranged between 25-1500 °C. In the present study, analysis were performed from 25-1000 °C with a heating rate of 10°C/min under nitrogen atmosphere.

Figure 3.18. EXSTAR SII TG/DTA6300 Analyzer

3.3.6. Scanning Electron Microscope (SEM)

Zeiss EVO LS10 Scanning Electron Microscope (Figure 3.19) operating in beam mode at 20 kV with secondary electron detector was used to characterize the morphological structure of the produced scaffolds and hydroxyapatite. The solid samples were coated by gold-palladium for 45 seconds in argon plasma with Quorum SC7620 Sputter Coater shown in Figure 3.20.

Figure 3.19. Zeiss EVO LS10 Scanning Electron Microscope

Figure 3.20. Quorum SC7620 Sputter Coater

3.3.7. Transmission Electron Microscopy (TEM)

Transmission electron images GO and scaffold D were recorded on JEOL JEM 2100 HRTEM (Figure 3.21) operating at 200 kV. Images were taken by Gatan Model 794 Slow Scan CCD Camera and also by Gatan Model 833 Orius SC200D CCD Camera. Carbon support film coated copper TEM grids (Electron Microscopy Sciences, CF200-Cu, 200 mesh) were used. The TEM images were taken in TÜBİTAK Marmara Research Center.

Figure 3.21. JEOL JEM 2100 HRTEM

3.3.8. Brunauer-Emmett-Teller (BET) Surface Area Analysis

The specific surface area of the produced scaffolds were analyzed using Quantachrome Quadrosorb SI (Figure 3.22) at 77 K. All the samples were degassed (at 393 K for 3 h) before the measurements and nitrogen was used to adsorbate gas.

Figure 3.22. Quantachrome Quadrosorb SI surface and pore size analyzer

3.3.9. Cell Viability Analysis

The cytotoxicity of the scaffolds codded A, B, C, D, E and F were assessed using the MTT (3-(4,5-dimethyl-2-yl)-2,5-diphenyltetrazolium bromide) assay. This study was carried out to investigate the cell viability and proliferation on the prepared scaffolds.

The MC3T3-E1 cells were incubated at 37°C in a moist environment of 5% CO_2 and then, the medium was removed and the cells were washed with PBS (phosphate buffered saline). Afterwards, the cells were plated on 24 well plates with the scaffolds (three samples were used for each type of scaffolds) in α-MEM culture media with 10% FBS (v/v), 1% penicillin-streptomycin (v/v) at a density of $1x10^5$ cells/mL and the plates were incubated at 37°C in 5% CO_2 to observe the cytotoxic and proliferative effects. The cells plated without the scaffold were used as negative control and the cells treated with DMSO (dimethyl sulfoxide) were used as positive control. Afterwards, 50 µL MTT solution was added to each well and incubated for 3 h at 37°C and the formation of formazan crystals were observed due to the reduction of MTT by viable cells. Then, 500 µL DMSO was added to dissolve the formazan crystals. After 30 min, the absorbans value of the plates at 570 nm were measured with Elisa Reader. The absorbans value is directly proportional to the amount of viable cells. The results were expressed by comparing the absorbans values of the cell-scaffold construct

with the control groups. In this respect, the negative control group absorbance was standardized as 100% viability and the relative cell viability (RCV) was calculated as in Equation 3.4.

$$RCV\% = ((Abs_{sample} - Abs_{Negative\ control}) / Abs_{Negative\ control}) * 100 \quad (3.4)$$

3.3.10. Mechanical Testing Instrument

Scaffold B and D were mechanically tested by a Universal Instron Mechanical Testing System (Instron 5982) (Figure 3.23) and their compressive strength values were compared to determine the GO effect on the mechanical properties of the produced scaffolds.

In the present study the cylindrical samples with a diameter of 1 cm and a high of 1 cm were used for the mechanical testing. The cross head speed of the instrument was adjusted to 0.5 mm/min and each measurement was repeated three times. The average compressive strength values were calculated by dividing of the maximum load (N) with the cross sectional area of the produced scaffolds.

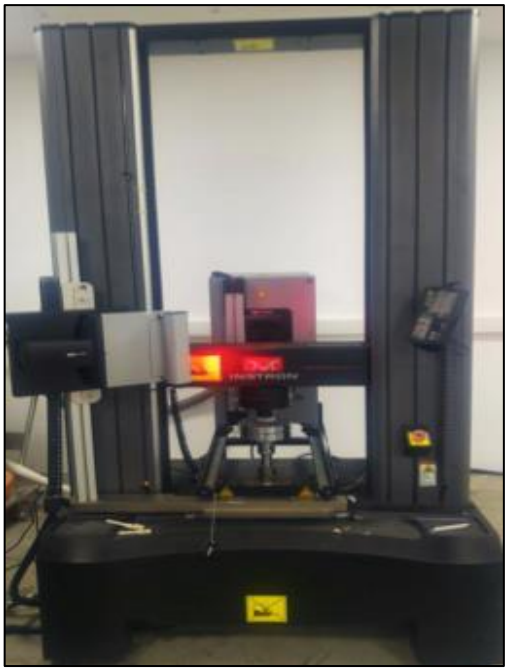

Figure 3.23. Instron 5982 Universal Testing Machine

4. RESULTS

4.1. Characterization Studies of Eggshells

Eggshell powder was prepared using the eggshells by applying the steps such as washing, boiling and grinding as given in Section 3.2.1.Then, the prepared eggshell powder was calcined for the formation of calcium oxide (CaO). FTIR and XRD analysis were performed on the calcined eggshell powder to confirm the formation of CaO which was used as calcium precursor for the wet chemical precipitation of HAp.

4.1.1. FTIR Analysis

FTIR analyses of eggshell powder (calcium carbonate) and calcined eggshell powder (calcium oxide) were represented in Figure 4.1.

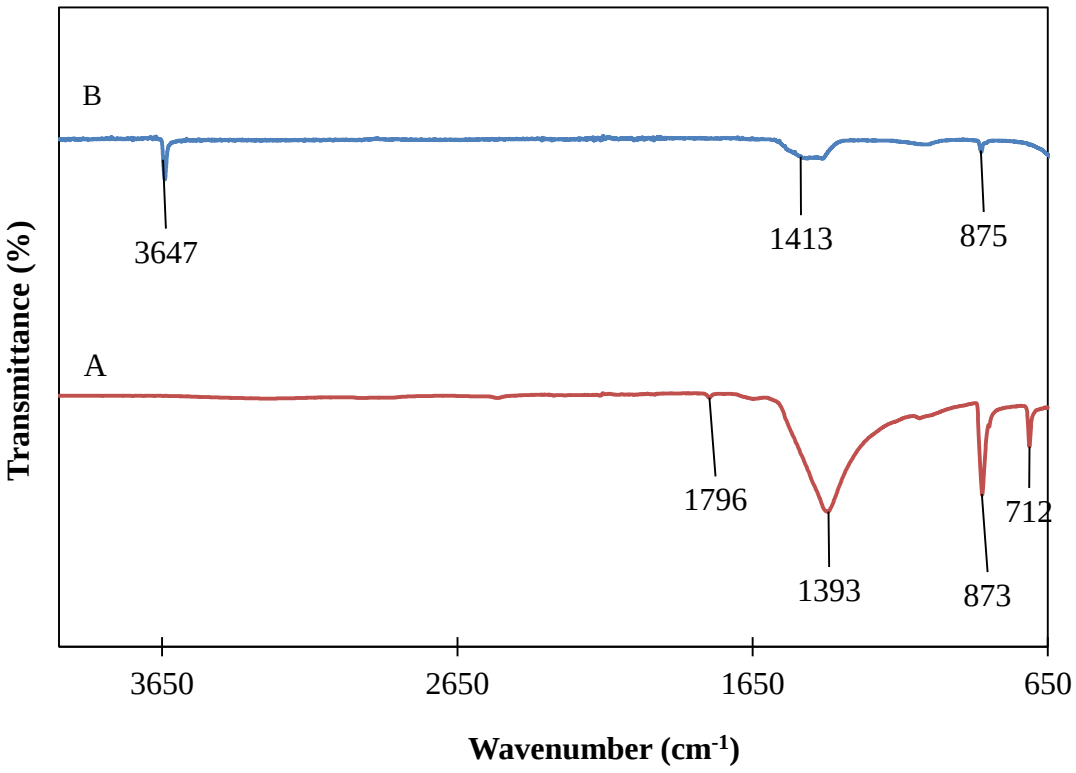

Figure 4.1. FTIR spectra of A) eggshell powder and B) calcined eggshell powder

The peak observed at 1796 cm^{-1} corresponded to combination modes of different CO_3^2. Other peaks observed at 1393, 873 and 712 cm^{-1} were characteristic peaks of carbonate group in $CaCO_3$ (Kamalanathan *et al.*, 2014).

After the calcination, $CaCO_3$ was successfully transformed to CaO phase as a calcium precursor for hydroxyapatite synthesis as confirmed by FTIR spectrum analysis (Figure 4.1). Three frequency bands specific for the presence of CaO were clearly observed (Kamalanathan *et al.*, 2014). The bands at 1413 and 875 cm^{-1} were associated with the C–O stretching, and the sharp peak observed at 3647 cm^{-1} indicated the formation of OH groups attached to the calcium atoms. It was concluded that the calcination process provided increasing of the CaO presence (Engin *et al.*, 2006).

4.1.2. XRD Analysis

The XRD patterns of crushed and calcined eggshell samples were given in Figure 4.2. The intense and narrow peaks in calcined solids define the crystalline structure of the material.

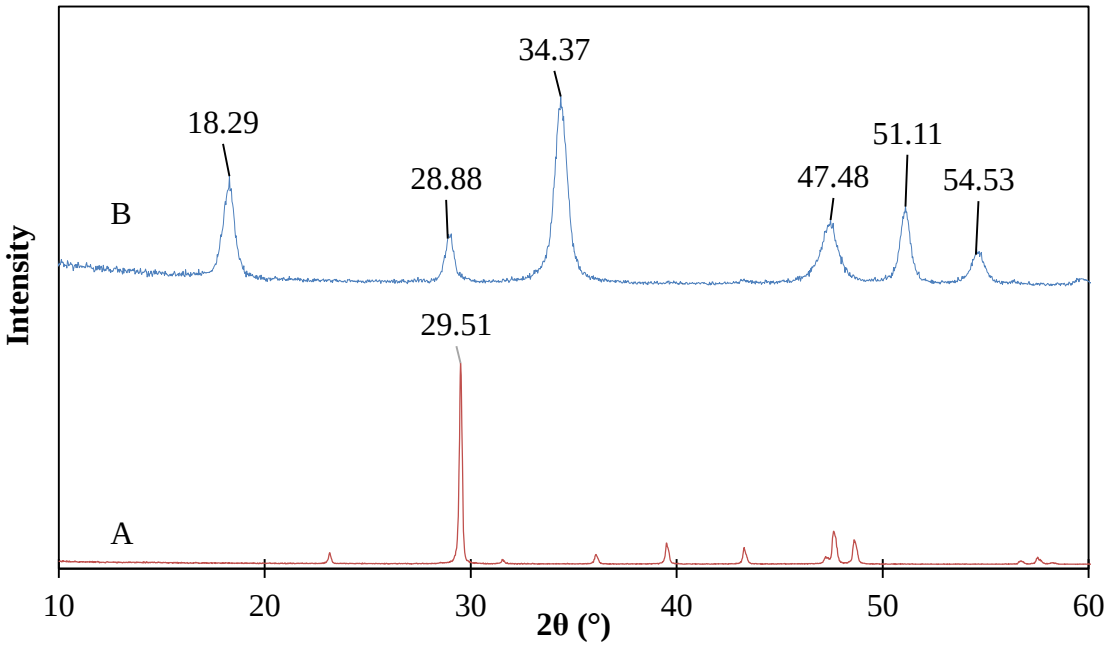

Figure 4.2. XRD patterns of A) eggshell powder and B) calcined eggshell powder

The major and intense peak appeared at 2θ values of 29.51 was attributed to the presence of $CaCO_3$. After the calcination, it was clearly seen that the intense of this peak was decreased because of the transformation of calcium carbonate to calcium oxide. The diffraction peaks obtained within 2θ values of 28.88, 34.37 and 54.53 corresponded to the presence of calcium oxide phase. Other diffraction peaks within 2θ values of 18.29, 47.48 and 51.11 were attributed to the presence of $Ca(OH)_2$ phase (Putra *et al.*, 2017).

4.2. Characterization Studies of Eggshell Derived HAp

HAp was synthesized by wet chemical precipitation method (Kamalanathan *et al.*, 2014) using the eggshells as a calcium and ortho-phosphoric acid as a phosphor precursor, respectively. The synthesis steps were given in Section 3.2.1. The synthesized HAp was characterized by FTIR, XRD, TGA, SEM and EDS analysis to confirm the formation of HAp.

4.2.1. FTIR Analysis

FTIR spectra of hydroxyapatite before and after calcination were given in Figure 4.3. In Figure 4.3a, the broad peak observed at 3370 cm^{-1} was attributed to OH^- stretching vibration. Weak bands of CO_3^{2-} were observed at 1456 cm^{-1}, 1416 cm^{-1} and 870 cm^{-1} (Gergely *et al.*, 2010). Bands observed at 1024 cm^{-1}, 961 cm^{-1}, 604 cm^{-1}, 600 cm^{-1} and 559 cm^{-1} were assigned to vibrations of the phosphate group, PO_4 (Koutsopoulos, 2002).

The bands obtained after the calcination (Figure 4.3b) indicated the pure formation of hydroxyapatite with complete removal of carbonates from the resultant structure as the peaks at 1456 cm^{-1}, 1416 cm^{-1} and 870 cm^{-1} were absent. (Koutsopoulos, 2002), (Florencio-Silva *et al.*, 2015). The sharp and strong band at 3573 cm^{-1} corresponded to characteristic stretching mode of OH^- vibration on HAp. The peak observed at 628 cm^{-1} was attributed to OH^-. The bands observed at 1088 cm^{-1}, 1026 cm^{-1}, 963 cm^{-1}, 599 cm^{-1} and 566 cm^{-1} were assigned to vibrations of the phosphate group, PO_4 (Koutsopoulos, 2002).

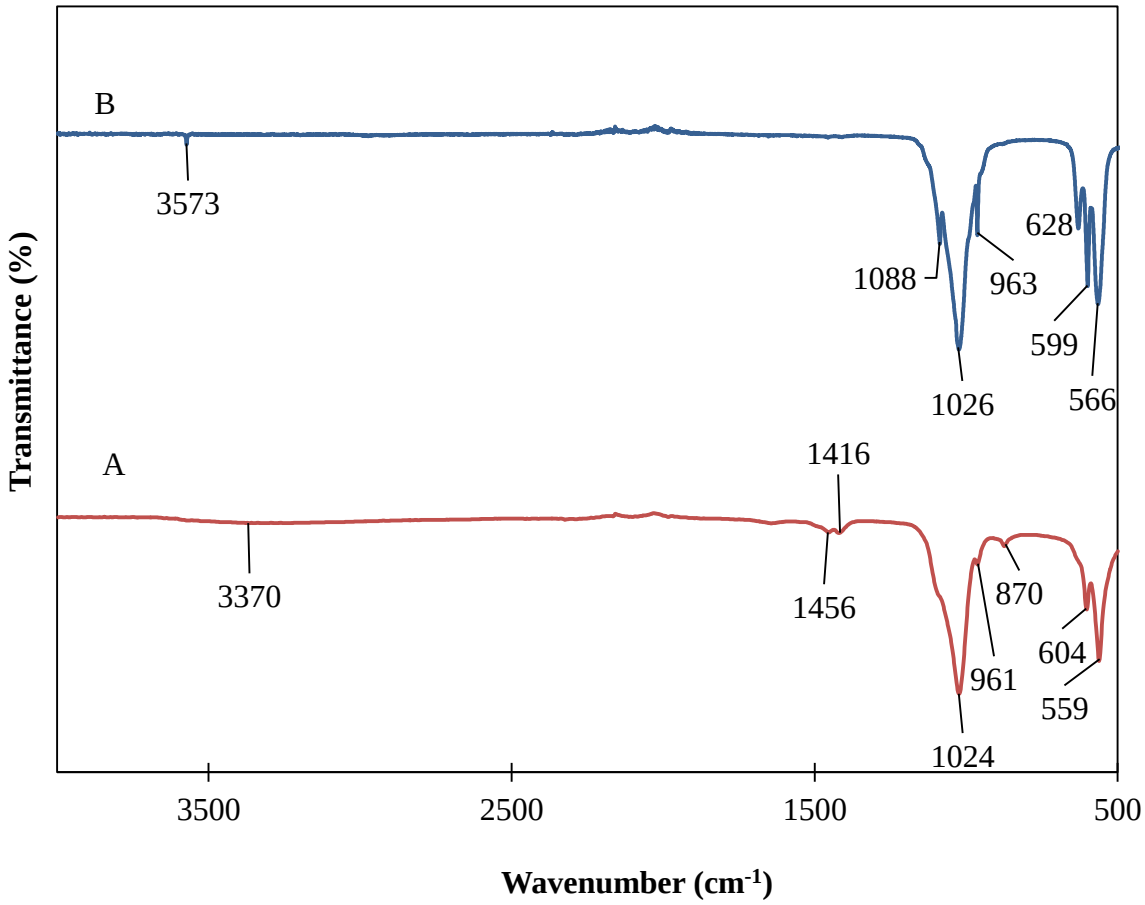

Figure 4.3. FTIR spectra of synthesized hydroxyapatite A) before calcination and B) after calcination

4.2.2. XRD Analysis

The XRD patterns of uncalcined and calcined hydroxyapatite were represented in Figure 4.4. The highest intensity peak of hydroxyapatite was obtained at a 2θ value of 32.04 in agreement with literature (Kamalanathan *et al.*, 2014). Another characteristic diffraction peak of hydroxyapatite was observed at a 2θ value of 26.18. These two characteristic peaks were associated with (002) and (211) reflections of hydroxyapatite, respectively. The crystallite size of the synthesized eggshell derived hydroxyapatite powder based on the (002) peak was found as 20.63 nm by using Scherer formula (Equation 3.3).

The intensity of the diffraction peaks had become more intense after the calcination of eggshell hydroxyapatite at 900°C for 2 h. The highest intensity of the diffraction peak had increased and become more intense. This revealed that the crystallinity degree of HAp was increased with high temperature calcination.

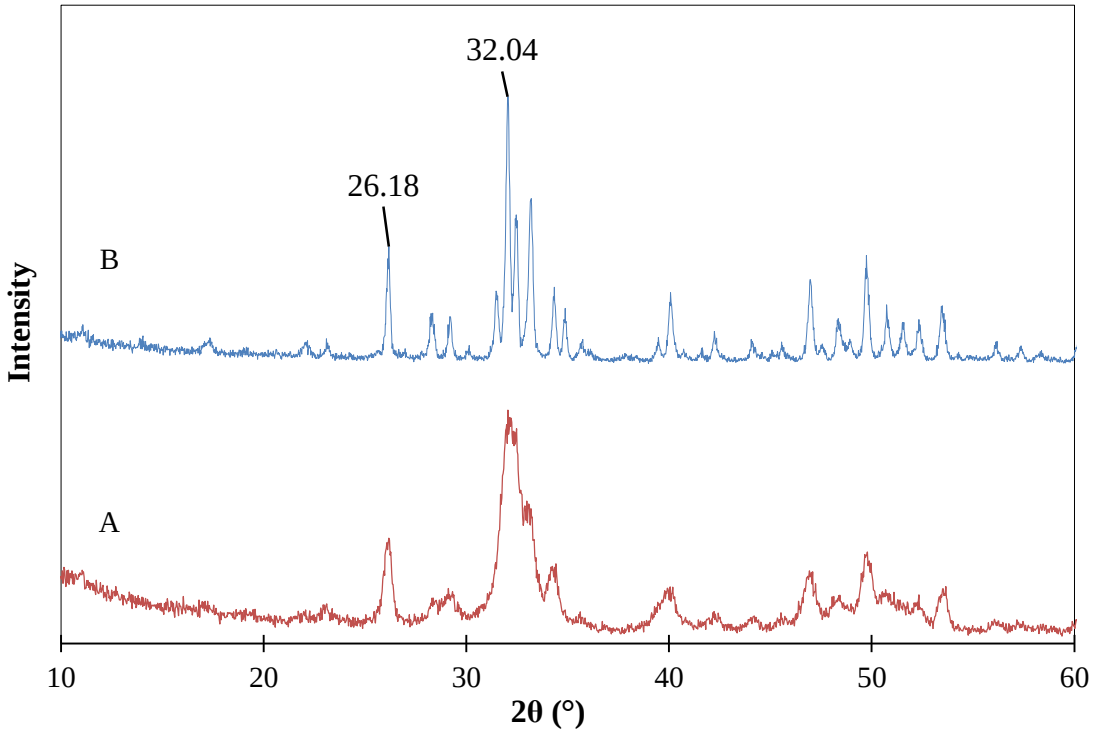

Figure 4.4. XRD patterns of A) hydroxyapatite and B) calcined hydroxyapatite

4.2.3. Thermogravimetric Analysis (TGA)

The thermogravimetric profile of pure HAp was given in Figure 4.5. From the profile given in this figure, no significant change on the weight of HAp even at high temperature values was observed. This case indicated that HAp maintained its stability.

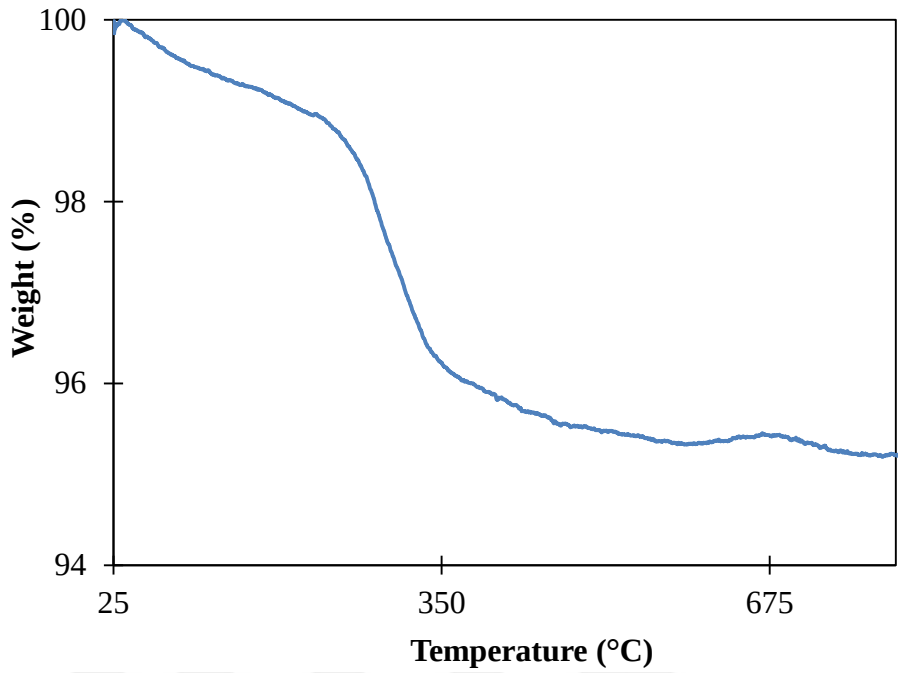

Figure 4.5. TGA profile of HAp

4.2.4. SEM Analysis

The SEM images of synthesized HAp at 5000X and 50000X magnifications were represented in Figure 4.6. From the SEM images, the agglomeration tendency of HAp particles could be seen clearly.

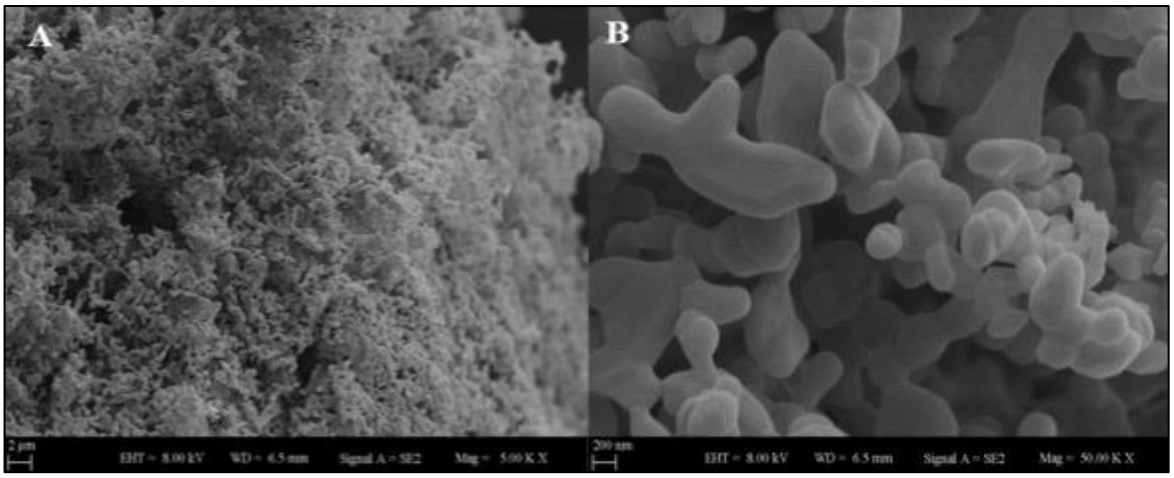

Figure 4.6. SEM images of HAp A) at 5000X and B) at 50000X

4.2.5. Energy Dispersive X-Ray Spectroscopy (EDS) Analysis

Elemental composition of the synthesized HAp was detected using EDS analysis and the results were given in Figure 4.7 and Table 4.1. In Figure 4.7, the presence of Ca, P and O elements in the sample can be seen clearly. The negligible amount of Au and Pd elements were detected due to coating of the HAp sample for SEM analysis.

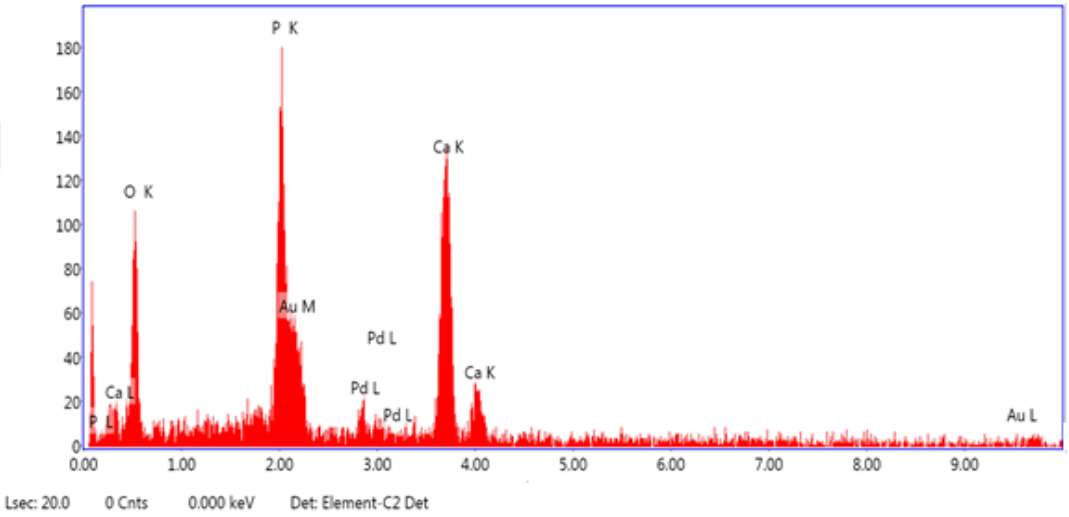

Figure 4.7. EDS pattern of HAp

According to the data given in Table 4.1, the stoichiometric ratio of Ca/P was found as 1.68, similarly with pure hydroxyapatite found in bone tissue (Lin and Chang, 2015).

Table 4.1. Elemental composition of synthesized HAp

Element	Atomic %
O	53.9
P	16.2
Au	1.8
Pd	0.8
Ca	27.3

4.3. Characterization Studies of GO

GO was synthesized by Improved Hummers Method (Marcano *et al.*, 2010), which includes $KMnO_4$, H_2SO_4 and H_3PO_4 as oxidation agents, as given in Section 3.2.2. The formation of GO was confirmed by UV-Vis spectroscopy, FTIR, XRD, Raman spectroscopy, TGA and TEM analyses.

4.3.1. UV-Visible Spectroscopy Analysis

The UV-Visible spectrum of aqueous GO measured in 200-800 nm wavelength range was given in Figure 4.8.

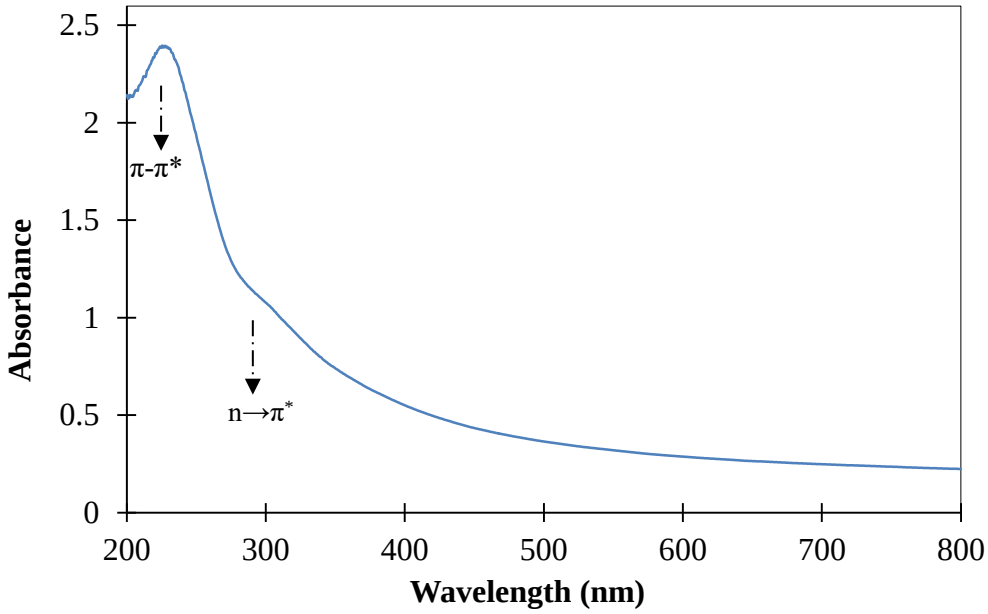

Figure 4.8. UV-Visible spectrum of GO aqueous solution

The spectrum of GO obtained was in an agreement with the characteristic sharp absorption peak at ~228 nm and broad shoulder at ~300 nm as seen in Figure 4.8 (Saxena *et al.*, 2011). The broad shoulder was assigned to $n \rightarrow \pi^*$ transitions of precedence of epoxide (C-O-C) and peroxide (R-O-O-R) like linkages (Marcano *et al.*, 2010). The sharp absorption peak appearance at approximately ~228 nm corresponded to a π-π^* transition of the aromatic C-C bonds (Alam *et al.*, 2017).

4.3.2. FTIR Analysis

Figure 4.9 shows the FTIR spectrum of GO prepared by Improved Hummers Method. The stretching and bending vibration of OH groups were seen as a broad peak observed between of 3000-3700 cm^{-1} in high frequency area (Marcano *et al.*, 2010) due to the strong hydrophilicity of GO.

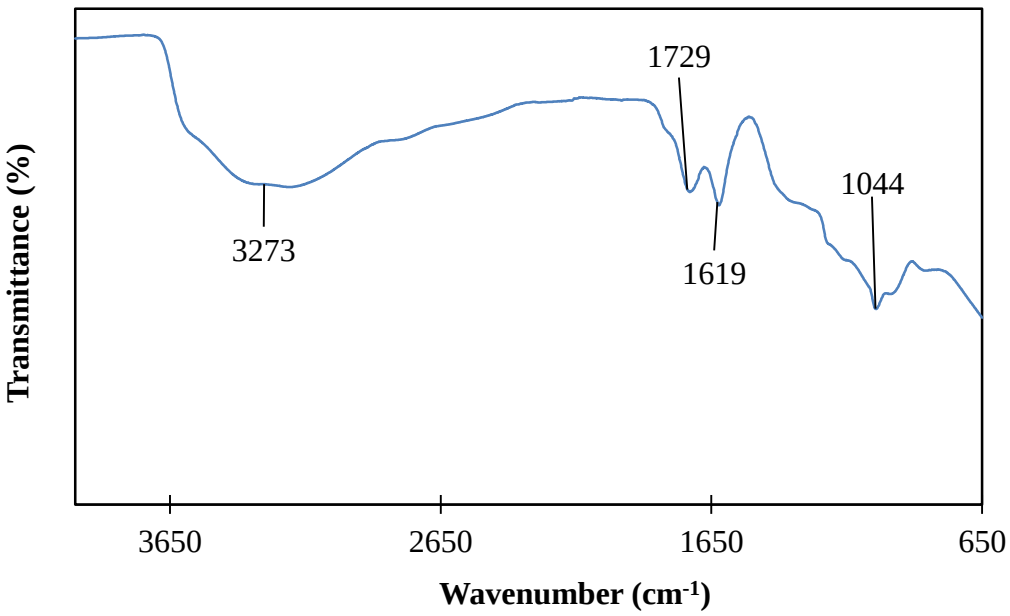

Figure 4.9. FTIR spectrum of GO

The characteristic peak of carboxyl C=O stretching vibrations was seen in 1729 cm^{-1}. The peak corresponding to the C=C from unoxidized sp^2 CC bonds was observed at 1619 cm^{-1} and the peaks observed at 1044 cm^{-1} are identified as C-O-C vibrations (Marcano *et al.*, 2010).

4.3.3. XRD Analysis

The XRD pattern of GO was represented in Figure 4.10. The sharp characteristic peak of GO appeared at 2θ=9.85. The additional peaks especially associated with the graphite flakes could not be seen in the XRD pattern due to high ordered oxidation of graphite (Lavin-Lopez *et al.*, 2016).

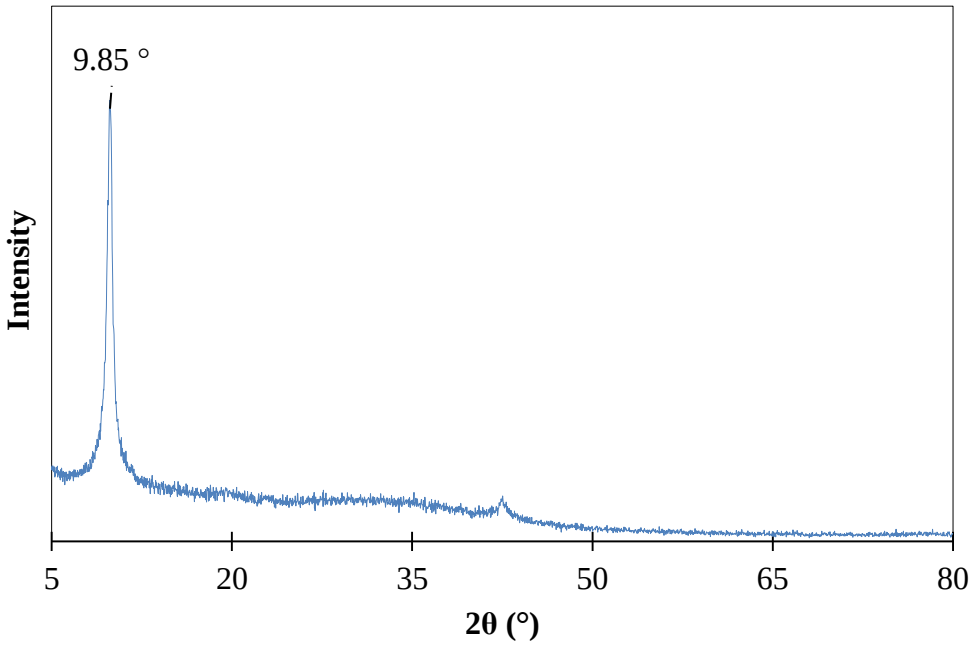

Figure 4.10. XRD pattern of GO

4.3.4. Raman Spectroscopy Analysis

The Raman spectrum is a sensitive and informative technique to determine the disorders originated from sp^2 carbon hexagonal networks with strong covalent bonds (Wu *et al., 2018).* The D band became prominent at ~1350 cm^{-1} in Raman spectrum of GO. This was associated with the presence of defects in graphitic materials. The G band located at 1580−1620 cm^{-1} due to the graphitic order (Lavin-Lopez *et al.*, 2016).

Figure 4.11 shows the Raman spectrum of GO. In this figure, two characteristic peaks of GO were indicated. The D peak appeared at 1358 cm^{-1} and the G peak was detected at 1598 cm^{-1}. The prominent D peak is a sign of a reduction in the size of the sp^2 domains originated from the oxidation process. Additionally, the high intensity ratio of these two peaks (I_D/I_G) indicates the number of defects due to the oxidation process (Lavin-Lopez *et al.*, 2016). This ratio generally was in the range of 0.7-1.0 and calculated as 1.01 for the synthesized graphene oxide sample.

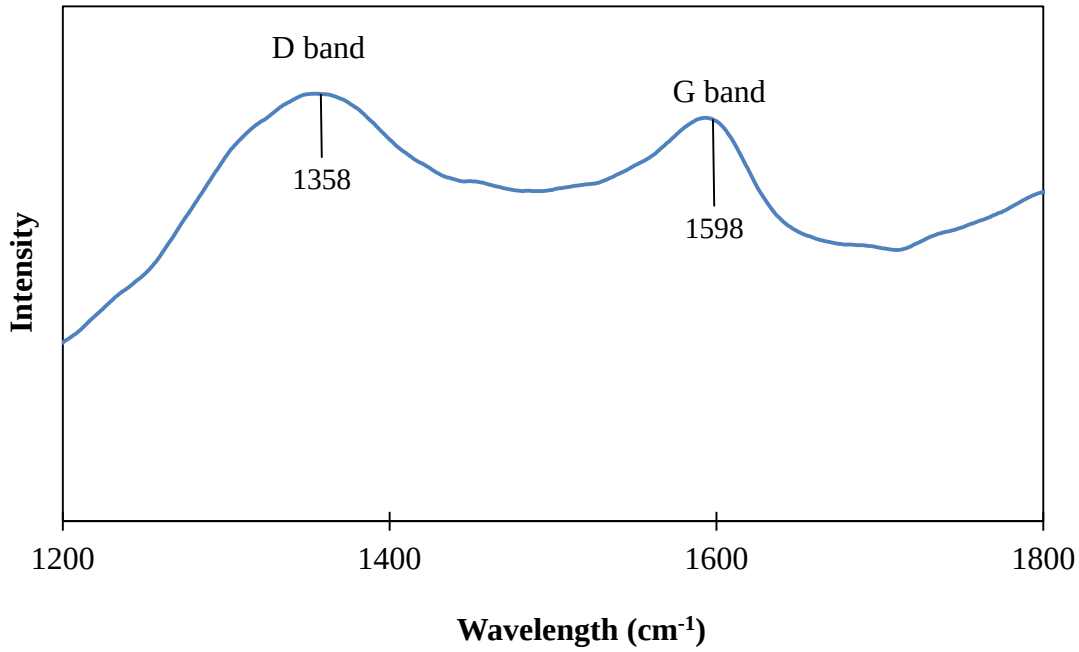

Figure 4.11. Raman spectrum of GO

4.3.5. Thermogravimetric Analysis (TGA)

The thermogravimetric analysis of GO was given in Figure 4.12. As seen from this figure, the relatively rapid weight loss of GO was observed at below 100°C due to the evaporation of water molecules. The destruction of functional groups containing oxygen atoms led to the second weight loss around 150 °C. The final weight loss was obtained around 230 °C due to the combustion of the carbon skeleton of GO (Mohandes and Salavati-Niasari, 2014).

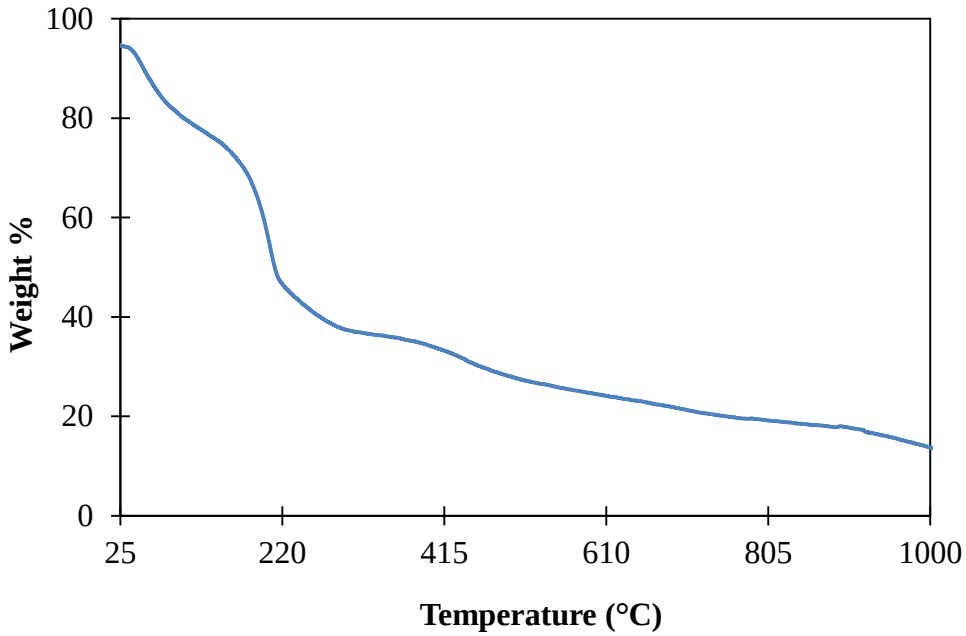

Figure 4.12. TGA profile of GO

4.3.6. TEM Analysis

TEM was used to confirm the nanosheet morphology of GO, and the images were represented in Figure 4.13. According to the TEM images, the wrinkled layer morphology of GO was clearly observed (Xu *et al.*, 2010).

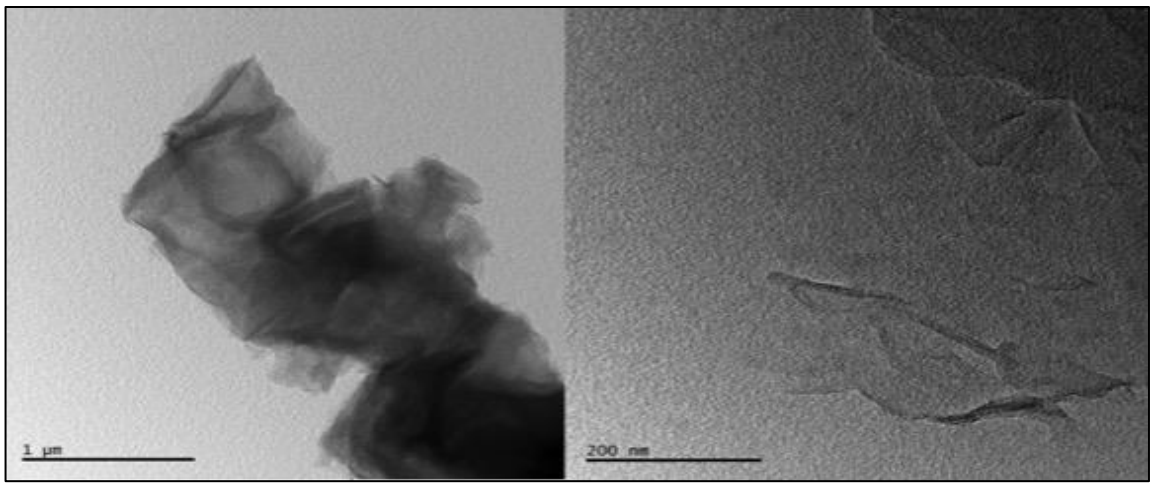

Figure 4.13. TEM images of GO

4.4. Characterization Studies of Chitosan

The chitosan supplied from Acros firm with 9012-76-4 CAS number was characterized by FTIR, XRD and TGA analyses.

4.4.1. FTIR Analysis

The FTIR spectrum of pure chitosan was given in Figure 4.14. The stretching vibrations of υ(C-H) at 2867 and 1374, υ (O-C-O) at 1056 and 1027, υ (NH_2) at 3290 and 1418 were obtained in FTIR spectrum of chitosan. The characteristic peaks of chitosan observed at 1652, 1587 and 1321 were attributed to the amide I (C-O), amide II (-NH) and amino (NH_2) groups (Mohandes and Salavati-Niasari, 2014). The peaks observed at 1149 and 892 were attributed to the –C–O–C– group vibration of saccharides (Cordero-Arias *et al.*, 2013).

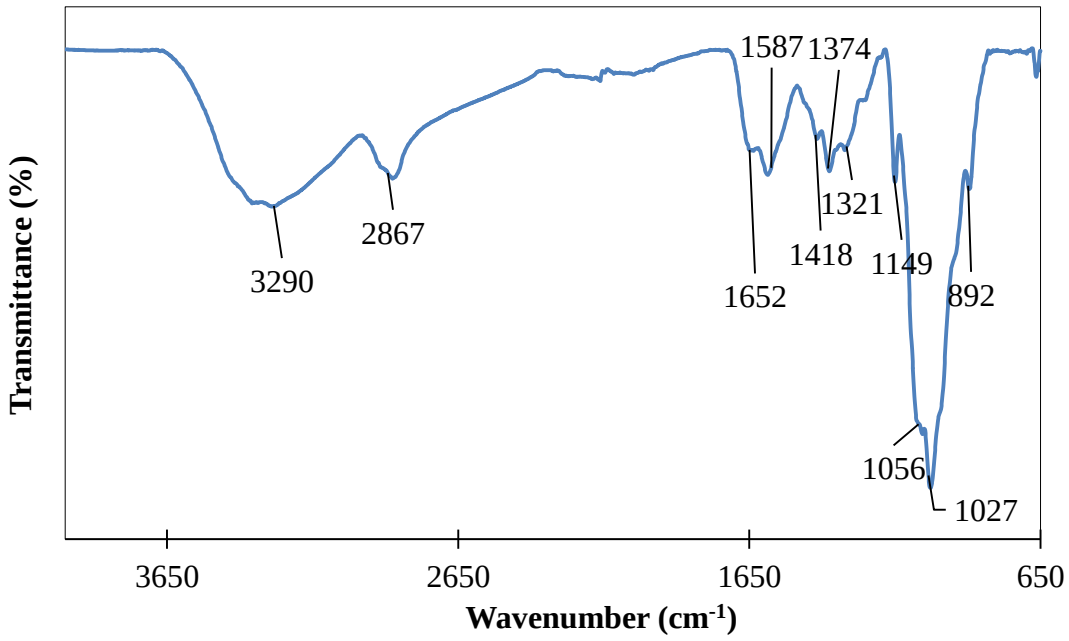

Figure 4.14. FTIR spectrum of chitosan

4.4.2. XRD Analysis

The XRD pattern of the chitosan was represented in Figure 4.15. The characteristic peak of chitosan with maximum intensity was observed at 2θ value of 19.91.

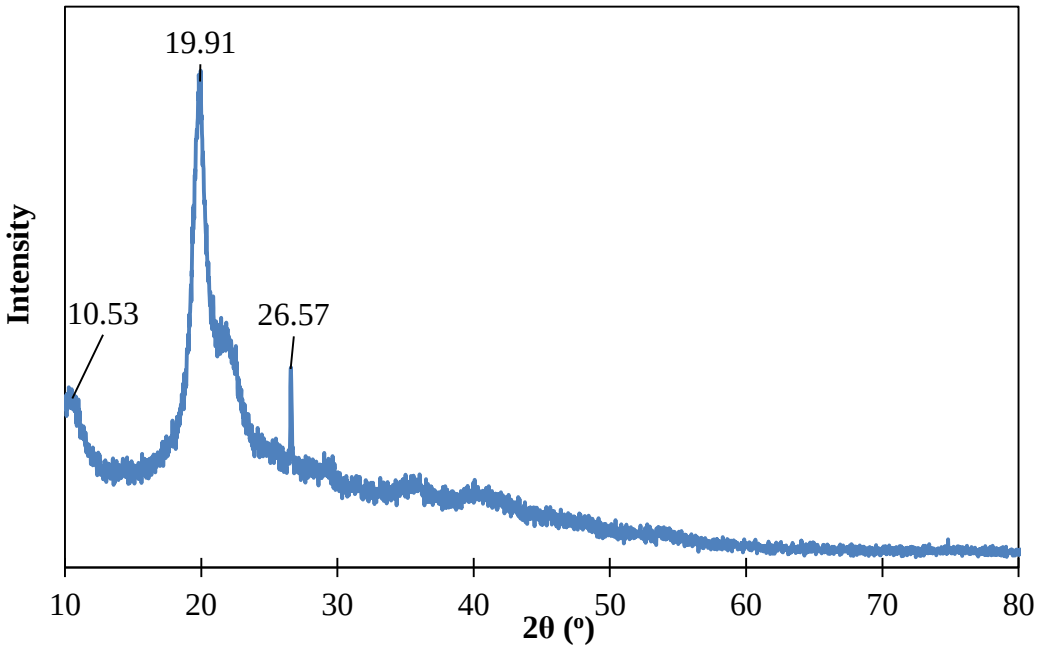

Figure 4.15. XRD pattern of chitosan

4.4.3. Thermogravimetric Analysis (TGA)

The TGA profile of pure chitosan given in Figure 4.16 showed that thermal degradation of chitosan occurred in two stages. The first stage occurred in the range of 25-177 °C due to loss of water molecules. At the second stage, the primary degradation of chitosan started at 256°C, and it was completely degraded at approximately 815 °C.

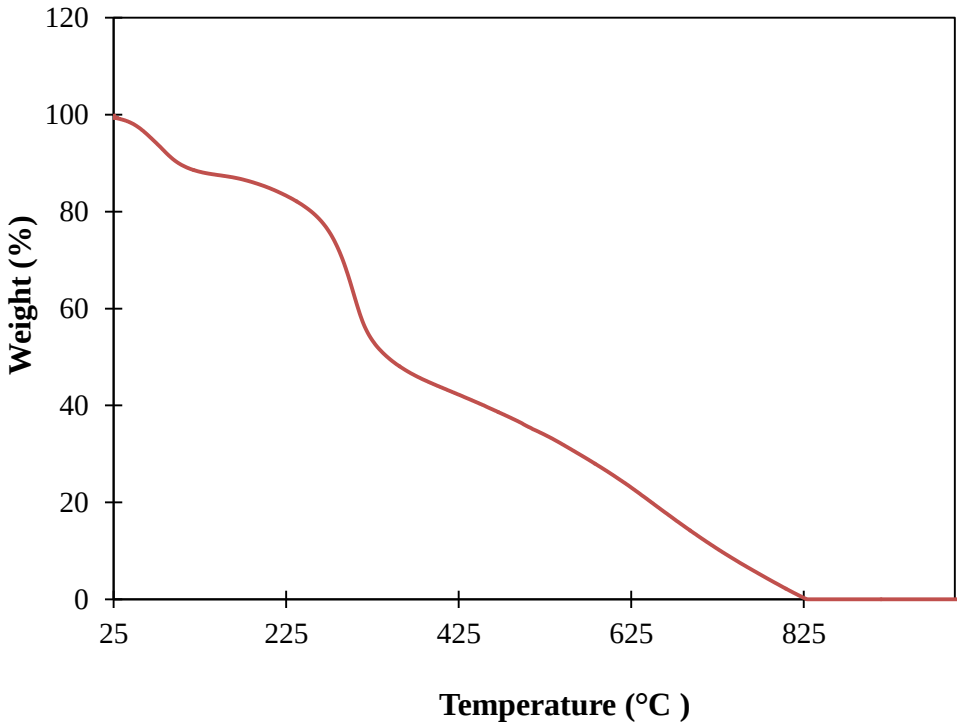

Figure 4.16. TGA profile of chitosan

4.5. Characterization Studies of Produced Scaffolds

Scaffolds were prepared by blending of the solutions of HAp, GO and CS, and then, this scaffold mixture was moulded and freezed as given in Section 3.2.3. Following the step of water-acetone substitution, the supercritical gel drying procedure was applied as given in Section 3.2.4.

In-vitro cell viability analysis was carried out for all produced scaffolds mentioned in Section 3.2.3 Table 3.1 since biocompatibility is the critical property of produced scaffolds. The in-vitro cell viability results of produced scaffolds were given in Table 4.3 in Section 4.5.7. According to the results obtained, the scaffold named as “scaffold D”, including 60% of HAp, 1% of GO and 39% of CS, had the highest relative cell viability. Therefore, for the determination of physical, chemical and biological properties of scaffold D, the characterization techniques were carried out.

4.5.1. FTIR Analysis

The FTIR spectra of CS, GO, HAp and scaffold D were shown in Figure 4.17. In the FTIR spectrum of scaffold D, all the characteristic peaks of individual components were obtained showing the dispersion of HAp and GO in CS. Additionally, slight shift of characteristic peak values and reduced peak values were obtained, and this could be explained by the interactions occurred between the components.

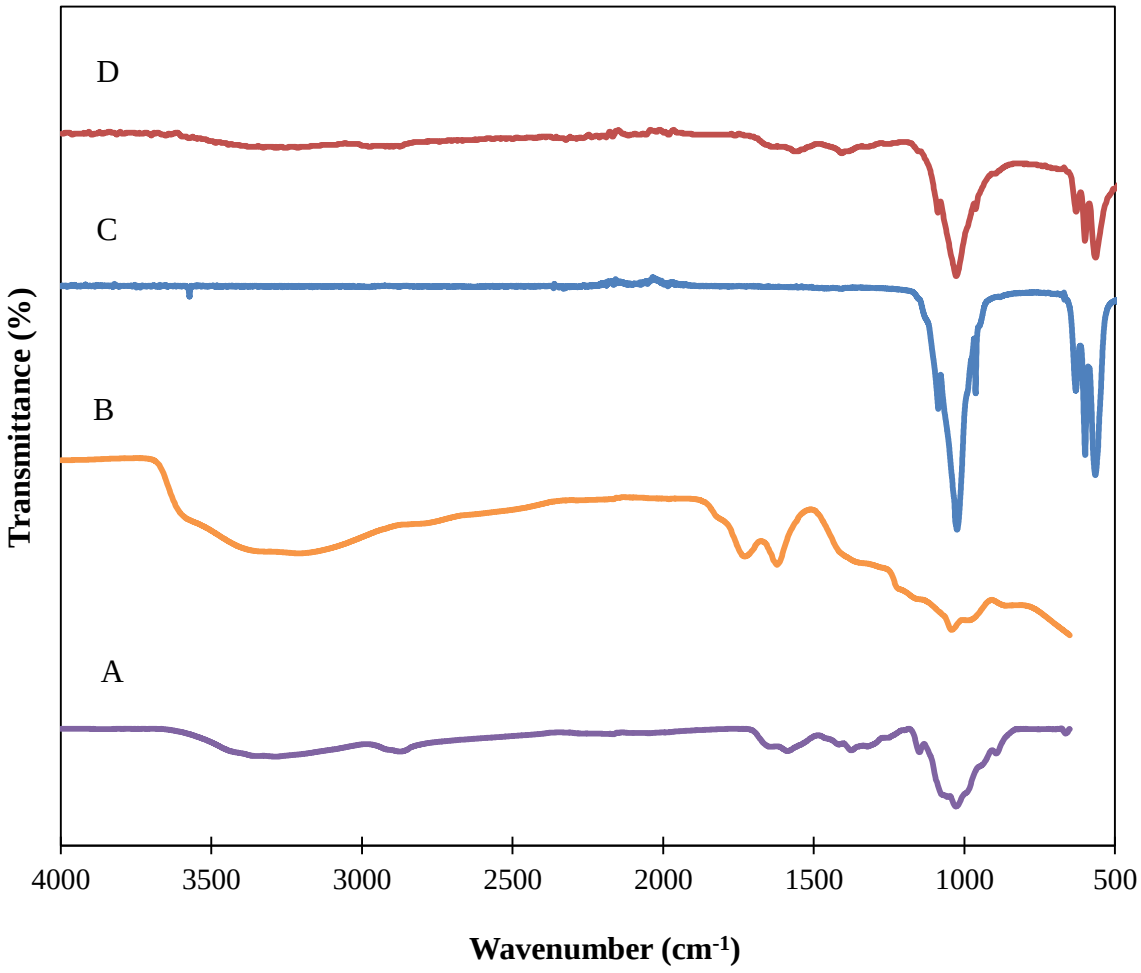

Figure 4.17. FTIR spectra of A) CS, B) GO, C) HAp and D) scaffold D

4.5.2. XRD Analysis

Phase and crystallinity of scaffold D was determined using XRD analysis and shown in Figure 4.18. The XRD pattern of the produced scaffolds confirmed the interactions between HAp, GO and CS.

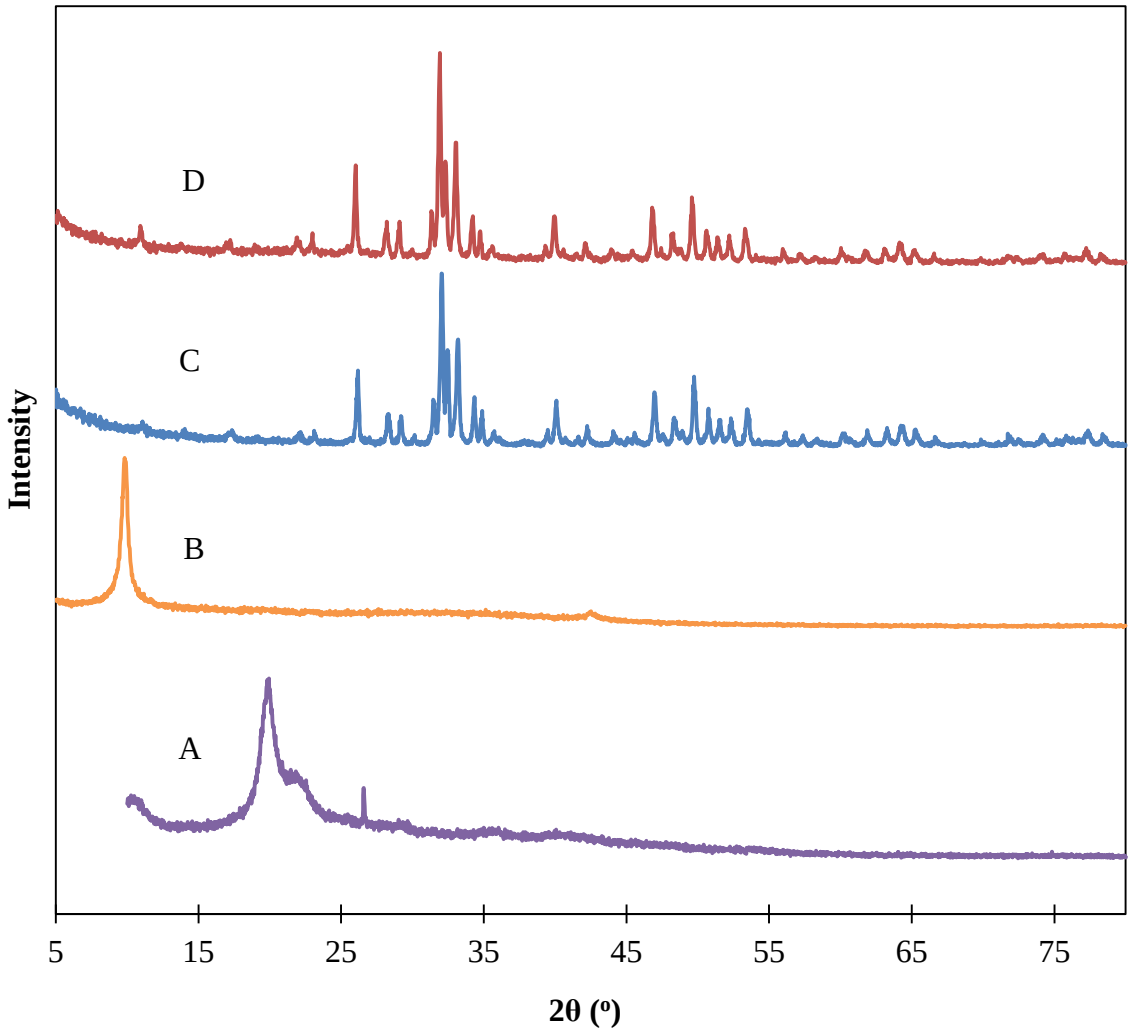

Figure 4.18. XRD patterns of A) CS, B) GO, C) HAp and D) scaffold D

4.5.3. Thermogravimetric Analysis

The thermogravimetric analysis of scaffold D was given in Figure 4.19. From the TGA profile of scaffold D, the first weight loss was observed between 75 ℃ and 200 ℃ due to removal of absorbed water molecules. The second weight loss was observed between 200 ℃ and 500 ℃ due to thermal decomposition of chitosan and graphene oxide. The negligible amount of weight loss was observed above 600 ℃ indicating the thermal stability of HAp and GO.

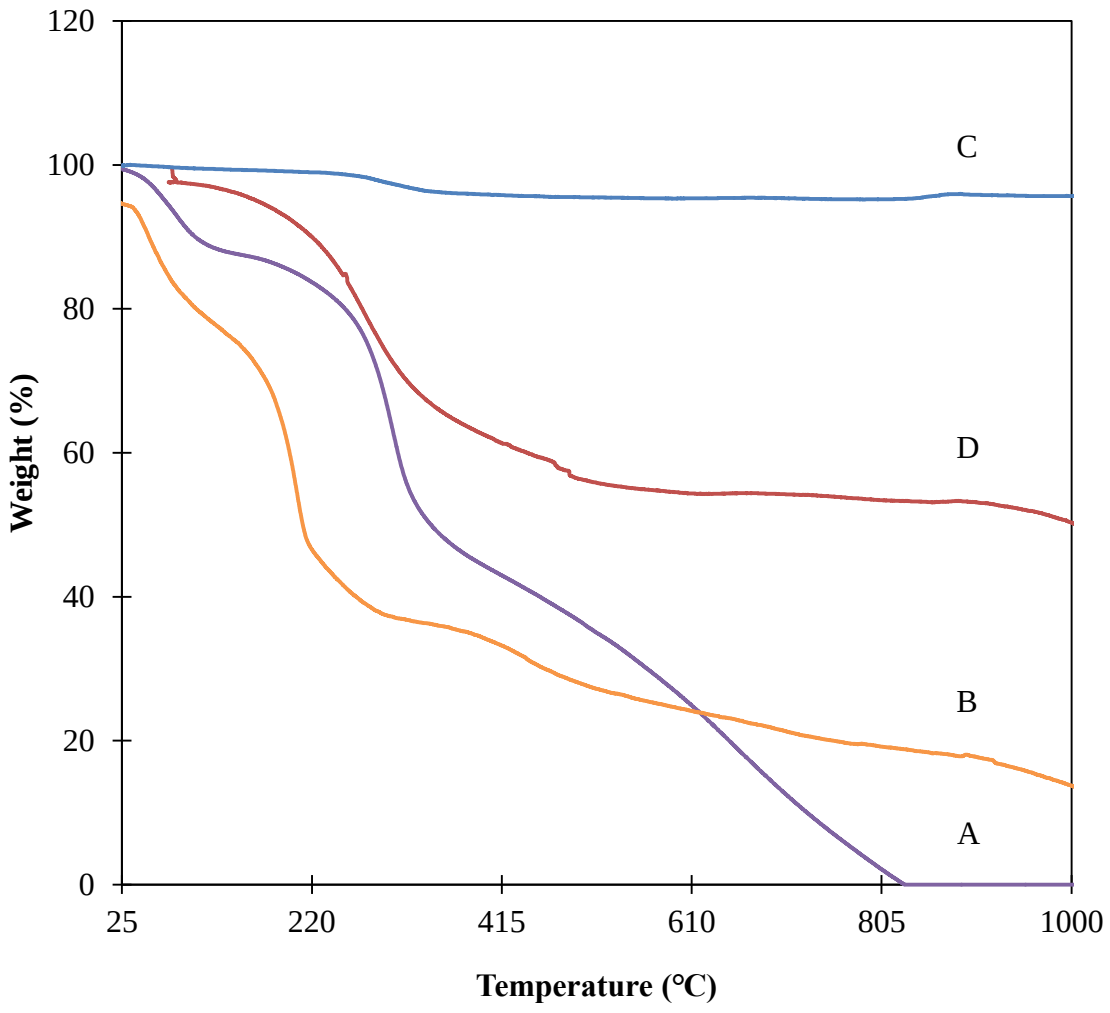

Figure 4.19. TGA profiles of A) CS, B) GO, C) HAp and D) scaffold D

4.5.4. SEM Analysis

The morphological structure of scaffold D was investigated by SEM analysis since the porous nature is an important parameter in terms of the cell growth. The SEM images of scaffold D at various magnifications were given in Figure 4.20. The porous structure of scaffold D (Figure 4.20b) and hydroxyapatite agglomerations at high magnification (Figure 4.20d) was clearly observed. The macropores with pore sizes of 130-160 μm were observed at SEM images as given in Figure 4.21.

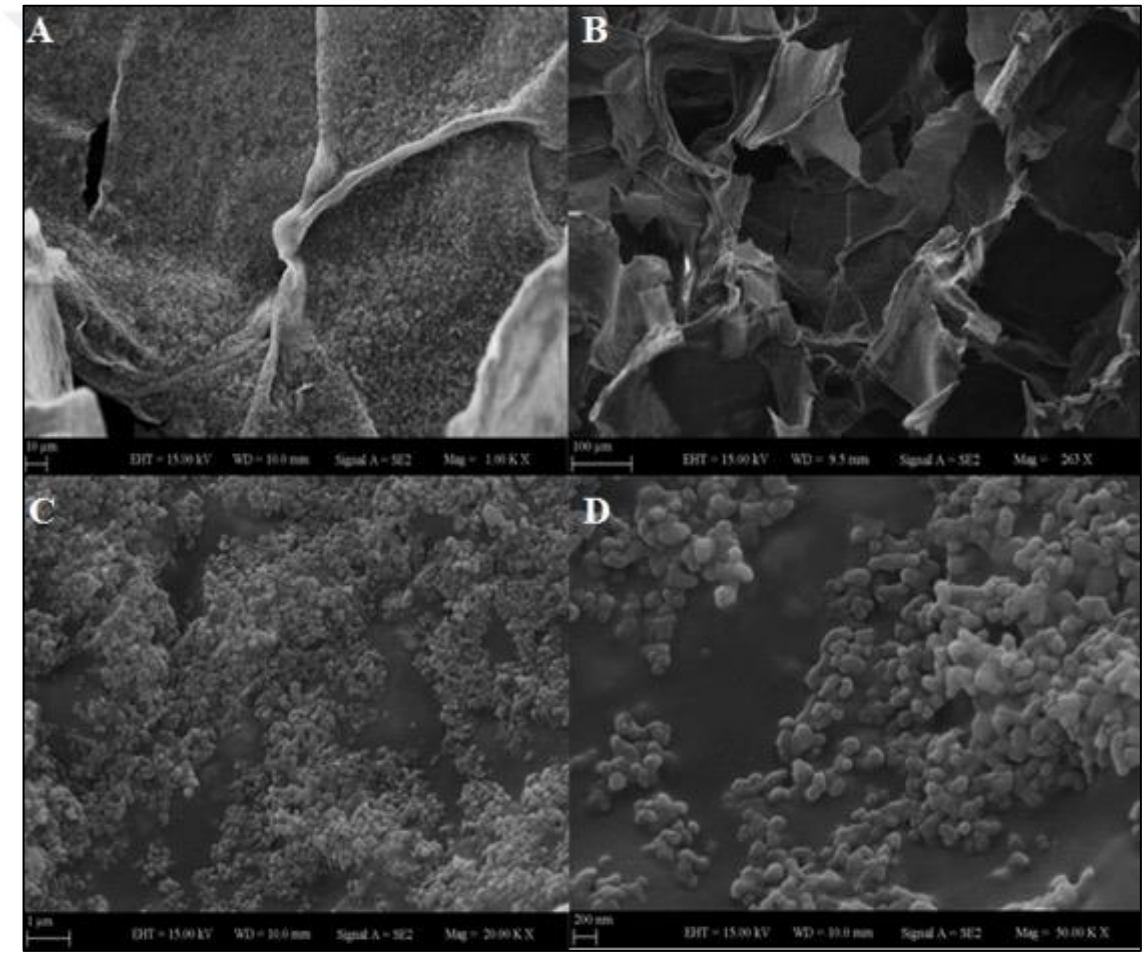

Figure 4.20. SEM images of scaffold D at various magnifications

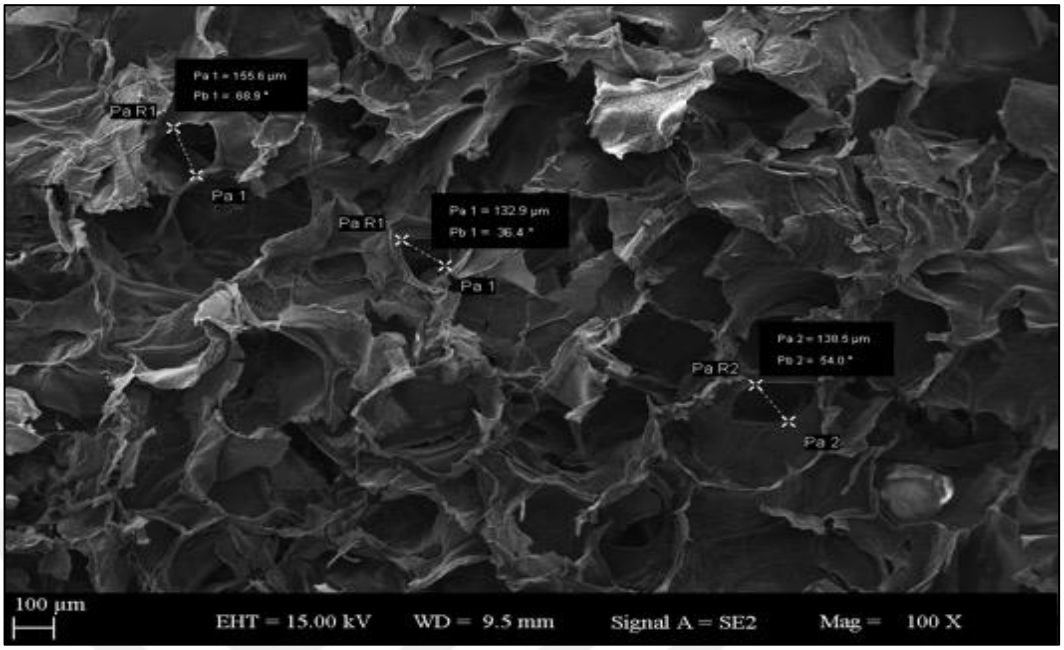

Figure 4.21. Measured pore size of scaffold D at 100X magnification

4.5.5. TEM Analysis

TEM images of scaffold D were taken to obtain further insight of its morphological structure and represented in Figure 4.22. According to the images, the hydroxyapatite agglomeration on GO-CS sheets was observed.

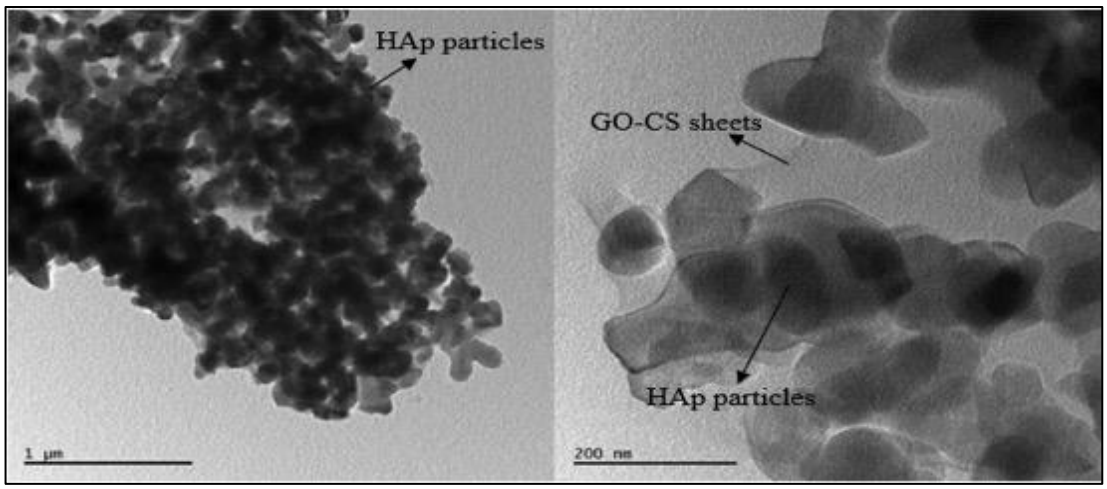

Figure 4.22. TEM images of scaffold D

4.5.6. BET Analysis

Specific surface area and pore size of scaffold D were characterized by the Brunauer–Emmett–Teller (BET) surface area. The N_2 adsorption-desorption isotherm of scaffold D was represented in Figure 4.23. According to the observed isotherm curve, it was determined that this curve had a similar structure with Type IV isotherm with a H3 hysteresis (Sing, 1982). This type of curve indicates the presence of the mesopores in the sample.

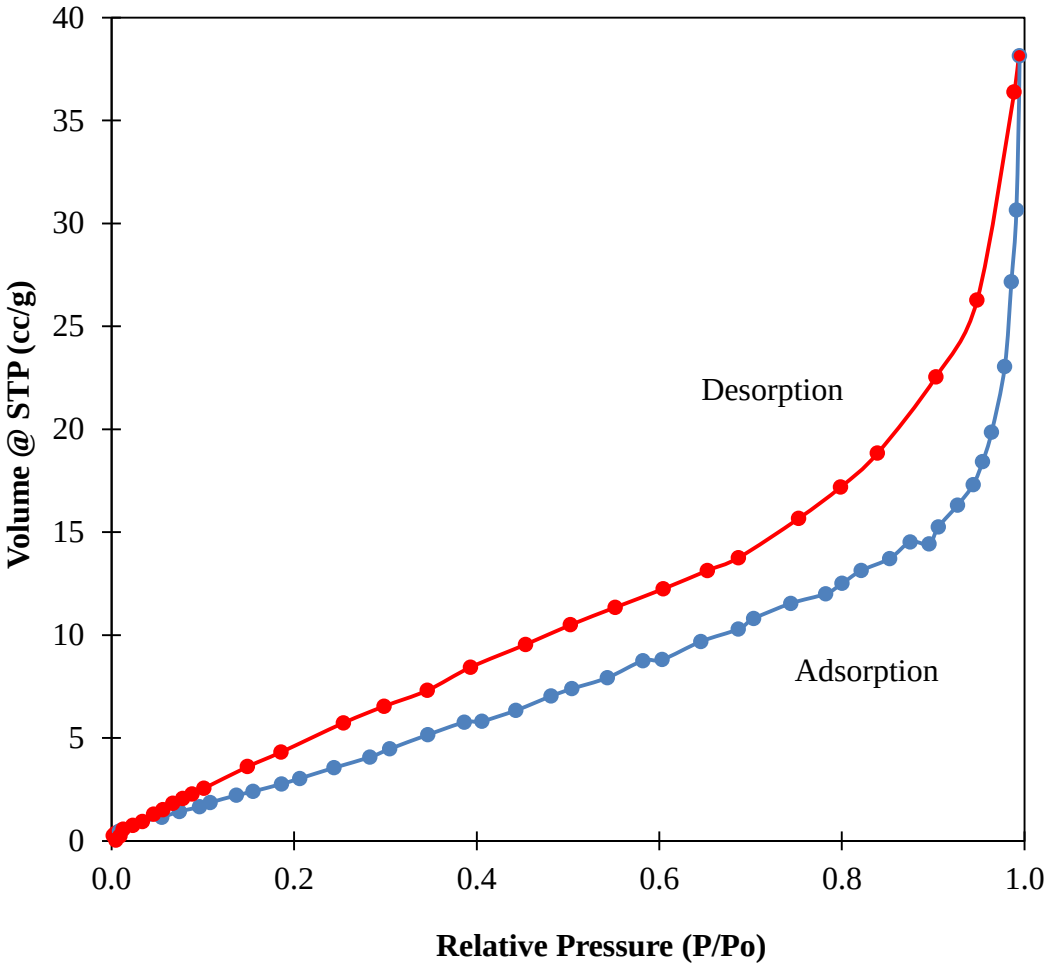

Figure 4.23. Nitrogen adsorption–desorption isotherm of scaffold

The corresponding parameters such as surface area, average pore diameter and pore volume obtained from the BET analysis was given in Table 4.2. These values were calculated by Barrett–Joyner–Halenda (BJH) equation.

Table 4.2. Surface area and porosity analysis of scaffold D

Parameters	Value
Surface area (m^2/g)	15.345
Pore volume($_{BJH\ adsorption}$) (cm^3/g)	0.058
Pore volume($_{BJH\ desorption}$) (cm^3/g)	0.055
Average pore diameter (nm)	15.3
Total pore volume (cm^3/g)	0.059

The pore size distribution of the scaffold obtained by BJH equation from the adsorption branch of the isotherm showed that the mesoporous structure was mainly distributed at 3.71 nm (Figure 4.24).

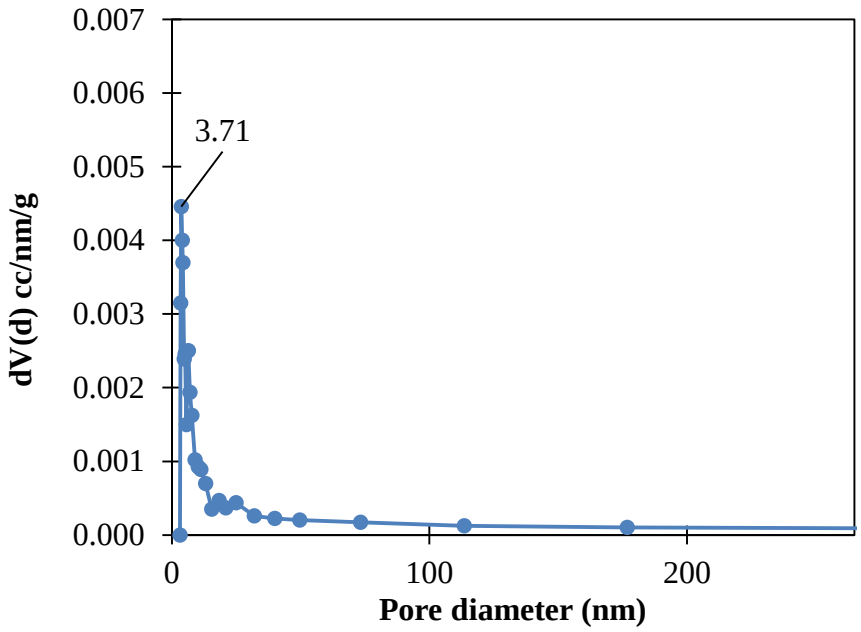

Figure 4.24. Pore size distribution of scaffold D

4.5.7. Cell Viability Analysis

The MTT assay analysis was performed for 1 day to evaluate the in-vitro cytotoxicity of produced scaffolds on MC3T3-E1 cells. For this purpose, the cells seeded on a tissue culture without scaffold were taken as a negative control. The absorbance values of negative control and cell-seeded scaffolds were measured, and the relative cell viability values were calculated using Equation 3.4 in Section 3.3.9. The values were expressed as mean ± relative standard deviation, which is <%7.83 as in Table 4.3.

Table 4.3. The relative cell viability values of produced scaffolds

Name	Scaffold Components	Ratio of Components (w/w)	Relative Cell Viability (%)	Relative Standard Deviation (%)
A	Graphene Oxide	1%	30.58	4.95
	Chitosan	99%		
B	Hydroxyapatite	60%	72.59	3.63
	Chitosan	40%		
C	Hydroxyapatite	60%	77.65	0.37
	Graphene Oxide	0.5%		
	Chitosan	39.5%		
D	Hydroxyapatite	60%	159.26	2.51
	Graphene Oxide	1%		
	Chitosan	39%		
E	Hydroxyapatite	60%	71.27	7.83
	Graphene Oxide	2%		
	Chitosan	38%		
F	Hydroxyapatite	60%	38.65	2.25
	Graphene Oxide	4%		
	Chitosan	36%		

In the present study, two-component scaffolds, A and B, were used to determine the three-component scaffold effect on the cell viability. As can be seen in Table 4.3 and Figure 4.25, the lowest cell proliferation was observed on scaffold A. This result could be explained by lack of 3D and porous structure of scaffold A. Scaffold B had higher cell viability than A and slightly lower cell viability than C. These results indicated that GO addition had proliferative effect on MC3T3-E1 cells.

MTT assay analysis was also performed for the three-component scaffolds including various ratios of GO such as 0.5% , 1% , 2% and 4% (w/w) called as C, D, E and F, respectively, to determine the toxicity effect of GO. The results showed that scaffold D had highest proliferative effect on MC3T3-E1 cell line. The reason of this can be explained by the addition of GO which had osteoconductive effect even at 1% (w/w) ratio. However, the increased GO ratio was inversely proportional with the MC3T3-E1 cell proliferation due to GO toxicity on the MC3T3-E1 cell line. As a result, the MTT assay analysis showed that scaffold D provided a well-suited environment for the proliferation of MC3T3-E1 cells.

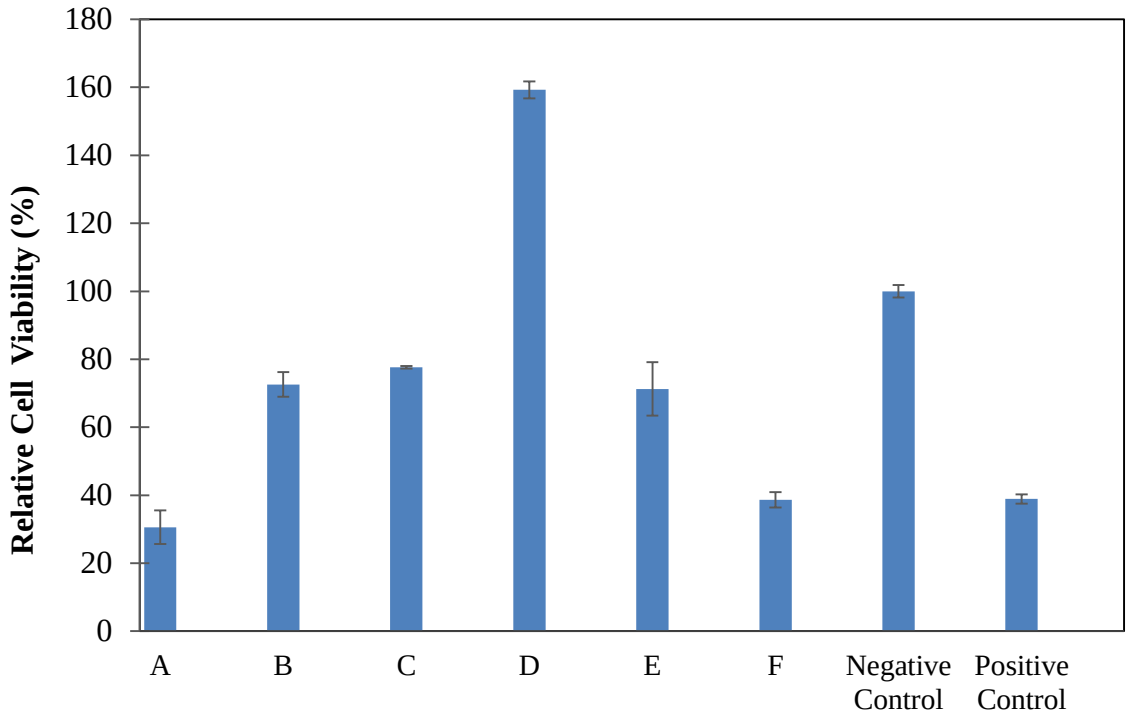

Figure 4.25. MTT assay analysis of produced scaffolds

4.5.8. Mechanical Analysis

The ideal scaffold should provide the mechanical support for the cells to stimulate them for the adhesion, proliferation and differentiation. For this reason, the mechanical characterization of the scaffold B and D were performed using the universal mechanical testing instrument, and the results were given in Figure 4.26. The values were expressed as mean ± relative standard deviation that is <%1.35.

In the present study, scaffolds B (0% GO w/w) and D (1% GO w/w) were used to determine the GO effect on their mechanical properties. According to the data obtained, the compressive strength values were found as 128 kPa and 244 kPa for scaffold B and D, respectively. This result showed that even small amount of GO addition (1% w/w) provided the significant improvement on the compressive strength.

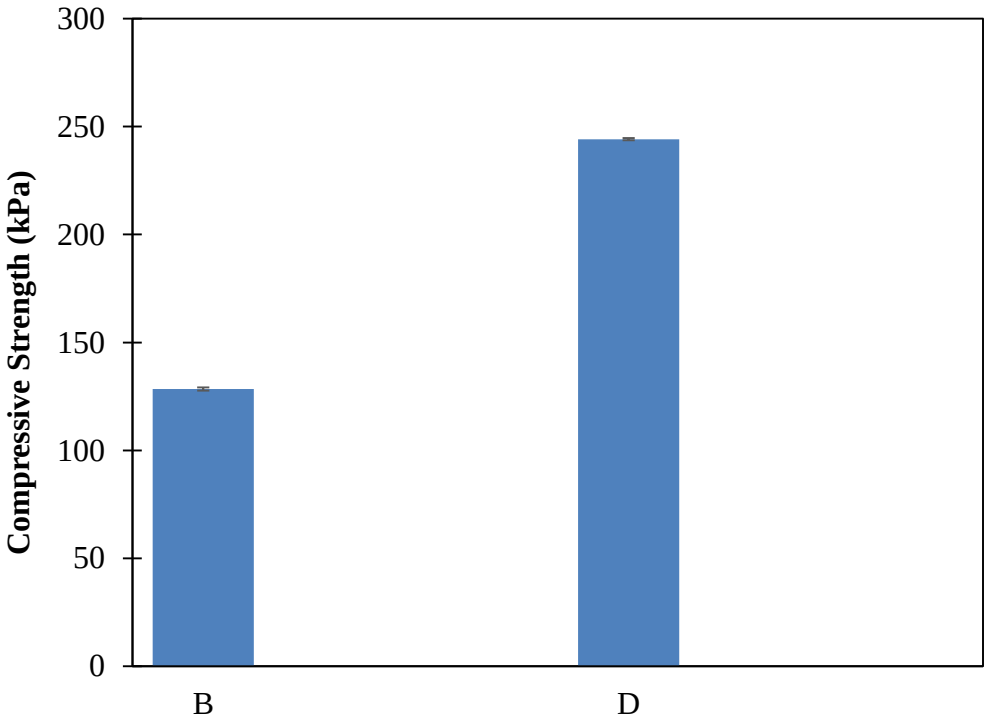

Figure 4.26. Compressive strength of the scaffolds

The obtained compressive strength value, 244 kPa, for scaffold D produced in the present study is in agreement with the previously reported three-component scaffolds produced by freeze drying method. El-Meliegy *et al.* (2018) used HAp as an incorporated material into the polymer matrix Dextran/Chitosan to obtain a composite scaffold by freeze drying technique. The produced scaffolds had 200 kPa-900 kPa compressive strength values depending on the proportion of the HAp. On the other hand, Kim *et al. (*2015) produced the three-component scaffold including HAp, alginate (AG) and chitosan (CS) utilizing AG as a dispersing agent for nano-HAp and CS. The HAp addition to the scaffolds at various proportions led to improvement of compressive strength values from 200 to 680 kPa.

5. CONCLUSIONS and RECOMMENDATIONS

5.1. Conclusions

In the present study, three-component scaffolds composed of HAp-GO-CS were produced by SC-CO_2 assisted procedure and characterized in terms of their physical, chemical and biological properties. To the best of our knowledge, no studies have been conducted on the investigation of the production of three-component scaffold, which is composed of hydroxyapatite (HAp) derived from eggshells, graphene oxide (GO), chitosan (CS), by using the supercritical gel drying method, and on the examination of the possible toxicity effects of GO additions.

In the context of this study, firstly, HAp was synthesized via precipitation method, and eggshells were utilized as calcium precursor. Secondly, the GO was synthesized by Improved Hummers method. Then, the scaffolds were prepared by blending of the solutions of HAp, GO and CS, and this scaffold mixture was moulded and freezed. After the water-acetone substitution step, the supercritical gel drying procedure was applied, and this was the final step for the production of the scaffolds. The produced scaffolds were coded as A, B, C, D, E, F, and their compositions were given in Table 3.1 Section 3.2.3. The characterization studies were applied on the components and produced scaffolds. According to the results obtained, the major findings can be given as follows;

- The FTIR spectra and XRD patterns confirmed that the HAp was successfully synthesized via precipitation method by using the eggshells. Additionally, the characterization studies to reveal the thermogravimetric behavior, morphological structure and elemental composition of HAp were carried out.
- According to the SEM analysis, HAp particles had a tendency to being agglomerate. The thermogravimetric analysis confirmed HAp's thermal stability which is expected behavior for all calcium phosphate based materials. Finally, the elemental composition of HAp was determined by EDS analysis, and the stoichiometric ratio of Ca/P was found as 1.68 similarly with pure hydroxyapatite found in bone tissue.

- The chemical structure of GO was characterized by UV-Vis Absorption Spectroscopy, FTIR and XRD. According to the results, synthesized GO had all characteristic peaks. Besides, the peaks belonging to unoxidized graphite sample were not detected. The Raman Spectroscopy analysis also confirmed that the oxidation of graphite powder was successfully carried out. The morphological structure of GO was analyzed by TEM. The result showed the full exfoliation of GO into individual sheets.

- The characterization studies of scaffolds were carried out by using scaffold D due to its high cell viability ratio. The FTIR and XRD analysis showed the individual peaks of the components. These peaks confirmed that the blending of the components were performed successfully.

- The morphological structure of scaffold D was analyzed by using SEM and TEM. The results showed that the scaffold had porous structure which is essential property for its applications in tissue engineering.

- The surface area, average pore size and pore size distribution of the scaffold D were measured by BET analysis. The results showed that the isotherm curve had a similar structure with Type IV isotherm with a H3 hysteresis. The surface area (m^2/g), pore volume (BJH adsorption), pore volume (BJH desorption), average pore diameter (nm) and total pore volume (cm^3/g) were found as 15.345, 0.058, 0.055, 15.3, and 0.059, respectively.

- The MTT assay analysis was carried out to reveal the toxic effect of produced scaffolds on pre-osteoblast cell line, MC3T3-E1 cells. The relative cell viability values of scaffold A, B, C, D, E and F were calculated and expressed as mean ± relative standard deviation is <%7.83. According to the results obtained, it was found that scaffold D had highest cell viability, and the increased GO ratio, above 1%, into scaffolds was found to be toxic on MC3T3-E1 cells.

- The universal testing machine instrument was used to determine the mechanical properties of scaffold B and D. According to the results, compressive strength of scaffolds was found as 128 kPa and 244 kPa for scaffold B and D, respectively. The obtained compressive strength value for scaffold D produced in the present study is in

agreement with the previously reported three-component scaffolds produced by freeze drying method (El-Meliegy *et al.,* 2018; Kim *et al.*, 2015).

Consequently, the present study represents the production of 3D three-component scaffolds composed of HAp-GO-CS by using supercritical gel drying method. According to the results obtained, scaffold D has 3D porous structure, highest cell viability and reasonable mechanical properties. Therefore, scaffold D, having those properties mentioned, could be a promising candidate for the bone tissue engineering applications.

5.2. Recommendations

Apart from all the studies performed within the framework of the thesis, the swelling behavior and degradation rate of scaffold D could be investigated for further studies. These properties are significant for examination of the physiological fluids absorption, transfer of nutrients and metabolites in bone tissue engineering applications.

REFERENCES

Akram, M. *et al.* (2014) 'Extracting hydroxyapatite and its precursors from natural resources', *Journal of Materials Science*, 49(4), pp. 1461–1475. doi: 10.1007/s10853-013-7864-x.

Alam, S. N., Sharma, N. and Kumar, L. (2017) 'Synthesis of Graphene Oxide (GO) by Modified Hummers Method and Its Thermal Reduction to Obtain Reduced Graphene Oxide (rGO)*', *Graphene*, 06(01), pp. 1–18. doi: 10.4236/graphene.2017.61001.

Athira, K. S., Sanpui, P. and Chatterjee, K. (2014) 'Fabrication of Poly(Caprolactone) Nanofibers by Electrospinning', *Journal of Polymer and Biopolymer Physics Chemistry*, 2(4), pp. 62–66. doi: 10.12691/jpbpc-2-4-1.

Bedian, L. *et al.* (2017) 'Bio-based materials with novel characteristics for tissue engineering applications -A review, *International Journal of Biological Macromolecules*. Elsevier B.V., 98, pp. 837–846. doi: 10.1016/j.ijbiomac.2017.02.048.

Bhattacharjee, P. *et al.* (2017) 'Silk scaffolds in bone tissue engineering: An overview', *Acta Biomaterialia*. Acta Materialia Inc. doi: 10.1016/j.actbio.2017.09.027.

Boukhvalov, D. W. and Katsnelson, M. I. (2009) 'Chemical functionalization of graphene', *Journal of Physics: Condensed Matter*, 21(34), p. 344205. doi: 10.1088/0953-8984/21/34/344205.

Cengiz, B. *et al.* (2008) 'Synthesis and characterization of hydroxyapatite nanoparticles', *Colloids and Surfaces A: Physicochemical and Engineering Aspects*, 322 (1–3), pp. 29–33. doi: 10.1016/j.colsurfa.2008.02.011.

Chan, B. P. and Leong, K. W. (2008) 'Scaffolding in tissue engineering: General approaches and tissue-specific considerations', *European Spine Journal*, 17 (SUPPL. 4). doi: 10.1007/s00586-008-0745-3.

Chen, D., Feng, H. and Li, J. (2004) 'Graphene Oxide : Preparation , Functionalization , and Electrochemical Applications'. doi: 10.1021/cr300115g.

Chetty, A. *et al.* (2012) 'Hydroxyapatite : Synthesis, properties and applications', *Nova Science Publishers*, pp. 91–132.

Chowdhury, S. and Balasubramanian, R. (2014) 'Recent advances in the use of graphene-family nanoadsorbents for removal of toxic pollutants from wastewater', *Advances in Colloid and Interface Science*. Elsevier B.V., 204, pp. 35–56. doi: 10.1016/j.cis.2013.12.005.

Compton, O. C. and Nguyen, S. T. (2010) 'Graphene oxide, highly reduced graphene oxide, and graphene: Versatile building blocks for carbon-based materials', *Small*, 6(6), pp. 711–723. doi: 10.1002/smll.200901934.

Cordero-Arias, L. *et al.* (2013) 'Electrophoretic deposition of nanostructured-TiO2/chitosan composite coatings on stainless steel', *RSC Advances*, 3(28), p. 11247. doi: 10.1039/c3ra40535d.

Dimiev, A. M. and Eigler, S. (eds) (2016) *Graphene Oxide: Fundamentals and Applications*. Wiley.

Dimiev, A. M. and Eigler, S. (2017) *Graphene Oxide Fundamentals and Applications*. 1st edn. John Wiley & Sons.

Dong, Y. *et al.* (2018) 'Fabrication of novel bioactive hydroxyapatite-chitosan-silica hybrid scaffolds: Combined the sol-gel method with 3D plotting technique', *Carbohydrate Polymers*. Elsevier, 197(April), pp. 183–193. doi: 10.1016/j.carbpol.2018.05.086.

Dreyer, D. R. *et al.* (2015) 'The chemistry of graphene oxide', *Graphene Oxide: Reduction Recipes, Spectroscopy, and Applications*, pp. 61–95. doi: 10.1007/978-3-319-15500-5_3.

Dutta, R. C. *et al.* (2017) 'Competent processing techniques for scaffolds in tissue engineering', *Biotechnology Advances*. Elsevier Inc., 35(2), pp. 240–250. doi: 10.1016/j.biotechadv.2017.01.001.

El-Meliegy, E. *et al.* (2018) 'Improvement of physico-chemical properties of dextran-chitosan composite scaffolds by addition of nano-hydroxyapatite', *Scientific Reports*, 8(1), p. 12180. doi: 10.1038/s41598-018-30720-2.

Engin, B., Demirtaş, H. and Eken, M. (2006) 'Temperature effects on egg shells investigated by XRD, IR and ESR techniques', *Radiation Physics and Chemistry*, 75(2), pp. 268–277. doi: 10.1016/j.radphyschem.2005.09.013.

Florencio-Silva, R. *et al.* (2015) 'Biology of Bone Tissue: Structure, Function, and Factors That Influence Bone Cells', *BioMed Research International*, 2015. doi: 10.1155/2015/421746.

García-González, C. A. *et al.* (2012) 'Supercritical drying of aerogels using CO 2: Effect of extraction time on the end material textural properties', *Journal of Supercritical Fluids*. Elsevier B.V., 66, pp. 297–306. doi: 10.1016/j.supflu.2012.02.026.

Georgakilas, V. *et al.* (2016) 'Noncovalent Functionalization of Graphene and Graphene Oxide for Energy Materials, Biosensing, Catalytic, and Biomedical Applications', *Chemical Reviews*, 116(9), pp. 5464–5519. doi: 10.1021/acs.chemrev.5b00620.

Gergely, G. *et al.* (2010) 'Preparation and characterization of hydroxyapatite from eggshell', *Ceramics International*, 36(2), pp. 803–806. doi: 10.1016/j.ceramint.2009.09.020.

Goenka, S., Sant, V. and Sant, S. (2014) 'Graphene-based nanomaterials for drug delivery and tissue engineering', *Journal of Controlled Release*. Elsevier B.V., 173(1), pp. 75–88. doi: 10.1016/j.jconrel.2013.10.017.

Goloshchapov, D. L. *et al.* (2013) 'Synthesis of nanocrystalline hydroxyapatite by precipitation using hen's eggshell', *Ceramics International*. Elsevier, 39(4), pp. 4539–4549. doi: 10.1016/j.ceramint.2012.11.050.

Guerrero-Contreras, J. and Caballero-Briones, F. (2015) 'Graphene oxide powders with different oxidation degree, prepared by synthesis variations of the Hummers method', *Materials Chemistry and Physics*. Elsevier B.V, 153, pp. 209–220. doi: 10.1016/j.matchemphys.2015.01.005.

Islam, S., Bhuiyan, M. A. R. and Islam, M. N. (2016) 'Chitin and Chitosan: Structure, Properties and Applications in Biomedical Engineering', *Journal of Polymers and the Environment*. Springer US, 25(3), pp. 1–13. doi: 10.1007/s10924-016-0865-5.

Jayakumar, R. *et al.* (2010) 'Biomedical applications of chitin and chitosan based nanomaterials - A short review', *Carbohydrate Polymers*. Elsevier Ltd., 82(2), pp. 227–232. doi: 10.1016/j.carbpol.2010.04.074.

Kamalanathan, P. *et al.* (2014) 'Synthesis and sintering of hydroxyapatite derived from eggshells as a calcium precursor', *Ceramics International*. Elsevier, 40(PB), pp. 16349–16359. doi: 10.1016/j.ceramint.2014.07.074.

Keane, T. J. and Badylak, S. F. (2014) 'Biomaterials for tissue engineering applications', *Seminars in Pediatric Surgery*. Elsevier, 23(3), pp. 112–118. doi: 10.1053/j.sempedsurg.2014.06.010.

Khan, Z. U. *et al.* (2016) 'A review of graphene oxide, graphene buckypaper, and polymer/graphene composites: Properties and fabrication techniques', *Journal of Plastic Film and Sheeting*, 32(4), pp. 336–379. doi: 10.1177/8756087915614612.

Khandelwal, H. and Prakash, S. (2016) 'Synthesis and Characterization of Hydroxyapatite Powder by Eggshell', *Journal of Minerals and Materials Characterization and Engineering.*, 4(March), pp. 119–126. doi: http://dx.doi.org/10.4236/jmmce.2016.42011.

Kim, H. L. *et al.* (2015) 'Preparation and characterization of nano-sized hydroxyapatite/alginate/chitosan composite scaffolds for bone tissue engineering', *Materials Science and Engineering C*. Elsevier B.V., 54, pp. 20–25. doi: 10.1016/j.msec.2015.04.033.

Koutsopoulos, S. (2002) 'Synthesis and characterization of hydroxyapatite crystals: A review study on the analytical methods', *Journal of Biomedical Materials Research*, 62(4), pp. 600–612. doi: 10.1002/jbm.10280.

Lan Levengood, S. and Zhang, M. (2015) 'Chitosan-based scaffolds for bone tissue engineering Sheeny', *J Mater Chem B Mater Biol Med.*, 2(21), pp. 3161–3184. doi: 10.1039/C4TB00027G.Chitosan-based.

Lavin-Lopez, M. D. P. *et al.* (2016) 'Influence of different improved hummers method modifications on the characteristics of graphite oxide in order to make a more easily scalable method', *Industrial and Engineering Chemistry Research*, 55(50), pp. 12836–12847. doi: 10.1021/acs.iecr.6b03533.

Lee, E. J., Kim, H. W. and Knowles, J. C. (2015) 'Ceramic Biomaterials as Tissue Scaffolds', in *Stem Cell Biology and Tissue Engineering in Dental Sciences*. Elsevier Inc., pp. 163–174. doi: 10.1016/B978-0-12-397157-9.00014-X.

Lee, J. *et al.* (2016) 'Biosensors based on graphene oxide and its biomedical application', *Advanced Drug Delivery Reviews*. Elsevier B.V., 105, pp. 275–287. doi: 10.1016 /j.addr.2016.06.001.

Lerf, A. *et al.* (1998) 'Structure of Graphite Oxide Revisited ', *The Journal of Physical Chemistry B*, 102(23), pp. 4477–4482. doi: 10.1021/jp9731821.

Levengood, S. L. and Zhang, M. (2014) 'Chitosan-based scaffolds for bone tissue engineering', *J Mater Chem B Mater Biol Med*, 2(21), pp. 3161–3184. doi: 10.1039/C4TB00027G.

Li, F. *et al.* (2015) 'Graphene oxide: A promising nanomaterial for energy and environmental applications', *Nano Energy*. Elsevier, 16, pp. 488–515. doi: 10.1016/j.nanoen.2015.07.014.

Lin, K. and Chang, J. (2015) *Structure and properties of hydroxyapatite for biomedical applications*, *Hydroxyapatite (HAp) for Biomedical Applications*. Elsevier Ltd. doi: 10.1016/B978178242033000001-8.

Logithkumar, R. *et al.* (2016) 'A review of chitosan and its derivatives in bone tissue engineering', *Carbohydrate Polymers*. Elsevier Ltd., 151, pp. 172–188. doi: 10.1016/j.carbpol.2016.05.049.

Lu, T., Li, Y. and Chen, T. (2013) 'Techniques for fabrication and construction of three-dimensional scaffolds for tissue engineering', *International Journal of Nanomedicine*, 8, pp. 337–350. doi: 10.2147/IJN.S38635.

Marcano, D. C. *et al.* (2010) 'Improved synthesis of graphene oxide', *ACS Nano*, 4(8), pp. 4806–4814. doi: 10.1021/nn1006368.

Mohandes, F. and Salavati-Niasari, M. (2014) 'Freeze-drying synthesis, characterization and in vitro bioactivity of chitosan/graphene oxide/hydroxyapatite nanocomposite', *RSC Advances*, 4(49), p. 25993. doi: 10.1039/c4ra03534h.

Monmaturapoj, N. (2008) 'Nano-size Hydroxyapatite Powders Preparation by Wet-Chemical Precipitation Route', *Journal of Metals, Materials and Minerals*, 18(1), pp. 15–20.

Muxika, A. *et al.* (2017) 'Chitosan as a bioactive polymer: processing, properties and applications', *International Journal of Biological Macromolecules*. Elsevier B.V. doi: 10.1016/j.ijbiomac.2017.07.087.

Nanda, S. S., Papaefthymiou, G. C. and Yi, D. K. (2015) 'Functionalization of Graphene Oxide and its Biomedical Applications', *Critical Reviews in Solid State and Materials Sciences*, 40(5), pp. 291–315. doi: 10.1080/10408436.2014.1002604.

Pallela, R. *et al.* (2012) 'Biophysicochemical evaluation of chitosan-hydroxyapatite-marine sponge collagen composite for bone tissue engineering', *Journal of Biomedical Materials Research - Part A*, 100 A(2), pp. 486–495. doi: 10.1002/jbm.a.33292.

Pei, S. and Cheng, H. (2011) 'The reduction of graphene oxide', *Carbon*. Elsevier Ltd, 50(9), pp. 3210–3228. doi: 10.1016/j.carbon.2011.11.010.

Perreault, F., Fonseca de Faria, A. and Elimelech, M. (2015) 'Environmental applications of graphene-based nanomaterials', *Chem. Soc. Rev.*, 44(16), pp. 5861–5896. doi: 10.1039/C5CS00021A.

Phiri, J., Gane, P. and Maloney, T. C. (2017) 'General overview of graphene: Production, properties and application in polymer composites', *Materials Science & Engineering B*. Elsevier B.V., 215, pp. 9–28. doi: 10.1016/j.mseb.2016.10.004.

Putra, R. S. *et al.* (2017) 'Enhanced Electro-Catalytic Process on the Synthesis of FAME Using CaO from Eggshell', *Energy Procedia*. The Author(s), 105(May), pp. 289–296. doi: 10.1016/j.egypro.2017.03.316.

Quirk, R. A. *et al.* (2004) 'Supercritical fluid technologies and tissue engineering scaffolds', *Current Opinion in Solid State and Materials Science*, 8(3–4), pp. 313–321. doi: 10.1016/j.cossms.2003.12.004.

Ray, S. C. (2014) *Chapter 2. Application and Uses of Graphene Oxide and Reduced Graphene Oxide, Applications of Graphene and Graphene-Oxide based Nanomaterials*. Elsevier Inc. doi: 10.1016/B978-0-323-37521-4.00002-9.

Ray, S. C. (2015) *Applications of Graphene and Graphene-Oxide Based Nanomaterials, Applications of Graphene and Graphene-Oxide Based Nanomaterials*. doi: 10.1016/B978-0-323-37521-4.00003-0.

Ray, S. C. (2015) 'Application and Uses of Graphene Oxide and Reduced Graphene Oxide', *Applications of Graphene and Graphene-Oxide Based Nanomaterials*, (May), pp. 39–55. doi: 10.1016/B978-0-323-37521-4.00002-9.

Reverchon, E. and Cardea, S. (2012) 'Supercritical fluids in 3-D tissue engineering', *Journal of Supercritical Fluids*. Elsevier B.V., 69, pp. 97–107. doi: 10.1016/j.supflu. 2012.05.010.

Rivera-Muñoz, E. M. (2011) 'Hydroxyapatite-Based Materials: Synthesis and Characterization', in Fazel, P. R. (ed.) *InTech*. Mexico, pp. 75–99. doi: http:// dx. doi.org/10.5772/62527.

Rodríguez-Vázquez, M. *et al.* (2015) 'Chitosan and Its Potential Use as a Scaffold for Tissue Engineering in Regenerative Medicine', *BioMed Research International*, 2015. doi: 10.1155/2015/821279.

Roseti, L. *et al.* (2017) 'Scaffolds for Bone Tissue Engineering: State of the art and new perspectives', *Materials Science and Engineering C*. Elsevier B.V., 78, pp. 1246–1262. doi: 10.1016/j.msec.2017.05.017.

Sadat-Shojai, M. *et al.* (2013) 'Synthesis methods for nanosized hydroxyapatite with diverse structures', *Acta Biomaterialia*. Acta Materialia Inc., 9(8), pp. 7591–7621. doi: 10.1016/j.actbio.2013.04.012.

Salgado, A. J., Coutinho, O. P. and Reis, R. L. (2004) 'Bone tissue engineering: State of the art and future trends', *Macromolecular Bioscience*, 4(8), pp. 743–765. doi: 10.1002/mabi.200400026.

Saravanan, S., Leena, R. S. and Selvamurugan, N. (2016) 'International Journal of Biological Macromolecules Chitosan based biocomposite scaffolds for bone tissue engineering', *International Journal of Biological Macromolecules*. Elsevier B.V., 93, pp. 1354–1365. doi: 10.1016/j.ijbiomac.2016.01.112.

Saxena, S. *et al.* (2011) 'Investigation of structural and electronic properties of graphene oxide', *Applied Physics Letters*, 99(1), pp. 2011–2014. doi: 10.1063/1.3607305.

Shahbazarab, Z. *et al.* (2018) 'Fabrication and characterization of nanobiocomposite scaffold of zein/chitosan/nanohydroxyapatite prepared by freeze-drying method for bone tissue engineering', *International Journal of Biological Macromolecules*. Elsevier B.V., 108, pp. 1017–1027. doi: 10.1016/j.ijbiomac.2017.11.017.

Shavandi, A. *et al.* (2015) 'Development and characterization of hydroxyapatite/β-TCP/chitosan composites for tissue engineering applications', *Materials Science and Engineering C*. Elsevier B.V., 56, pp. 481–493. doi: 10.1016/j.msec.2015.07.004.

Sing, K. S. W. (1982) ‘Reporting physisorption data for gas/solid systems with special reference to the determination of surface area and porosity (Provisional)’, *Pure and Applied Chemistry*, 54(11). doi: 10.1351/pac198254112201.

Siva, A. P. S. and Ansari, M. N. M. N. M. (2015) ‘A Review on Bone Scaffold Fabrication Methods’, *International Research Journal of Engineering and Technology*, 2(6), pp. 1232–1238. Available at: https://www.irjet.net/archives/V2/i6/IRJET-V2I6185.pdf.

Sivashankari, P. R. and Prabaharan, M. (2016) ‘Prospects of chitosan-based scaffolds for growth factor release in tissue engineering’, *International Journal of Biological Macromolecules*. Elsevier B.V., 93, pp. 1382–1389. doi: 10.1016/j.ijbiomac. 2016.02.043.

Subia, B., Kundu, J. and Kundu, C., S. (2010) ‘Biomaterial Scaffold Fabrication Techniques for Potential Tissue Engineering Applications’, *Tissue Engineering*, (3), pp. 141–159. doi: 10.5772/8581.

Türk, S. *et al.* (2018) ‘3D porous collagen/functionalized multiwalled carbon nanotube/chitosan/hydroxyapatite composite scaffolds for bone tissue engineering’, *Materials Science and Engineering C*, 92(January), pp. 757–768. doi: 10.1016/j.msec.2018.07.020.

Velasco, M. A., Narvaez-Tovar, C. A. and Garzon-Alvarado, D. A. (2015) ‘Design, materials, and mechanobiology of biodegradable scaffolds for bone tissue engineering.’, *BioMed research international*, 2015, p. 729076. doi: 10.1155/2015/729076.

Venkatesan, J. *et al.* (2011) ‘Preparation and characterization of carbon nanotube-grafted-chitosan - Natural hydroxyapatite composite for bone tissue engineering’, *Carbohydrate Polymers*. Elsevier Ltd., 83(2), pp. 569–577. doi: 10.1016/j.carbpol.2010.08.019.

Venkatesan, J. *et al.* (2012) ‘Chitosan–amylopectin/hydroxyapatite and chitosan–chondroitin sulphate/hydroxyapatite composite scaffolds for bone tissue engineering’, *International Journal of Biological Macromolecules*. Elsevier B.V., 51(5), pp. 1033–1042. doi: 10.1016/j.ijbiomac.2012.08.020.

Venkatesan, J., Kim, S. K. and Wong, T. W. (2015) *Chitosan and Its Application as Tissue Engineering Scaffolds*, *Nanotechnology Applications for Tissue Engineering*. Elsevier Inc. doi: 10.1016/B978-0-323-32889-0.00009-1.

Venkatesan, J., Kim, S. and Wong, T. W. (2015) *Chapter 9. Chitosan and Its Application as Tissue Engineering Scaffolds*, *Nanotechnology Applications for Tissue Engineering*. Elsevier Inc. doi: 10.1016/B978-0-323-32889-0.00009-1.

Wahl, D. A. *et al.* (2007) ‘Controlling the processing of collagen-hydroxyapatite scaffolds for bone tissue engineering’, *Journal of Materials Science: Materials in Medicine*, 18(2), pp. 201–209. doi: 10.1007/s10856-006-0682-9.

Wang, P. *et al.* (2010) ‘Effects of synthesis conditions on the morphology of hydroxyapatite nanoparticles produced by wet chemical process’, *Powder Technology*. Elsevier B.V., 203(2), pp. 315–321. doi: 10.1016/j.powtec.2010.05.023.

Wu, J.-B. *et al.* (2018) ‘Raman spectroscopy of graphene-based materials and its applications in related devices’, *Chemical Society Reviews*. Royal Society of Chemistry, pp. 1822–1873. doi: 10.1039/C6CS00915H.

Xu, J. *et al.* (2010) ‘Hierarchical nanocomposites of polyaniline nanowire arrays on graphene oxide sheets with synergistic effect for energy storage’, *ACS Nano*, 4(9), pp. 5019–5026. doi: 10.1021/nn1006539.

Yang, Y. *et al.* (2013) ‘Graphene based materials for biomedical applications’, *Materials Today*. Elsevier Ltd., 16(10), pp. 365–373. doi: 10.1016/j.mattod.2013.09.004.

Yu, P. *et al.* (2017) ‘Self-assembled high-strength hydroxyapatite/graphene oxide/chitosan composite hydrogel for bone tissue engineering’, *Carbohydrate Polymers*. Elsevier Ltd., 155, pp. 507–515. doi: 10.1016/j.carbpol.2016.09.001.

Zaaba, N. I. *et al.* (2017) ‘Synthesis of Graphene Oxide using Modified Hummers Method: Solvent Influence’, *Procedia Engineering*. Elsevier B.V., 184(184), pp. 469–477. doi: 10.1016/j.proeng.2017.04.118.